THEORETICAL STUDY OF MAGNETIC AND CONDUCTING PROPERTIES OF TRANSITION METAL NANOWIRES

Zahra Tabookht

Dipòsit Legal: T-1807-2011

Zahra Tabookht

Theoretical Study of Magnetic and Conducting Properties of Transition Metal Nanowires

PhD Thesis

Supervised by

Dr. Xavier López and Dr. Coen de Graaf

Department of Physical and Inorganic Chemistry

UNIVERSITAT ROVIRA I VIRGILI

Tarragona

2011

UNIVERSITAT ROVIRA I VIRGILI
THEORETICAL STUDY OF MAGNETIC AND CONDUCTING PROPERTIES OF TRANSITION METAL NANOWIRES
Zahra Tabookht
DL:T-1807-2011

UNIVERSITAT ROVIRA I VIRGILI

Departament de Química Física i Inorgànica

Xavier López, investigador Ramón y Cajal, i Coen de Graaf, investigador ICREA, del Departament de Química Física i Inorgànica de la Universitat Rovira i Virgili,

Fem constar que la present memòria, titulada:

"Theoretical Study of Magnetic and Conducting Properties of Transition Metal Nanowires"

ha estat realitzada sota la nostra direcció al Departament de Química Física i Inorgànica de la Universitat Rovira i Virgili per Zahra Tabookht per a l'obtenció del títol de Doctor i que acompleix els requeriments per poder optar a Menció Europea.

Tarragona, 24 d'Octubre de 2011

Els directors de la tesi doctoral

Dr. Xavier López Dr. Coen de Graaf

UNIVERSITAT ROVIRA I VIRGILI
THEORETICAL STUDY OF MAGNETIC AND CONDUCTING PROPERTIES OF TRANSITION METAL NANOWIRES
Zahra Tabookht
DL:T-1807-2011

UNIVERSITAT ROVIRA I VIRGILI
THEORETICAL STUDY OF MAGNETIC AND CONDUCTING PROPERTIES OF TRANSITION METAL NANOWIRES
Zahra Tabookht
DL:T-1807-2011

Acknowledgements

I would like to present my deep appreciation to my supervisors Dr. Xavier López and Dr. Coen de Graaf for their management on this thesis and beneficial and instructive discussions carried out during the last four years.

I want to acknowledge the Universitat Rovira i Virgili (URV) for the four-year PhD grant and for providing me a great and peaceful scientific atmosphere, and also the Spanish Ministry of Science and Innovation for the three-month mobility grant.

Université Paul Sabatier (IRSAMC) in Toulouse-France (Prof. Nathalie Guihéry) is really appreciated for my three-month research stay.

My special thanks are to José Ortiz and Elisenda Mas for all computer support given during my PhD in the URV.

All personnel of the “department of physical and inorganic chemistry” are sincerely acknowledged for their warm and helpful collaborations. Without them, the fulfillment of the thesis might not be materialized.

Deep appreciations are dedicated to all members of the “Quantum Chemistry group” with whom I enjoyed a fantastic social and scientific life in Tarragona.

… and finally

I would like to thank Kaveh, my husband, and my parents whose spiritual support and their patience are always the best encouragement for me.

Table of Contents

Chapter 1

General Introduction

1.1. Nanotechnology

Materials reduced to the nanoscale can show different properties compared to what they exhibit in the macroscopic world, enabling unique applications. For instance, opaque substances become transparent (copper); stable materials turn combustible (aluminium); insoluble materials become soluble (gold). A material such as gold, which is chemically inert at normal scales, can serve as a potent chemical catalyst at the nanoscale.

Nanotechnology is the creation of useful materials, devices, and systems through the manipulation of matter at the molecular scale. Much of today's nanoscale research is designed to reach a better understanding of how matter

behaves at this small scale. The factors that govern larger systems do not necessarily apply at the nanoscale. Because nanomaterials have large surface areas relative to their volumes, phenomena like friction and sticking are more important than in larger systems.

There are two basic approaches for creating nanodevices. The 'top-down' approach involves molding or etching materials into smaller components. In this approach, nano-objects are constructed from larger entities without atomic-level control.[1] This approach has traditionally been used in making parts for computers and electronics. In the 'bottom-up' approach, materials and devices are built from molecular components that assemble themselves chemically by principles of molecular recognition. The concept of molecular recognition is especially important: molecules can be designed so that a specific configuration or arrangement is favoured due to non-covalent intermolecular forces. Such bottom-up approaches should be capable of producing devices in parallel and are in principle much cheaper than top-down methods, although the control of the process can become rather complex as the size and complexity of the desired assembly increases. These approaches utilize the concepts of molecular self-assembly and/or supramolecular chemistry to automatically arrange themselves into some useful conformation.

1.2. Ligand Field Theory

TM complexes play an important role in various processes in nature, such as inorganic catalysts or as reactive sites of enzymes in bioinorganic chemistry.[2-4] Their great role in living organisms, for example, iron in transport and storage of O_2, copper and iron in respiratory cycle and cobalt in vitamin B_{12} and also their huge industrial usages, such as iron in steel, copper in wiring and pipes, titanium in painting, platinum and palladium in catalysis and silver as the best conductor of heat and electricity, all are evidences of their essential position in science and technology developments.

Ligand Field Theory (LFT)[5-9] has been the basic concept to understand the origin of the spectral and magnetic properties of TM complexes for a long time. In 1929, Bethe[10] studied the effect of the surrounding ions on the electron

distribution for all the TM ions in a NaCl-type lattice. He supposed that the ions are rigid spheres and that their mutual interactions are solely the result of the electrostatic potentials set up by their charges. The effect of such a potential on the electrons of a central ion that is part of a lattice is nowadays known as the *crystal field*. One of the major consequences of crystal field theory is that the repulsion between the metal and ligand electrons causes a non-uniform energy shift of the d orbitals with respect to the free ion that can be parameterized within an electrostatic model. However, it was found that only few of the outcomes of crystal field theory depend on the existence of an extended lattice. This observation naturally leads to an important concept of coordination chemistry: that of the *coordination cluster,* defined as the moiety formed by a central metal ion and a number of attached ligands, the whole forming a distinguishable entity and possibly bearing a net electrical charge. Coordination clusters pack themselves into a lattice in the solid state. This packing is not considered of primary importance, because the principal contribution to the potential at the central metal ion comes from the atoms closest to it —the donor atoms.

In the more general model of a coordination compound, the electrons of the central ion are subject to a potential arising from the ligand atoms, not necessarily of simple electrostatic origin as considered in crystal field theory. LFT covers all aspects in which the physical properties of an ion or atom are influenced by its nearest neighbours. LFT, then, contains crystal field theory as a limiting special case. According to the above definition, LFT includes all theories of chemical bonding between an atom and its neighbours like the strength of the metal-ligand bond and coordination bond.

Many results of LFT depend largely on the approximate symmetry of the ligand distribution around the central metal ion rather than on the exact nature of the ligands or the details of their locations. The relative disposition of the ligands about the metal ion decides the pattern of the TM-d orbital splitting, which is the main factor to explain some basic properties of the complex. The major disadvantage of the LFT approach is that the number of adjustable parameters increases when the symmetry of the complex lowers.

Within the Angular Overlap Model (AOM),[11-13] a variant of LFT, the d orbital splitting is expressed in terms of weak covalent σ- and π-bonding interactions with ligand orbitals. The AOM gave LFT a chemically sound language allowing one to interpret the strength of the ligands in terms of σ and π (donation and back-donation) mechanisms instead of the more physically oriented crystal field language. This model describes the TM-ligand interaction under a basic assumption that the strength of a bond formed using *atomic orbitals* on two atoms is related to the magnitude of overlap of the two orbitals.

Although LFT is semi-empirical in nature, it provides a tremendous amount of insight into the electronic structure, spectroscopy, thermochemistry, stereochemistry, photochemistry and kinetics of transition metal complexes. The great achievement of LFT has been that with a minimum amount of empirical parameters a great variety of properties could be explained and even reproduced with good numerical accuracy. However, charge transfer transitions, super-hyperfine couplings and coupling of electronic and nuclear motions cannot be explained and more sophisticated quantum mechanical approaches are needed.

1.3. Beyond Ligand Field Theory

Ever since the description of the chemical bond in the H_2^+ molecule by Heitler and London,[14] two competing approaches have been developed within the realm of molecular quantum chemistry. After the initial success of Valence Bond (VB) theory in the 1930s and 1940s, Molecular Orbital (MO) theory took over in the second half of the twentieth century. In particular, the Hartree-Fock (HF) self-consistent field (SCF) implementation of MO theory proved to be extremely powerful[15-17] In fact, the HF theory became the undisputed standard *ab initio* method for molecules[18] upon which further improvements can be built. Despite the correct treatment of electronic exchange within HF theory, electron correlation is completely missing. This is easily shown for the H_2 molecule where the MO wave function is a mixture of four configurations when written in terms of atomic-like orbitals:

$$\Psi = \left|\sigma_g \overline{\sigma}_g\right| = \left|(a+b)\left(\overline{a}+\overline{b}\right)\right| = \left|a\overline{b}\right| + \left|b\overline{a}\right| + \left|a\overline{a}\right| + \left|b\overline{b}\right|$$

The uncorrelated nature of the two electrons is obviated by the fact that the ionic configurations with two electrons on the same atom have exactly the same weight as the neutral configurations with one electron on each side of the molecule. Hence, the position of electron 1 is not correlated with the position of electron 2, while it is obvious that electrons 1 and 2 prefer to be in opposite sides of the molecule at any moment. This complete lack of electron correlation in the HF wave function allows defining the correlation energy as the difference between the HF energy (in the complete basis set limit) and the *exact* energy, as introduced by Löwdin in 1955.[19] On the other hand, the simple VB wave function is based on the first two configurations only, yielding a fully correlated wave function. The optimal wave function will be somewhere in between these two extremes and, depending on the importance of electron correlation it will resemble more the HF or the VB description. In any case, the HF description of the electronic structure is usually a good starting point and electron correlation effects can be added by perturbation theory (typically with a Møller-Plesset[20] partition of the Hamiltonian), configuration interaction (CI) or coupled cluster (CC) methodologies.

The progressive treatment of the ligand atoms as point charges to a simple molecular orbital (MO) model is a step in the good direction. It does not provide a complete quantitative description of the ligand field effect, but it provides a way to rationalize the decrease of the central ion d electron repulsion and spin-orbit coupling parameters below the values known for the free ion, as well as phenomena related to the delocalization of electrons over both the central and the ligand atoms. The flexibility of molecular orbital-based methods allows improving the description in a step-by-step approach, in principle converging to a quantitative complete picture.

1.4. Extended Metal Atom Chains

In the past 30 years, multinuclear transition metal complexes have attracted much attention due to their diverse applications in nanoscale electronic devices.[21-25] Ligand-supported[26] linear metal complexes, also named Extended Metal Atom Chains (EMACs), are a family of one-dimensional polymetallic

compounds. They are linear strings of TM metal atoms surrounded by purposely-designed polydentate organic ligands, whose number of binding sites determines the nuclearity of the chain. The chain is normally capped by axial ligands, which may be halogen atoms ($L = Cl^-$, Br^-) or molecular anions such as BF_4^-,[27] NCS^-, CN^-, CH_3CN[28] and $N(CN)_2^-$.[29] Many systems belonging to this family have been synthesized and their properties have been characterized.[30-40] Over the last ten years, experimentalists have tried to synthesize EMACs with increasingly long metal backbones.[41-49] Longer molecular systems can be obtained either by designing equatorial ligands with a larger number of binding sites or by making connections between small metallic complexes. The main limitation of the first approach lies in the design, as well as the instability and insolubility problems associated to large ligands.[26] In order to extend the molecular wires by making connection between shorter metallic complexes the properties of axial ligands play a crucial role.[50] Peng's group achieved an 11-nickel molecular string, the current record in 2011.[51-52]

The simplest prototype of this class of atomic-sized metal chains, is the trimetallic complex, $M^{II}_3(dpa)_4X_2$ (dpa = di(2-pyridyl) amido), shown in Figure 1.1. These linear clusters have been synthesized with various metals of the first and second transition rows (M = Cu, Ni, Co, Rh, Ru, and Cr).[27,53-61] Among these complexes, tricobalt and trichromium complexes have attracted the largest attention because they can exhibit structures with either symmetric (delocalized) or unsymmetric (localized) metal-metal bonding, depending on the composition of the crystal and the nature of the axial ligands.[30,32,34,38,54,62-63] The symmetric form of Cr_3 has a significantly larger electrical conductivity[64] than other trimetal complexes as Ni_3 and Co_3. In general, the metal-metal bond length varies upon oxidation or reduction, opening the possibility that the complexes function as molecular switches. For instance, one-electron oxidation of $Ni_3(dpa)_4Cl_2$ leads to a remarkable shortening of the Ni-Ni distances, 0.15 Å, inducing a change from a localized to a delocalized electronic configuration for the ground state.[65-66]

Trinuclear heterometallic complexes are not uncommon and many have been recently synthesized, including symmetric derivatives such as CoPdCo,[67] CuMCu (M = Pd, Pt),[68] and asymmetric compounds like MMM´ (M = Cr, Mo,

W and M´= Fe, Zn)[69] or CuCuM (M = Pd, Pt)[70] or RuRuM (M = Cu, Ni) derivatives.[71]

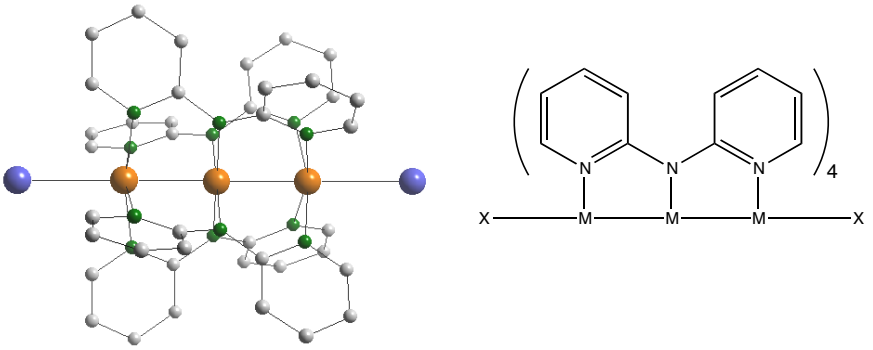

Figure 1.1. Ball-and-stick (left) and schematic 2D representations of the structure of $M_3(dpa)_4Cl_2$. Blue: chlorine; magenta: metals; green: nitrogen; gray: carbon. Hydrogen atoms have been omitted for clarity.

The already mentioned dipyridylamido anion is the most common ligand used to construct EMACs. It contains two pyridylic and one amido coordination sites as shown schematically in Figure 1.1. The central nitrogen is significantly more basic than the other two and its interaction with the metal is stronger. The two pyridine rings are twisted due to the steric hindrance between adjacent hydrogen atoms. Usually four dpa ligands wrapped around the metals hold the EMAC together. But other variants have also been synthesized. The trimetallic chains can also be cocooned by two interlocking heptadentate dianions derived from a chain of five pyridyl groups linked at the 2, or 2 and 6, positions by four amide nitrogen atoms (mpeptea, shown in Chart 1) instead of four tridentate dpa ligands.[31] Theses trimetallic EMACs differ from the former ones in that the axial positions are now part of the entire ligand. Their general formula is $[M_3L_2]^{2+}$ where L = mpeptea. Yet another class of trimetallic EMACs is formed by the $[M_3(BPAP)_4]^{2-}$ or $[M_3(Lpts)_4]^{2-}$ complexes, with BPAP = 2,6-bis(phenylamido)pyridine[72] and Lpts = N,N´-bis-(*p*-toluenesulfonyl)-

pyridyldiamide[73] (see Chart 1). In such cases, the terminal metal atoms feature low-spin configurations as a consequence of the square planar field induced by the more basic amido ends, preventing the acceptance of axial coordination by them. Introduction of one or more nitrogen-rich aromatic rings such as pyrazine to the dpa ligands significantly improves the reactivity of complex resulting to a new family of EMACs.[74]

One of the features that make EMACs an interesting object of study is that they represent a family of transition metal complexes in which neighbouring metal atoms are constrained to remain in a range of distances typically comprised between 2.25 and 2.6 Å. Such metal-metal close contacts are not so common in coordination chemistry and are determinant for the appearance of their appealing magnetic and conducting properties.[34,75-81]

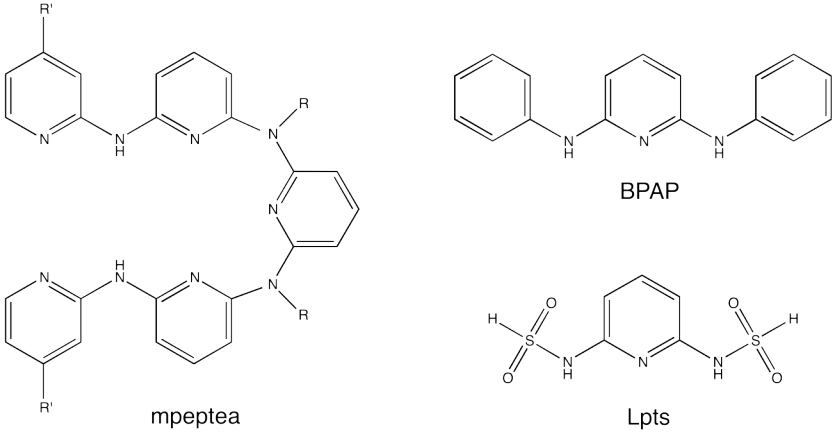

Chart 1

Before the beginning of the present work, theoretical studies on EMAC systems were exclusively performed with DFT schemes, mainly due to their relatively large size.[82-84] The goal of most of these studies was the understanding and interpretation of magnetic and conducting properties of EMACs through the calculation and analysis of their electronic structure. This has been done on the basis of MO diagrams obtained by quantum chemistry methods. Figure 1.2

shows the MOs generated by linear combinations of d atomic orbitals in trimetallic $M_3(dpa)_4X_2$ complexes with D_4 symmetry. Their energy sequence schematized in Figure 1.2 is a result of ligand fields on the metal sites experienced from axial positions and equatorial coordinations.[65,82-83] The nature of the electronic ground state and the associated structural features depend on the distribution of metallic electrons over these fifteen MOs with predominant metal character.

Reproducing and predicting magnetic exchange parameters in existing and hypothetical EMAC systems have been the most important task of theoreticians.[67,85-89] The magnetic interactions in EMACs are, in general, antiferromagnetic (AF) and they usually arise from the well-known superexchange mechanism,[90] which occurs via the bridging ligands and the diamagnetic metal centers (if exist) in the middle of the chain. The latter one includes the metal-metal interaction that contributes to the AF coupling.[90] Another interesting issue in theoretical study of EMAC complexes has been the electron delocalization over the metal-metal backbone[91-92] which makes them potentially useful as electrical conductors in nanocircuits.

A controversy that lasted for years between the groups of Prof. Peng (Taiwan) and Prof. Cotton (Texas) about the existence of symmetric and unsymmetric structures for the $Co_3(dpa)_4Cl_2$ complex was resolved through a quantum chemical study by Pantazis and McGrady, who showed that the two structural forms result from different electronic configurations.[62]

DFT geometry optimizations have always been the preliminary step to perform electronic structure calculations. Different basis sets and density functionals have been examined to reproduce the experimental geometries. Some methods, techniques and definitions that have been used in theoretical study of EMACs will be explained in the next chapter.

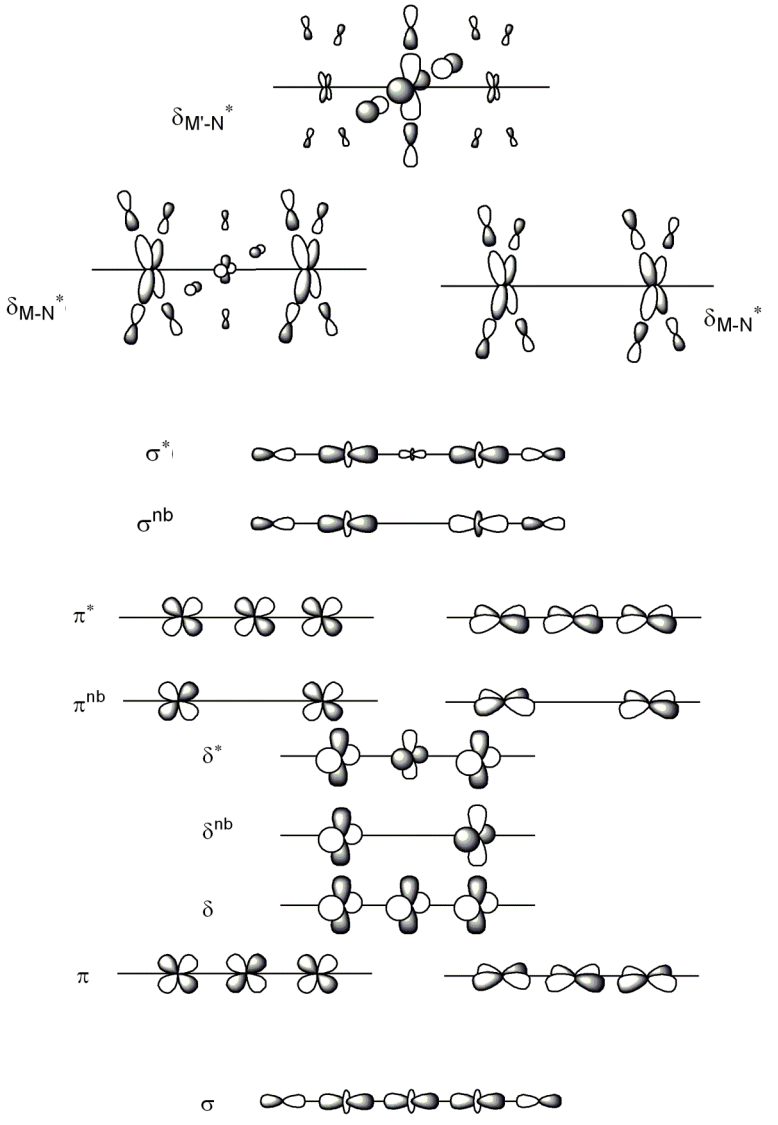

Figure 1.2. Schematic view of the sequence of metallic molecular orbitals in trimetallic EMAC complexes.

1.5. Objectives

As discussed in the previous section, EMACs have received much attention due to their possible applications as molecular magnets,[93] which may be used as magnetic memories or building blocks in quantum devices[94] and also as promising candidates for nanowires[21-22] due to the metal–metal interactions. Experimental studies are often not sufficient to entirely determine and understand the physical properties of these special TM clusters. The spatial distribution of the unpaired electrons in the ground state as well as in relevant states of higher energy, and the energies which are required to switch from one spin state to another, are notoriously difficult to fully determine from experimental studies. Quantum chemical methods are a valuable source of additional information. The combination of experimental and theoretical studies can potentially provide a complete and reliable description of the physical properties of TM complexes. However, the investigation of TM clusters by means of quantum chemistry methods is non-trivial. Because of the presence of unpaired electrons, such systems have to be accurately described by open-shell wave functions, requiring a multi-determinantal description in many cases.[95] TM complexes typically involve significant near-degeneracy effects ('static correlation') that are difficult to treat with single-determinantal methods. Thus, multi-determinantal approaches are often necessary to achieve quantitatively accurate results. Nevertheless, multi-determinantal methods are complicated, time-consuming and the size of TM complexes often restricts these calculations to single-determinant methods. However, efficient multi-determinantal approaches combined with the enormous increase in available computer power make plausible the extension of the *ab initio* treatment on TM complexes of significant size to low-cost personal computers. This dissertation aims to advance in the application of both DFT- and wave function-based methods to the study of polynuclear TM complexes. Moreover, as the accurate description of the electronic structure of polynuclear TM complexes is much more challenging than TM mono- and di-nuclear clusters,[96-100] the goal of this study is also to

establish a reliable strategy for the *ab initio* treatments on polynuclear TM complexes.

A comprehensive discussion of the magnetic exchange parameter of unpaired electrons in a series of trinuclear EMACs is given in chapter three. We compare wave function-based methods, complete active space self-consistent field (CASSCF) and CAS second-order perturbation theory (CASPT2), to earlier DFT-based treatments.

Previous DFT-based studies on the trimetallic Ni EMAC[91] showed a marked difference between calculated and experimental magnetic coupling strength. In chapter four we will explore the origin of this discrepancy. We will work out the hypothesis that this difference can (at least partially) be ascribed to the deviations from the Heisenberg behaviour. Due to the direct metal–metal contacts, these deviations are possibly larger than in systems in which magnetic centers are bridged with non-metallic ligands.[101] The origin of the difference between DFT results and experiments will also be explored in terms of the geometry and the choice of the density functional. Systems with stronger magnetic interactions deviate more from the Heisenberg behaviour. Hence, it is expected that the deviations to the ordinary Heisenberg behaviour increase when 3d TM ions are replaced by TM ions of the second or third period. We will address the issue of the usefulness of fitting the magnetic susceptibility in such systems with the standard Heisenberg Hamiltonian. We are also interested in the determination of the relative weights of the two types of magnetic interactions, σ- and δ- like, in Ni and other complexes where each magnetic site carries two unpaired electrons.

Among trimetallic EMACs, we have also studied some heterometallic MM'M derivatives as potential candidates for having closed-shell ground states. Most EMACs known to date, as those studied in chapter three, are magnetic systems with localized spin momenta and hence are not suitable as conducting systems. Conductivity along a metal chain is often related to mobile electrons in orbitals delocalized along the chain. In chapter five we investigate the hypothesis that larger TM ions of the second and third series destabilize these highly localized orbitals due to increasing antibonding metal-ligand interactions,

and at the same time improve the overlap of the σ orbitals. This would lead to some realistic candidates for conduction.

The last study focuses on a similar family of compounds, namely the one-dimensional MMX chains, $[Ni_2(dta)_4I]_\infty$ and $[Pt_2(dta)_4I]_\infty$ (dta = $CH_3CS_2^-$). These compounds have been previously characterized and studied, notably the larger conductivity observed for the $[Pt_2(dta)_4I]_\infty$ chain in comparison to the $[Ni_2(dta)_4I]_\infty$ chain, which at first sight may be explained simply by the larger size of the Pt ions. In chapter six, their properties are explained through the extraction of electronic structure parameters using multi-determinantal configuration interaction methods. We explore the correlation of these different electrical conductivities with the geometry, the hopping integrals and the on-site Coulomb repulsion. First, preliminary data from periodic DFT calculations performed on both chains is obtained. Then, the extraction of electronic structure parameters from *ab initio* calculations, through the Effective Hamiltonian approach, is presented. The main goal is to determine the charge-ordering states for both chains, a matter of debate in the case of Ni compound, and to relate these results with the measured electrical conductivities. In chapter two, the computational methods and theories applied throughout this study will be briefly outlined.

References

[1] P. Rodgers, Nature Nanotechnology, 2006.

[2] J. J. R. Frausto de Silva, R. J. P. Williams, *The Biological Chemistry of the Elements*, Clarendon Press, Oxford, 2001.

[3] S. J. Lippard, J. M. Berg, *Principles of Bioinorganic Chemistry*, Univ. Science Books, Mill Valley, CA, 1994.

[4] W. Kaim, B. Schwederski, *Bioinorganic Chemistry: Inorganic Elements in the Chemistry of Life*, Second edn., John Wiley &Sons, New York, 2007.

[5] C. J. Ballhausen, *Introduction to Ligand Field Theory*, McGraw-Hill, New York, 1962.

[6] C. J. Ballhausen, H. B. Gray, *Molecular Orbital Theory*, Benjamin, New York, 1964.

[7] C. K. Jorgensen, *Adv. Chem. Phys*. 5 (1963) 33.

[8] C. K. Jorgensen, *Struct. Bond*. 1 (1966) 3.

[9] C. K. Jorgensen, *Struct. Bond*. 6 (1969) 94.

[10] H. Bethe, *Ann. Phys*. 3 (1929) 133.

[11] C. E. Schaffer, C. K. Jorgensen, *Mol. Phys*. 9 (1965) 401.

[12] H. H. Schmidtke, *Theor. Chim. Acta* 20 (1971) 92.

[13] L. G. Vanquickenborne, A. Ceulemans, *Coord. Chem. Rev*. 48 (1983) 157.

[14] W. Heitler, F. London, *Z. Physik* 44 (1927) 455 .

[15] A. Szabo, N. S. Ostlund, *Modern Quantum Chemistry: Introduction to Advanced Electronic Structure Theory*, McGraw-Hill, New York, 1989,

[16] C. C. J. Roothaan, *Rev. Mod. Phys.* 23 (1951) 6989.

[17] C. C. J. Roothaan, Self-consistent field theory for open shells of electronic systems, *Rev. Mod. Phys*. 32 (1960) 179185.

[18] W. J. Hehre, L. Radom, P. v. R. Schleyer, J. A. Pople, *Ab Initio Molecular Orbital Theory*, Wiley, New York, 1986.

[19] P. O. Löwdin, *Phys. Rev.* 97 (1955) 1474.

[20] C. Møller, M. S. Plesset, *Phys. Rev*. 46 (1934) 618.

[21] J. S. Miller, *Extended Linear Chain Compounds*; Plenum: New York, 1982, Vol. 1-3.

[22] P. Day, H. J. Keller, *Low-Dimensional Cooperative Phenomena*; Plenum: New York, 1974, p. 191.

[23] R. J. H. Clark, D. E. Brown, *Mixed Valence Compounds*; Reidel, Dordrecht, 1982, p.271.

[24] T. Murahashi, Y. Higuchi, T. Katoh, H. Kurosawa, *J. Am. Chem. Soc*. 124 (2002) 14288.

[25] T. Ruffer, M. Ohashi, A. Shima, H. Mizomoto, Y. Kaneda, K. Mashima, *J. Am. Chem. Soc.* 126 (2004) 12244.

[26] J. K. Bera, K. R. Dunbar, *Angew. Chem. Int. Ed*. 41 (2002) 4453.

[27] F. A. Cotton, L. M. Daniels, G. T. Jordan IV, C. A. Murillo, *J. Am. Chem. Soc*. 119 (1997) 10377.

[28] R. Clérac, F. A. Cotton, K. R. Dunbar, T. Lu, C. A. Murillo, X. Wang, *Inorg. Chem*. 39 (2000) 3065.

[29] R. Clérac, F. A. Cotton, S. P. Jeffery, C. A. Murillo, X. Wang, *Inorg. Chem*. 40 (2001) 1265.

[30] J. F. Berry, F. A. Cotton, T. Lu, C. A. Murillo, B. K. Roberts, X. Wang, *J. Am. Chem. Soc*. 126 (2004) 7082.

[31] F. A. Cotton, H. Chao, C. A. Murillo, Q. Wang, *Dalton Trans.* (2006) 5416.

[32] F. A. Cotton, L. M. Daniels, C. A. Murillo, I. Pascual, *J. Am. Chem. Soc*. 119 (1997) 10233.

[33] F. A. Cotton, L. M. Daniels, C. A. Murillo, I. Pascual, *Inorg. Chem. Commun*. 1 (1998) 1.

[34] C. J. Hsiao, S. H. Lai, I. C. Chen, W. Z. Wang, S. M. Peng, *J. Phys. Chem. A* 112 (2008) 13528.

[35] S. H. Lai, C. J. Hsiao, J. W. Ling, W. Z. Wang, S. M. Peng, I. C. Chen, *Chem. Phys. Lett*. 456 (2008) 181.

[36] G. C. Huang, I. P. C. Liu, J. H. Kuo, Y. L. Huang, C. Y. Yeh, G. H. Lee, S. M. Peng, *Dalton Trans*. (2009) 2623.

[37] S. M. Peng, C. C. Wang, Y. L. Jang, Y. H. Chen, F. Y. Li, C. Y. Mou, M. K. Leung, *J. Magn. Magn, Mater*. 209 (2000) 80.

[38] R. Clérac, F. A. Cotton, K. R. Dunbar, T. Lu, C. A. Murillo, X. Wang, *J. Am. Chem. Soc*. 122 (2000) 2272.

[39] J. F. Berry, F. A. Cotton, L. Peng, C. A. Murillo, *Inorg. Chem*. 42 (2003) 377.

[40] R. Clérac, F. A. Cotton, K. R. Dunbar, C. A. Murillo, I. Pascual, X. Wang, *Inorg. Chem*. 38 (1999) 2655.

[41] S. A. Hua, G. C. Huang, I. P. C. Liu, J. H. Kuo, C. H. Jiang, C. L. Chiu, C. Y. Yeh, G. H. Lee, S. M. Peng, *Chem. Commun*. 46 (2010) 5018.

[42] C. Yin, G. C. Huang, C. K. Kuo, M. D. Fu, H. C. Lu, J. H. Ke, K. N. Shih, Y. L. Huang, G. H. Lee, C. Y. Yeh, C. H. Chen, S. M. Peng, *J. Am. Chem. Soc*. 130 (2008) 10090.

[43] J. F. Berry, F. A. Cotton, C. S. Fewox, T. Lu, C. A. Murillo, X. Wang, *Dalton Trans*. (2004) 2297.

[44] I. P. C. Liu, M. Bénard, H. Hasanov, I. W. P. Chen, W. H. Tseng, M. D. Fu, M. M. Rohmer, C. H. Chen, G. H. Lee, S. M. Peng, *Chem. Eur. J*. 13 (2007) 8667.

[45] I. P. C. Liu, W. Z. Wang, S. M. Peng, *Chem. Commun*. (2009) 4323.

[46] C. Y. Yeh, C. H. Chou, K. C. Pan, C. C. Wang, G. H. Lee, Y. O. Su, S. M. Peng, *J. Chem. Soc. Dalton Trans*. (2002), 2670.

[47] C. Y. Yeh, Y. L. Chiang, G. H. Lee, S. M. Peng, *Inorg. Chem*. 41 (2002) 4096.

[48] C. C. Wang, W. C. Lo, C. C. Chou, G. H. Lee, J. M. Chen, S. M. Peng, *Inorg. Chem*. 37 (1998) 4059.

[49] S. Y. Lai, T. W. Lin, Y. H. Chen, C. C. Wang, G. H. Lee, M. H. Yang, M. K. Leung, S. M. Peng, *J. Am. Chem. Soc*. 21 (1999) 250.

[50] J. F. Berry, F. A. Cotton, C. A. Murillo, *Dalton Trans*. (2003) 3015.

[51] J. H. Kuo, T. B. Tsao, G. H. Lee, H. W. Lee, C. Y. Yeh, S. M. Peng, *Eur. J. Inorg. Chem*. (2011) 2025.

[52] R. H. Ismayilov, W. Z. Wang, G. H. Lee, C. Y. Yeh, S. A. Hua, Y. Song, M. M. Rohmer, M. Bénard, S. M. Peng, *Angew. Chem. Int. Ed*. 50 (2011) 2045.

[53] G. J. Pyrka, M. El-Mekki, A. A. Pinkerton, *J. Chem. Soc., Chem. Commun*. (1991), 84.

[54] R. Clérac, F. A. Cotton, L. M. Daniels, K. R. Dunbar, C. A. Murillo, I. Pascual, *Inorg. Chem*. 39 (2000) 748.

[55] F. A. Cotton, L. M. Daniels, G. T. Jordan IV, *Chem. Commun*. (1997) 421.

[56] J. T. Sheu, C. C. Lin, I. Chao, C. C. Wang, S. M. Peng, *Chem. Commun*. (1996) 315.

[57] L. P. Wu, P. Field, T. Morrissey, C. Murphy, P. Nagle, B. J. Hathaway, C. Simmons, P. Thornton, *J. Chem. Soc. Dalton Trans.* (1990) 3835.

[58] S. Aduldecha, B. J. Hathaway, *J. Chem. Soc., Dalton Trans*. (1991) 993.

[59] E. C. Yang, M. C. Cheng, M. S. Tsai, S. M. Peng, *J. Chem. Soc., Chem. Commun*. (1994) 2377.

[60] F. A. Cotton, C. A. Murillo, X. Wang, *J. Chem. Soc., Dalton Trans.* (1999) 3327.

[61] K. N. Shih, M. J. Huang, H. C. Lu, M. D. Fu, C. K. Kuo, G. C. Huang, G. H. Lee, C. H. Chen, S. M. Peng, *Chem. Commun*. 46 (2010) 1338.

[62] D. A. Pantazis, J. E. McGrady, *J. Am. Chem. Soc*. 128 (2006) 4128.

[63] R. Clérac, F. A. Cotton, L. M. Daniels, K. R. Dunbar, C. A. Murillo, I. Pascual, *Inorg. Chem*. 39 (2000) 752.

[64] S. Y. Lin, I. W. P. Chen, C. H. Chen, M. H. Hsieh, C. Y. Yeh, T. W. Lin, Y. H. Chen, S. M. Peng, *J. Phys. Chem. B* 108 (2004) 959.

[65] J. F. Berry, F. A. Cotton, L. M. Daniels, C. A. Murillo, X. Wang, *Inorg. Chem*. 42 (2003) 2418.

[66] J. F. Berry, F. A. Cotton, T. Lu, C. A. Murillo, X. Wang, *Inorg. Chem*. 42 (2003) 3595.

[67] M. M. Rohmer, I. P. C. Liu, J. C. Lin, M. J. Chiu, C. H. lee, G. H. Lee, M. Bénard, X. López, S. M. Peng, *Angew. Chem. Int. Ed*. 46 (2007) 3533.

[68] I. P. C. Liu, G. H. Lee, S. M. Peng, M. Bénard, M. M. Rohmer, *Inorg. Chem*. 46 (2007) 9602.

[69] M. Nippe, E. Bill, J. F. Berry, *Inorg. Chem*. 50 (2011) 7650.

[70] I. P. C. Liu, C. H. Chen, C. F. Chen, G. H. Lee, S. M. Peng, *Chem. Commun*. (2009) 577.

[71] G. C. Huang, M. Bénard, M. M. Rohmer, L. A. Li, M. J. Chiu, C. Y. Yeh, G. H. Lee, S. M. Peng, *Eur. J. Inorg. Chem*. (2008) 1767.

[72] F. A. Cotton, L. M. Daniels, P. Lei, C. A. Murillo, X. Wang, *Inorg. Chem*. 40 (2001) 2778.

[73] M. Y. Huang, C. Y. Yeh, G. S. Lee, S. M. Peng, *Dalton Trans*. (2006) 5683.

[74] R. H. Ismayilov, W. Z. Wang, G. H. Lee, R. R. Wang, I. P. C. Liu, C. Y. Yeh, S. M. Peng, *Dalton Trans*. (2007) 2898.

[75] D. H. Chae, J. F. Berry, S. Jung, F. A. Cotton, C. A. Murillo, Z. Yao, *Nano Lett*. 6 (2006) 165.

[76] I. W. P. Chen, M. D. Fu, W. H. Tseng, J. Y. Yu, S. H. Wu, C. J. Ku, C. H. Chen, S. M. Peng, *Angew. Chem. Int. Ed*. 45 (2006) 5814.

[77] S. Y. Lin, I. W. Peter Chen, C. h. Chen, M. H. Hsieh, C. Y. Yeh, T. W. Lin, Y. H. Chen, S. M. Peng, *J. Phys. Chem. B* 108 (2004) 959.

[78] J. F. Berry, F. A. Cotton, C. A. Murillo, *Organometallics* 23 (2004) 2503.

[79] K. N. Shih, M. J. Huang, H. C. Lu, M. D. Fu, C. K. Kuo, G. C. Huang, G. H. Lee, C. h. Chen, S. M. Peng, *Chem. Commun*. 46 (2010**)** 1338.

[80] J. F. Berry, F. A. Cotton, L. M. Daniels, C. A. Murillo, *J. Am. Chem. Soc*. 124 (2002**)** 3212.

[81] J. F. Berry, F. A. Cotton, C. A. Murillo, B. K. Roberts, *Inorg. Chem*. 43 (2004) 2277.

[82] M. M. Rohmer, M. Bénard, *J. Am. Chem. Soc*. 120 (1998) 9372.

[83] M. M. Rohmer, A. Strich, M. Bénard, J. P. Malrieu, *J. Am. Chem. Soc*. 123 (2001) 9126.

[84] M. M. Rohmer, M. Bénard, *Chem. Soc. Rev*. 30 (2001) 340.

[85] I. P. C. Liu, G. H. Lee, S. M. Peng, M. Bénard, M. M. Rohmer, *Inorg. Chem*. 46 (2007) 9602.

[86] X. López, M. Bénard, M. M. Rohmer, *Inorg. Chem*. 46 (2007) 5.

[87] X. López, M. Bénard, M. M. Rohmer, *J. Mol. Struct. THEOCHEM* 777 (2006) 53.

[88] W. V. den Heuvel, L. F. Chibotaru, *Inorg. Chem*. 48 (2009) 7557.

[89] X. López, M. M. Rohmer, M. Bénard, *J. Mol. Struct*. 890 (2008) 18.

[90] M. Bénard, J. F. Berry, F. A. Cotton, C. Gaudin, X. López, C. A. Murillo, M. M. Rohmer, *Inorg. Chem*. 45 (2006) 3932.

[91] P. Kiehl, M. M. Rohmer, M. Bénard, *Inorg. Chem*. 43 (2004) 3151.

[92] V. P. Georgiev, J. E. McGrady, *Inorg. Chem*. 49 (2010) 5591.

[93] O. Kahn, *Molecular Magnetism*, Wiley VCH, New York, 1993.

[94] S. J. Blundell, F. L. Pratt, *J. Phys.: Condens. Matter* 16 (2004) R771.

[95] C. J. Calzado, J. Cabrero, J. P. Malrieu, R. Caballol, *J. Chem. Phys*. 116 (2002) 3985.

[96] T. Ayed, N. Guihéry, B. Tangour, J. C. Barthelat. *Theor. Chem. Acc*. 116 (2006) 497.

[97] C. J. Calzado, C. Angeli, D. Taratiel, R. Caballol, J. P. Malrieu. *J. Chem. Phys*. 131 (2009) 044327.

[98] C. J. Calzado, J. Cabrero, J. P. Malrieu, R. Caballol. *J. Chem. Phys*. 116 (2002) 3985.

[99] J. Zapata-Rivera, R. Caballol, C. J. Calzado. *J. Comput. Chem*. 32 (2011) 1144.

[100] J. Miralles, J. P. Daudey, R. Caballol. *Chem. Phys. Lett*. 198 (1992) 555.

[101] R. Bastardis, N. Guihéry, C. de Graaf. *J. Chem. Phys*. 129 (2008) 104102.

Chapter 2

Theoretical Background

2.1. Effective Hamiltonian Theory

The theory of effective Hamiltonians is a method for determining the interactions between particles (electrons) by mapping the complete set of interactions onto the essential part of problem. These efficient and simplified interactions, represented by the effective Hamiltonian, facilitate physical interpretations and it is also a valuable technical tool for the treatment of large systems, since *ab initio* quantum chemistry programs cannot, at present, afford the treatment of large polyatomic systems despite the great progress in computational facilities. This effort for simplification of the information has even been used for highly accurate *ab initio* treatment of small systems.

The term 'effective Hamiltonian' is used for Hamiltonians obtained by projections of some exact wave functions onto a finite model space. The concept

of *model space* plays a central role in effective Hamiltonian theory. It is a finite *M*-dimensional subspace *S* of the entire Hilbert space and it is chosen in such a way that it describes the most essential physics of the system. The term 'model Hamiltonian' is more general and it is used when some simplified form of an approximate Hamiltonian has been guessed from a preliminary physical analysis. In contrast with effective Hamiltonians, which can be obtained by means of well-defined mathematical procedures, model Hamiltonians are generally parameterized from experiment. Modeling involves a reduction or a simplification of the problem. This reduction may concern:

1. The basis set of atomic orbitals (AOs) in which the problem is supposed to be treated. All *ab initio* calculations use projected Hamiltonians since they work in finite basis sets.
2. The number of *N*-electron configurations (or determinants) in which one treats the electronic structure problem. Instead of handling with a huge number of configurations which span the Hamiltonian in a finite basis set (full configuration interaction), one may explain the behavior of the system in terms of a few leading configurations only, without spoiling the quality of the information. A remarkable example of this strategy is the Heisenberg Hamiltonian, which accurately describes the energies involved in the coupling of localized spin angular moments in paramagnetic systems, despite the fact that the model space contains neutral determinants only (spin degree of freedom, no charge degree of freedom).

2.2. The Bloch and des Cloizeaux Effective Hamiltonian

The basic idea of the Bloch effective Hamiltonian[1] is to pass from the exact Hamiltonian, *H*, to an effective Hamiltonian whose eigenvalues exactly coincide with a subset of the eigenvalues of *H*. In this approach, all the information of the other eigenvalues of *H* is lost. Suppose we know a large number of solutions of the exact Hamiltonian:

$$\hat{H}\left|\Psi_k\right\rangle = E_k \left|\Psi_k\right\rangle$$

Consider an *M*-dimensional subspace *S* spanned by *M* vectors Φ_m. The projection operator associated with *S* is:

$$\hat{P}_S = \sum_{m \in S} |\Phi_m\rangle\langle\Phi_m|$$

We define an effective Hamiltonian in *S* such that its *M* eigenvalues are exact and its eigenvectors are projections of the corresponding exact (in practice, the *ab initio*) eigenvectors in the model space *S*.

$$\hat{H}_{eff}^{Bloch} \left| \hat{P}_S \Psi_k \right\rangle = E_k \left| \hat{P}_S \Psi_k \right\rangle \qquad \text{or} \qquad \hat{H}_{eff}^{Bloch} \tilde{\Phi}_k = E_k \tilde{\Phi}_k$$

By projection techniques, the *ab initio* information is mapped onto a smaller model space that contains all the essential physics of interest. The Bloch effective Hamiltonian is non-Hermitian since its solutions are the projections of the exact solutions onto the model space. The hermitic variant of the Bloch effective Hamiltonian can be obtained by $S^{-1/2}$ orthonormalization of the projected eigenvectors leading to the des Cloizeaux effective Hamiltonian:[2]

$$H_{eff}^{desCloizeaux} = \sum_{k=1}^{M} |\Phi'_k\rangle E_k \langle\Phi'_k| \qquad \text{with} \qquad \Phi'_k = S^{-1/2} \tilde{\Phi}_k$$

Yet another orthogonalization procedure is the Gram-Schmidt method. If one is mainly interested in the lowest projected wave functions, it may be preferable to leave them unchanged and orthogonalize the highest projected wave functions with respect to the lowest ones. In this way, the information of the highest projected wave functions is sacrificed and only their energies are used in the construction of the effective Hamiltonian. This procedure can be advantageous when the higher states of the *S* space appear placed among other states not belonging to it. For these high-lying (quasi)degenerate states, linear combinations can be formed with other states giving rise to low projections onto the model space and wave functions that partially loose their significance.

2.3. Quasi-degenerate Perturbation Theory

Apart from providing a recipe to map complex, nearly exact wave functions on a smaller model space, the effective Hamiltonian can also be used to obtain exact energies and the projected wave functions starting from an approximate description in a small model space. When the eigenenergies and the eigenvectors of the exact Hamiltonian are not known, it is possible to build an effective Hamiltonian, spanned in a given model space *S*, using the quasi-degenerate perturbation theory (QDPT).[1-4] For an increasing order of perturbation, the eigenvalues and eigenvectors of the effective Hamiltonian tend to the exact energies and exact projections on *S* of the exact eigenvectors, respectively. The second-order expansion of the matrix elements of H_{eff} are given by

$$\langle \Phi_I | \hat{H}_{eff} | \Phi_J \rangle = \langle \Phi_I | \hat{H}_0 | \Phi_J \rangle + \sum_{\Phi_\alpha \notin S_0} \frac{\langle \Phi_I | \hat{V} | \Phi_\alpha \rangle \langle \Phi_\alpha | \hat{V} | \Phi_J \rangle}{E_J^{(0)} - E_\alpha^{(0)}}$$

where Φ_I and Φ_J belong to the model space. *V* is the perturbation operator, and H_0 a convenient choice of the zero-order Hamiltonian.[5-7] QDPT first accounts for the effect of the external determinants and then diagonalizes the resulting effective Hamiltonian of the model space *S*, in contrast to other multiconfigurational perturbation schemes (such as CASPT2 or NEVPT2), for which the Hamiltonian is first diagonalized within the model space *S* and then the effect of the external determinants is included for each state independently.

The QDPT expressions become rather complicated after 2nd order and not very practical to get really precise energies and vectors.[8] Nevertheless, the QDPT is an essential tool for analysis when starting from a simple model Hamiltonian.

2.4. Model Hamiltonians

Heisenberg Hamiltonian. The link between theory and experiments for magnetic systems with localized spin moments is often achieved via a vector coupling model such as the Heisenberg model, where the energies of the different spin states are given as the expectation values of a phenomenological Hamiltonian,[9-11]

$$\hat{H}^{H} = -\sum_{i<j} J_{ij}\,\hat{S}_i \cdot \hat{S}_j \qquad (1)$$

For a system with many spin sites, this Hamiltonian is written as a sum of pair-wise exchange interactions between adjacent spin sites, where S_i and S_j are the spin operators at sites i and j, respectively, and J_{ij} is the spin exchange parameter.

Magnetic susceptibility, neutron inelastic scattering or Raman scattering data are often analyzed on magnetic systems in terms of the Heisenberg Hamiltonian, the spin exchange parameter playing the role of a numerical fitting parameter needed to reproduce the experimental data. In many cases, the spin exchange parameters can be univocally derived from experiments but, sometimes, it is necessary to carry out appropriate electronic structure calculations to clarify the magnetic structure and to determine the size of the interactions. The successful description of such a delicate physical property lies in the correct mapping between the Heisenberg spin eigenstates and the suitable *ab initio* electronic states.

In the preceding section it has been recalled that an effective Hamiltonian projects a part of the physics of a system onto a low-dimensional model space. For those systems in which the physics can be reduced to a set of sites in which each site carries one unpaired electron only in a well-defined and localized magnetic orbital, the model space and the status of the Heisenberg Hamiltonian is rather clear. The lowest-energy eigenstates are given by linear combinations of all the Slater determinants with common closed-shell core orbitals and with all magnetic orbitals singly occupied. The spatial part of all these determinants is the same and they only differ by the spin distribution. The model space, in such a case, is spanned by the neutral valence bond (VB) determinants since they have the common feature of keeping one electron per site. The Heisenberg Hamiltonian acts as a spin only effective Hamiltonian for this simple model space.

In a system with two magnetic sites and two electrons, the Heisenberg Hamiltonian is simplified to

$$\hat{H}^{H} = -J\,\hat{S}_1 \cdot \hat{S}_2 \tag{2}$$

Knowing that

$$\hat{S}_1 = \hat{S}_{x1} + \hat{S}_{y1} + \hat{S}_{z1} \quad \text{and} \quad \hat{S}_2 = \hat{S}_{x2} + \hat{S}_{y2} + \hat{S}_{z2}$$

the inner product of two spin moments can be written as

$$\hat{S}_1 \cdot \hat{S}_2 = \hat{S}_{x1}\,\hat{S}_{x2} + \hat{S}_{y1}\,\hat{S}_{y2} + \hat{S}_{z1}\,\hat{S}_{z2}$$

$\hat{S}_x$ and $\hat{S}_y$ are defined in terms of spin raising and lowering operators as

$$\hat{S}_x = \frac{1}{2}(\hat{S}^{+} + \hat{S}^{-}) \qquad \text{and} \qquad \hat{S}_y = \frac{1}{2i}(\hat{S}^{+} - \hat{S}^{-})$$

then,

$$\hat{S}_{x1}\,\hat{S}_{x2} = \frac{1}{4}(\hat{S}_1^{+}\,\hat{S}_2^{+} + \hat{S}_1^{+}\,\hat{S}_2^{-} + \hat{S}_1^{-}\,\hat{S}_2^{+} + \hat{S}_1^{-}\,\hat{S}_2^{-})$$

$$\hat{S}_{y1}\,\hat{S}_{y2} = -\frac{1}{4}(\hat{S}_1^{+}\,\hat{S}_2^{+} - \hat{S}_1^{+}\,\hat{S}_2^{-} - \hat{S}_1^{-}\,\hat{S}_2^{+} + \hat{S}_1^{-}\,\hat{S}_2^{-})$$

$$\hat{S}_{x1}\,\hat{S}_{x2} + \hat{S}_{y1}\,\hat{S}_{y2} = \frac{1}{2}(\hat{S}_1^{+}\,\hat{S}_2^{-} + \hat{S}_1^{-}\,\hat{S}_2^{+})$$

therefore,

$$\hat{S}_1 \cdot \hat{S}_2 = \frac{1}{2}(\hat{S}_1^{+}\,\hat{S}_2^{-} + \hat{S}_1^{-}\,\hat{S}_2^{+}) + \hat{S}_{z1}\,\hat{S}_{z2} \tag{3}$$

The matrix representation of the Heisenberg Hamiltonian in the model space containing $|\alpha\beta\rangle$ and $|\beta\alpha\rangle$ determinants is:

	$\lvert\alpha\beta\rangle$	$\lvert\beta\alpha\rangle$
$\langle\alpha\beta\rvert$	$\frac{1}{4}J$	$-\frac{1}{2}J$
$\langle\beta\alpha\rvert$	$-\frac{1}{2}J$	$\frac{1}{4}J$

This model space can be represented also in terms of $|a\,\bar{b}\rangle$ and $|\bar{a}\,b\rangle$ determinants.

The diagonal matrix elements are calculated as follows:

$$\langle\alpha\beta|\hat{H}^H|\alpha\beta\rangle = -J\langle\alpha\beta|\hat{S}_1\cdot\hat{S}_2|\alpha\beta\rangle =$$

$$-J\langle\alpha\beta|\left[\frac{1}{2}(\hat{S}_1^+\hat{S}_2^- + \hat{S}_1^-\hat{S}_2^+) + \hat{S}_{z1}\hat{S}_{z2}\right]|\alpha\beta\rangle =$$

$$-J\langle\alpha\beta|\left[\frac{1}{2}\times 0 + \frac{1}{2}|\beta\alpha\rangle - \frac{1}{4}|\alpha\beta\rangle\right] = \frac{1}{4}J$$

and the off-diagonal terms:

$$\langle\alpha\beta|\hat{H}^H|\beta\alpha\rangle = -J\langle\alpha\beta|\hat{S}_1\cdot\hat{S}_2|\beta\alpha\rangle =$$

$$-J\langle\alpha\beta|\left[\frac{1}{2}(\hat{S}_1^+\hat{S}_2^- + \hat{S}_1^-\hat{S}_2^+) + \hat{S}_{z1}\hat{S}_{z2}\right]|\beta\alpha\rangle =$$

$$-J\langle\alpha\beta|\left[\frac{1}{2}|\alpha\beta\rangle + \frac{1}{2}\times 0 - \frac{1}{4}|\beta\alpha\rangle\right] = -\frac{1}{2}J$$

The eigenstates obtained after diagonalization of the Heisenberg Hamiltonian are triplet and singlet states:

$$\Psi^T = \frac{1}{\sqrt{2}}(|\alpha\beta\rangle + |\beta\alpha\rangle) \quad \text{and} \quad \Psi^S = \frac{1}{\sqrt{2}}(|\alpha\beta\rangle - |\beta\alpha\rangle)$$

Including the spatial part, they can also be represented as

$$\Psi^T = \frac{1}{\sqrt{2}}\left(|a\,\bar{b}\rangle + |\bar{a}\,b\rangle\right) \quad \text{or} \quad \Psi^T = \frac{1}{\sqrt{2}}\left(|a\,\bar{b}\rangle - |b\,\bar{a}\rangle\right)$$

$$\Psi^S = \frac{1}{\sqrt{2}}\left(|a\,\bar{b}\rangle - |\bar{a}\,b\rangle\right) \quad \text{or} \quad \Psi^S = \frac{1}{\sqrt{2}}\left(|a\,\bar{b}\rangle + |b\,\bar{a}\rangle\right)$$

The energy of the triplet state is obtained as follows:

$$\hat{H}^H \Psi^T = -J\,\hat{S}_1 \cdot \hat{S}_2 \Psi^T$$

$$= -J\left[\frac{1}{2}(\hat{S}_1^+ \hat{S}_2^- + \hat{S}_1^- \hat{S}_2^+) + \hat{S}_{z1}\hat{S}_{z2}\right]\frac{1}{\sqrt{2}}(|\alpha\beta\rangle + |\beta\alpha\rangle)$$

$$= -J\frac{1}{\sqrt{2}}\left[\frac{1}{2}(0 + \alpha\beta + \beta\alpha + 0) - \frac{1}{4}\alpha\beta - \frac{1}{4}\beta\alpha\right]$$

$$= -J\frac{1}{\sqrt{2}}\left[\frac{1}{2}(\alpha\beta + \beta\alpha) - \frac{1}{4}(\alpha\beta + \beta\alpha)\right]$$

$$= -J\frac{1}{\sqrt{2}}\left[\frac{1}{4}(\alpha\beta + \beta\alpha)\right]$$

$$= -\frac{J}{4}\left[\frac{1}{\sqrt{2}}(|\alpha\beta\rangle + |\beta\alpha\rangle)\right] = -\frac{1}{4}J\Psi^T$$

and, for the singlet:

$$\hat{H}^H \Psi^S = -J\,\hat{S}_1 \cdot \hat{S}_2 \Psi^S$$

$$= -J\left[\frac{1}{2}(\hat{S}_1^+ \hat{S}_2^- + \hat{S}_1^- \hat{S}_2^+) + \hat{S}_{z1}\hat{S}_{z2}\right]\frac{1}{\sqrt{2}}(|\alpha\beta\rangle - |\beta\alpha\rangle)$$

$$= -J\frac{1}{\sqrt{2}}\left[\frac{1}{2}(0 - \alpha\beta + \beta\alpha - 0) - \frac{1}{4}\alpha\beta + \frac{1}{4}\beta\alpha\right]$$

$$= -J\frac{1}{\sqrt{2}}\left[-\frac{1}{2}(\alpha\beta - \beta\alpha) - \frac{1}{4}(\alpha\beta - \beta\alpha)\right]$$

$$= -J\frac{1}{\sqrt{2}}\left[-\frac{3}{4}(\alpha\beta - \beta\alpha)\right]$$

$$= \frac{3}{4}J\left[\frac{1}{\sqrt{2}}(|\alpha\beta\rangle - |\beta\alpha\rangle)\right] = \frac{3}{4}J\Psi^S$$

Then, the energy difference between the singlet and triplet states is:

$$E^S - E^T = J$$

When each magnetic site carries more than one unpaired electron, the same procedure can be followed. However, it should be noted that the simple form of

the Heisenberg Hamiltonian (eq. (1)) is not strictly valid anymore and a more elaborate form may be required by taking into account higher-order terms. In chapter four these deviations from the simple Heisenberg Hamiltonian are evaluated through DFT calculations in Ni and Pd trimetallic EMAC complexes.

Hubbard Hamiltonian. Another important model Hamiltonian originally conceived for solid state physics is the Hubbard Hamiltonian.[12] It is one of the simplest models of interacting particles (electrons) including a kinetic term allowing for hopping of particles between sites (first term) and a potential term consisting of an on-site interaction (second term):

$$\hat{H}^{Hubbard} = -\sum_{\langle i,j \rangle} t_{ij} (\hat{a}_i^+ \hat{a}_j + \hat{a}_j^+ \hat{a}_i) + U \sum_i (\hat{a}_{i\alpha}^+ \hat{a}_{i\alpha} + \hat{a}_{i\beta}^+ \hat{a}_{i\beta})$$

where t_{ij} is the intersite hopping integral, U the on-site effective two-electron repulsion and a_i^+ and a_i are the creation and annihilation operators, respectively.

The model space built from two orthogonal magnetic local orbitals, *a* and *b*, is composed of four determinants, two neutral, $|a\bar{b}\rangle$and $|b\bar{a}\rangle$, and two ionic ones, $|a\bar{a}\rangle$and $|b\bar{b}\rangle$. The model Hamiltonian expressed in this model space takes the form

	$\|a\bar{b}\rangle$	$\|b\bar{a}\rangle$	$\|a\bar{a}\rangle$	$\|b\bar{b}\rangle$
$\langle a\bar{b}\|$	0	K_{ab}	t_{ab}	t_{ab}
$\langle b\bar{a}\|$	K_{ab}	0	t_{ab}	t_{ab}
$\langle a\bar{a}\|$	t_{ab}	t_{ab}	U	K'_{ab}
$\langle b\bar{b}\|$	t_{ab}	t_{ab}	K'_{ab}	U

where the energy of the neutral determinants is considered as the energy origin. K_{ab} is the exchange integral between the neutral configurations and K'_{ab} between the ionic ones. U is the energy difference between the ionic and the neutral determinants. The hopping integral, t_{ab}, is the coupling between the ionic and the neutral forms. Diagonalization of this model Hamiltonian leads to four solutions:

(a) a purely neutral triplet state, $|T_u\rangle = \frac{1}{\sqrt{2}}(|a\,\bar{b}\rangle - |b\,\bar{a}\rangle)$ with energy

$${}^3E_u = -K_{ab}$$

(b) a purely ionic singlet state, $|S_u\rangle = \frac{1}{\sqrt{2}}(|a\,\bar{a}\rangle - |b\,\bar{b}\rangle)$ with energy

$${}^1E_u = U - K_{ab}$$

(c) an essentially neutral singlet state,

$|S_g\rangle = c_1(|a\,\bar{b}\rangle + |b\,\bar{a}\rangle) + c_2(|a\,\bar{a}\rangle + |b\,\bar{b}\rangle)$ $c_1 >> c_2$ with energy

$${}^1E_g = K_{ab} + \frac{U - \sqrt{U^2 + 16t_{ab}^2}}{2}$$

(d) an essentially ionic singlet state,

$|S_g'\rangle = c_2(|a\,\bar{b}\rangle + |b\,\bar{a}\rangle) - c_1(|a\,\bar{a}\rangle + |b\,\bar{b}\rangle)$ $c_1 >> c_2$ with energy

$${}^1E_g' = K_{ab} + \frac{U + \sqrt{U^2 + 16t_{ab}^2}}{2}$$

where *u* and *g* stand for *gerade* and *ungerade* symmetries. The singlet-triplet energy separation is given by

$${}^1E_g - {}^3E_u = 2K_{ab} + \frac{U - \sqrt{U^2 + 16t_{ab}^2}}{2} \qquad (4)$$

which can be considered as the variational estimate of the Heisenberg J in the Hubbard model. When $U >> |t_{ab}|$, the following power expansion is possible:

$$\sqrt{1+x} \approx 1 + \tfrac{1}{2}x - \cdots$$

$$\sqrt{U^2 + 16t_{ab}^2} = U\sqrt{1 + \frac{16t_{ab}^2}{U^2}} \approx \left(U + \frac{8t_{ab}^2}{U}\right)$$

Inserting this result in eq. (4), the coupling constant is:[13,14]

$$J = 2K_{ab} - \frac{4t_{ab}^2}{U}$$

Figure 2.1 shows the relationship between experimental and theoretical (*ab initio* calculations) studies. The effective Hamiltonian theory (EHT) is a bridge between the accurate *ab initio* calculations, which are difficult to interpret, and the easily understandable effective Hamiltonian containing the exact energies. In the opposite direction, through the quasi-degenerate perturbation theory, the effective Hamiltonian can be built from a simple and approximate model space. A rigorous check on the validity of the model Hamiltonian, obtained by mapping from experiments, can be obtained by comparing it with an effective Hamiltonian spanned in the same basis and projected from the exact, *ab initio* information.

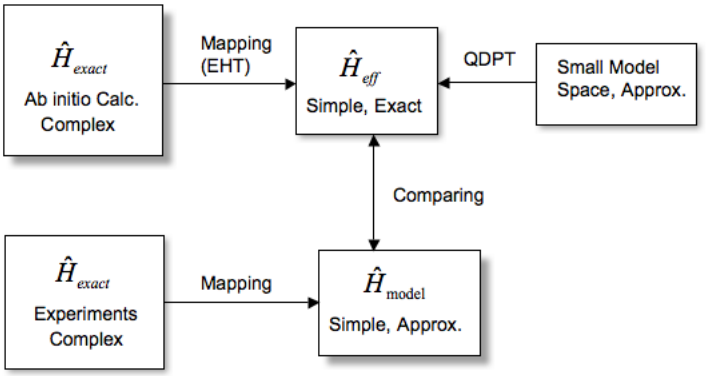

Figure 2.1. Schematic representation of the role of the effective Hamiltonian between experiments and theoretical *ab initio* calculations.

2.5. Broken-symmetry Approach

First principles electronic structure calculations can be used to obtain a quantitative description of spin exchange interactions in paramagnetic systems. While these calculations normally do not require a modeling of the magnetic unit in molecule-based magnets, the calculations of the exchange interactions in extended systems are often performed in the cluster approach.[15-18] The electronic states of the exact nonrelativistic Hamiltonian are projected onto the model space of the Heisenberg spin Hamiltonian $\hat{H} = -J\,\hat{S}_1 \cdot \hat{S}_2$. The electronic states

can be calculated by using either configuration interaction (CI) wave function methods or density functional theory (DFT).[19,20] In the former method, the electronic states are eigenstates of the S^2 operator. In DFT-based methods, the magnetic coupling is evaluated from the difference between the determinant with the maximum M_s value and the broken symmetry (*BS*) determinants. The single determinant nature of the Kohn-Sham implementation of DFT does not allow the use of pure spin eigenfunctions. The usual way in which DFT treats open shell systems is through the use of a spin-polarized, i. e. unrestricted, formalism in which α and β spin orbitals are allowed to have different spatial parts. The single determinant description of the high-spin state is not a problem, except for the small spin contamination inherent to the use of an unrestricted formalism. However, in the case of a low spin state one is forced to use a *BS* approach proposed by Noodleman et al.[21-22] in which the open-shell magnetic orbitals are localized in different centers with opposite net spin moments. This allows one to study spin exchange interactions on the basis of single-determinant electronic wave functions employed in DFT.

The calculation of the energies involved in spin exchange processes within the unrestricted formalism suffers from the usual intricate problem of spin contamination by higher multiplicity components. Consider a simple case with two magnetic sites with $S = 1/2$ spin angular moments. The unpaired electrons are localized on two orbitals *a* and *b* localized in different centers ($\langle a|b\rangle = 0$). In the broken symmetry approach the overlap between the spatial parts of orbitals *a* and *b* is not zero, $S_{ab} = \langle a|b\rangle \neq 0$, due to the unrestricted nature of the electron density (orbitals *a* and *b* have spins α and β, respectively). The unrestricted high spin and low spin states are the triplet T' and the *BS* solution, respectively. If the overlap is small one can assume that T' is a good approximation to the high spin state, $\langle HS|\hat{S}^2|HS\rangle \approx 2$. The expectation value of S^2 for the *BS* solution depends on the overlap between *a* and *b* as follows:

$$\left\langle \hat{S}^2 \right\rangle = \langle BS|\hat{S}^2|BS\rangle = 1 - |S_{ab}|^2$$

In systems where the two magnetic centers are far enough from each other, this overlap tends to zero and the expectation value of S^2 for the *BS* solution approaches 1. This means that the *BS* solution is strongly spin contaminated by the triplet state and one would expect for a ~50% admixture of singlet and triplet. Consequently, the *BS* state lies (approximately) halfway the singlet and the triplet in energy and the magnetic coupling constant is

$$E(BS) - E(HS) \approx \frac{J}{2} \qquad \text{(zero overlap limit)}$$

Now, we consider the case with four unpaired electrons in two magnetic sites with $S = 1$ each. Two magnetic orbitals are localized on center *a* (a_1 and a_2) and the other two on center *b* (b_1 and b_2). The unrestricted quintet state (Q') is the high spin state with $\left\langle \hat{S}^2 \right\rangle = \left\langle HS \left| \hat{S}^2 \right| HS \right\rangle \approx 6$ and the low spin state is the *BS* solution with $\left\langle \hat{S}^2 \right\rangle = \left\langle BS \left| \hat{S}^2 \right| BS \right\rangle \approx 2$, provided that $\left\langle a_1 \left| b_1 \right\rangle \approx 0$ and $\left\langle a_2 \left| b_2 \right\rangle \approx 0$. In this case, the energy difference between the high spin and *BS* solutions gives:[23]

$$E(BS) - E(HS) \approx 2J$$

A more rigorous relation between *J* and the energies of the different determinants can be obtained by projection of *BS* solutions onto the pure singlet state to eliminate the spin contamination. Yamaguchi proposed an approximate spin projection procedure:[24-27]

$$J = \frac{2(E_{BS} - E_{HS})}{\left\langle \hat{S}^2 \right\rangle_{HS} - \left\langle \hat{S}^2 \right\rangle_{BS}}$$

with $\left\langle \hat{S}^2 \right\rangle_{HS}$ and $\left\langle \hat{S}^2 \right\rangle_{BS}$ denoting the S^2 expectation values calculated in the high spin and in the *BS* solutions, respectively. In this way, for a system with two unpaired electrons localized on two magnetic sites, it is easy to show that[28]

$$J = \frac{2(E_{BS} - E_{T'})}{1 + S_{ab}^2} \qquad (5)$$

and for a system with four unpaired electrons localized on two magnetic sites, one may calculate J as

$$J = \frac{2(E_{BS} - E_{Q'})}{4 + S_{ab}^2} \tag{6}$$

E_{BS}, E_T' and E_Q' are the expectation values of the Heisenberg Hamiltonian for BS, triplet and quintet solutions. Equations (5) and (6) are often simplified by taking $S_{ab} = 0$ when a and b are far from each other.

2.6. Electronic Structure Methods to Study TM Complexes

Wave function-based methods. The single-determinantal nature of the Hartree-Fock (HF) method does not allow its applications on TM complexes, since the interaction between configurations is important for properly correlating the d electrons. Thus, multiconfigurational (MC) approaches are often employed to obtain a correct description of the electronic states of complexes containing TM atoms. In these methods, the many-electron wave function can be written as a linear combination of single Slater determinants (SD). The SDs are built from one-electron multi-center orbitals, that are commonly expanded in terms of basis functions. These form the *basis set* and limits the accuracy of the description of the MOs. The number of SDs included in the summation determines the *size* of the many-electron basis, and thus limits the description of the electron correlation. Often, the most difficult question arising in a multiconfigurational description of the wave function is the selection of the configuration space. In early applications, the configurations were selected individually, based on physical insight and intuition. Nowadays, the selection of the configurations proceeds in a more systematic manner, with whole classes of configurations selected simultaneously. The underlying idea of such selection is the partitioning of the orbital space into subspaces, characterized by certain restrictions with respect to the occupations of the configurations entering the multiconfigurational wave function.

The complete active space self-consistent field (CASSCF) method is one of the most usual and reliable ones for this sake. In CASSCF calculations, the total

orbital space is partitioned into a set of inactive orbitals, a set of active orbitals and a set of secondary orbitals. The inactive orbitals are doubly occupied in all configurations, the active orbitals are not subject to restrictions on their occupations, and secondary orbitals are unoccupied in all configurations. In the resulting wave functions, the CI and the MO coefficients have been variationally optimized.

Another shortcoming of monodeterminantal approaches in the accurate description of TM complexes arises from a completely different physical origin. In the independent particle model, the electrons are moving in the average field of the other electrons, which is obviously an approximation. In reality, the motions of electrons depend on their mutual instantaneous positions. That is, their motions are *correlated*. This fraction of the electron correlation is basically treated by Second-order Perturbation Theory[29] or Configuration Interaction[30] methods when a multiconfigurational reference wave function is required. Starting with a CASSCF wave function as the zeroth order wave function, the former theory gives a second order estimate to the energy contribution of all configurations that are, at most, doubly excited in a perturbative way with respect to the reference wave function (CAS). The method is not variational and does not guarantee obtaining energies higher than the exact energy. In CI methods, the CASSCF wave function is extended to a linear combination of many determinants in which the coefficients are variationally optimized by diagonalization of the Hamiltonian in the CI basis. The number of determinants included in the CI expansion must be reduced and the accuracy of the calculations depends on this reduction. CI methods, in the practical implementation (truncated CI), are not size extensive. By far the most common CI approximation is the truncation of the CI space expansion according to the degree of excitation relative to the reference state. The widely employed CI singles and doubles (CISD) wave function includes only those *N*-electron basis functions including single and double excitations of the reference state. Since the Hamiltonian operator includes only one- and two-electron terms, only singly and doubly excited configurations can interact directly with the reference, and they typically account for about 95% of the correlation energy in small molecules at

their equilibrium geometries.[31] The difference dedicated configuration interaction (DDCI) technique[32-33] has been designed for a direct evaluation of vertical energy differences. The truncation of the CI expansion in this method is based on the argument that the determinants involving two holes and two particles (2h + 2p) do not contribute to energy differences at the second order of perturbation and can be omitted in the CI expansion.

Density functional theory. As it was mentioned in section 1.2, the HF method completely neglects the electronic correlation and this is decisively important in compounds containing transition metal atoms. The wave function-related difficulties in incorporating correlation can be elegantly solved to an astonishingly accurate degree by moving away from the *N*-electron wave function and its corresponding Schrödinger equation and replacing them by a computational scheme which rests on the electron density $\rho(r)$. Density functional theory is an exact theory, at least in principle, and it includes both electronic exchange and correlation.[19,34] It is essentially based on two theorems of Hohenberg and Kohn[35] stating that the wave function of the ground state is a unique functional of the electron density $\rho(r)$. In addition, there is a variational principle such that the search for the lowest energy E_0 can be replaced by the search for the lowest energy electron density $\rho_0(r)$.

Formally, the functional of the total energy is expressed as

$$E[\rho(r)] = T_0[\rho(r)] + \frac{1}{2}\iint \frac{\rho(r)\,\rho(r')}{|r-r'|}\,dr\,dr' + E_{xc}[\rho(r)] + \int \rho(r)\,v(r)\,dr$$

including the kinetic energy of the system of noninteracting electrons, a classic Coulomb energy of the charge density, an energy functional for exchange and correlation, and the attractive Coulomb potential provided by the fixed nuclei. The ingenious trick used by Kohn and Sham[36] is the introduction of a reference system of noninteracting electrons with the same (spin) density. For a system of noninteracting electrons, the kinetic energy T_0 (leading part of the total energy) can be calculated by introducing *orbitals*. One may reduce gradually all electron-electron interactions to zero and in order to keep the same (spin)

density, introduce a little extra potential, that is, the system becomes a quasi-noninteracting system. The numerical success of DFT is a logical consequence of its smart strategy in treating the large energetic part (kinetic energy) as accurately as possible —by using orbitals— and approximating the small ones (exchange-correlation energies); all residual errors have been effectively dumped into these. The price to be paid for this *accurate but indirect* calculation is similar to that for HF theory ($3N$ variables).

The local density approximation (LDA)[36] is the main approximation for the electron density in which the exchange-correlation energy is considered for a homogeneous electrons gas. Clearly, this approximation is so crude that it seemed to be only applicable to systems with slowly varying electron densities. Another route has been followed by taking the gradient of the electron density. The idea is to include $\partial\rho(r)/\partial r$, as well as $\rho(r)$, to better describe the exchange hole which would improve the LDA especially in regions of low density. This functional is called generalized gradient approximation (GGA). In addition, the desire to further improve the numerical accuracy of DFT based methods has made people deliberately *mix* contributions of exchange and correlation that arise from different sources. One of the most widespread *hybrid* functionals, called B3LYP, is a three-parameter ansatz[37] including contributions from the LDA, HF theory, Becke's gradient-based exchange correction and the LYP correlation functional.

Nonetheless, both LDA and GGA fail, although to a different extent, if electronic correlation becomes strongly dominant. In reality, electron correlation leads to a localization of the electrons.[38] It has been known for a long time that such an underestimation of electron correlation can be easily corrected by introducing an additional electron repulsion parameter U, and this is the origin of a DFT patch called LDA+U method.

References

[1] C. Bloch, *Nucl. Phys*. 6 (1958) 329.

[2] J. des Cloizeaux, *Nucl. Phys*. 20 (1960) 321.

[3] J. H. Van Vleck, *Phys. Rev*. 33 (1929) 467.

[4] B. H. Brandow, *Int. J. Quantum Chem*. 15 (1979) 207.

[5] B. H. Brandow, *Rev. Mod. Phys*. 39 (1967) 771.

[6] I. Lindgren, J. Morrison, *Atomic Many Body Theory,* Springer-Verlag, Berlin, p.200, 1982.

[7] J. P. Malrieu and D. Maynau, *J. Am. Chem. Soc*. 104 (1982) 3021.

[8] I. de P. R. Moreira, N. Suaud, N. Guihéry, J. P. Malrieu, R. Caballol, J. M. Bofill, F. Illas. *Phys. Rev. B* 66 (2002) 134430.

[9] P. A. M. Dirac*, Proc. R. So. London, Ser. A* 112 (1926) 661; 123 (1929) 714.

[10] W. Z. Heisenberg, *Phys*. 38 (1926) 411.

[11] J. H. van Vleck, *Theory of electric and Magnetic Susceptibilities*, Oxford University Press, London, 1932.

[12] J. Hubbard, *Proc. R. Soc. Lond. A* 276 (1963) 238; 281 (1964) 401.

[13] P. W. Anderson, *Phys. Rev*. 79 (1950) 350.

[14] P. W. Anderson, *Theory of the Magnetic Interaction: Exchange in Insulators and Superconductors*, edited by F. Turnbull and F. Seitz, Academic Press, New York, Vol. 14, p. 99, 1963.

[15] F. Illas, J. Casanovas, M. A. Garcia-Bach, R. Caballol, O. Castell. *Phys. Rev. Lett*. 71 (1993) 3549.

[16] R. L. Martin. *Chem. Phys*. 98 (1993) 8691.

[17] C. de Graaf, I. de P. R. Moreira, F. Illas, R. L. Martin. *Phys. Rev. B* 60 (1999) 3457.

[18] F. Illas, I. de P. R. Moreira, C. de Graaf, V. Barone. *Theor. Chem. Acc*. 104 (2000) 265.

[19] R. G. Parr, W. Yang, *Density functional theory of atoms and molecules*, Oxford University Press, New York, 1989.

[20] R. M. Dreizler, E. K. U. Gross. *Density functional theory: an approach to the quantum many body problem*, Springer, Berlin Heidelberg, New York, 1990.

[21] L. Noodleman and J. G. Norman Jr., *J. Chem. Phys*. 70 (1979) 4903.

[22] L. Noodleman and E. R. Davidson, *Chem. Phys*. 109 (1986) 131.

[23] D. Dai, Whangbo. *J. Chem. Phys*. 118 (2003) 29.

[24] K. Yamaguchi, H. Fukui, T. Fueno. *Chem. Lett*. (1986) 625.

[25] K. Yamaguchi, Y. Takahara, T. Fueno, K. Nasu, *Jpn. J. Appl. Phys*. 26(1987) L1362.

[26] T. Onishi, T. Soda, Y. Kitagawa, Y. Takano, Y. Daisuke, S. Takamizawa, Y. Yoshikoda, K. Yamaguchi. *Mol. Cryst. Lig. Cryst*. 143 (2000) 133.

[27] T. Onishi, Y. Takano, Y. Kitagawa, T. Kawakami, Y. Yoshikoda, K. Yamaguchi. *Polyhedron* 20 (2001) 1177.

[28] R. Caballol, O. Castell, F. Illas, I. de P. R. Moreira, J. P. Malrieu, *J. Phys. Chem. A* 101 (1997) 7860.

[29] K. Andersson, P. Å. Malmqvist, B. O. Roos, A. J. Sadlej, K. Wolinski. *J. Phys. Chem.* 94 (1990) 5483.

[30] A. Szabo, N. S. Ostlund, *Modern Quantum Chemistry: Introduction to Advanced Electronic Structure Theory*, McGraw-Hill, New York, 1989.

[31] R. J. Harrison, N. C. Handy. *Chem. Phys. Lett*. 95 (1983) 386.

[32] J. Miralles, O. Castell, R. Caballol, J. P. Malrieu. *Chem. Phys*. 172 (1993) 33.

[33]J. Miralles, J. P. Daudey, and R. Caballol, *Chem. Phys. Lett*. 198 (1992) 555.

[34] R. O. Jones, O. Gunnarsson, *Rev. Mod. Phys*. 61 (1989) 689.

[35] P. Hohenberg, W. Kohn, *Phys. Rev*. 136 (1964) 864.

[36] W. Kohn, L. J. Sham, *Phys. Rev*. 140 (1965) 1133.

[37] P. J. Stephens, J. F. Devlin, D. F. Chabalowski, M. J. Frisch, *J. Phys. Chem*. 98 (1994) 11623.

[38] P. W. Anderson, *Phys. Rev*. 124 (1961) 41.

Chapter 3

Analysis of the Magnetic Coupling in $M_3(dpa)_4Cl_2$ Systems by *Ab initio* Methods

3.1. Introduction and Objectives

Previous theoretical studies on trimetallic EMAC systems have been mainly performed with density functional theory (DFT) schemes due to the size issue. These theoretical works, performed by Bénard and colleagues during the last decade, provided insight into the geometrical and electronic structures and also into the rationalization of their magnetic properties.[1-10] However, it is well known that DFT is an approximate way to treat magnetic problems, mainly due to the monodeterminantal nature of the Kohn-Sham implementation. For the first time, we apply correlated *ab initio* methods to compute the magnetic exchange parameter in EMACs to evaluate their performance compared with the DFT method. We herein employ a multiconfigurational (MC) approach, which

properly accounts for the multideterminantal nature of the electronic states, and hence describes all spin states as eigenstates of the total spin operator.

The complete active space self-consistent field (CASSCF) method is, in principle, a good technique for this aim, but the dimension of the active space limits its applicability. However, in most problems related to magnetism, the number of electrons and orbitals that have to be included in the CAS remains below this limit and good results can be obtained by combining CASSCF with a second computational technique to account for the remaining electron correlation, such as the complete active space second-order perturbation theory (CASPT2)[11-12] or the difference dedicated configuration interaction (DDCI).[13] A second drawback of this approach is the number of basis functions that can be treated in a straightforward routine-like fashion. Until recently, the CASPT2 and DDCI methods have mostly been applied to relatively small molecules, but the development of new formulations based on the Cholesky decomposition of the integrals[14-16] and/or local electron correlation methods[17-20] significantly widen the range of applicability of these MC approaches. Since highly correlated treatments of TM complexes with magnetic interactions have been devoted only to modestly large complexes,[21] this work explores the possibilities of applying such methods to larger molecules. Here, we analyze the exchange coupling constants obtained for a series of EMACs using the CASPT2 methodology.[11-12] This method uses a CAS wave function as zeroth-order wave function and accounts for the remaining part of the electron correlation by second-order perturbation theory. In general, CASPT2 gives rather satisfactory results provided that the CAS is large enough and properly chosen.[22-28] This latter issue is important in the discussion of the results.

The *ab initio* data herein presented for $Ni_3(dpa)_4Cl_2$ (**1**), $Pd_3(dpa)_4Cl_2$ (**2**), $Cu_3(dpa)_4Cl_2$ (**3**), $Cu_3(dpa)_4Cl_2^+$ (**3**$^+$), $Ag_3(dpa)_4Cl_2$ (**4**) and $Ag_3(dpa)_4Cl_2^+$ (**4**$^+$) are discussed and compared to those computed before at the DFT level. The presentation of the results is organized in two main parts: first the string complexes containing two magnetic centers (**1**, **2** and **3**$^+$, **4**$^+$), and then the compounds with three magnetic centers (**3** and **4**). A schematic representation of the electronic structure of the compounds discussed in the present study, which

are actually the singly occupied molecular orbitals involved in magnetic interactions, is shown in Figure 3.1.

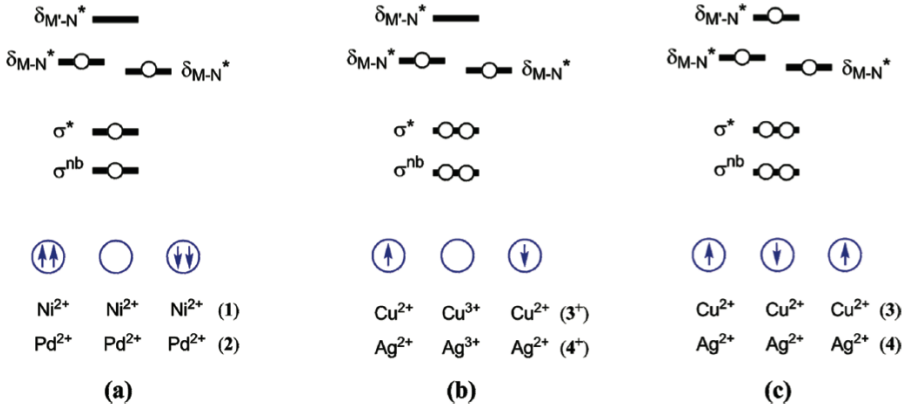

Figure 3.1. Schematic view of the electron distribution involved in the magnetic coupling in (a) **1** and **2**, (b) $\mathbf{3}^+$ and $\mathbf{4}^+$, and (c) **3** and **4** string complexes. The molecular orbitals shown are the upper five of the set of fifteen orbitals containing the metal valence electrons. The energy separation between the orbitals represented is not scaled.

3.2. Computational Details

Geometry optimizations were carried out for $Ni_3(dpa)_4Cl_2$, $Cu_3(dpa)_4Cl_2$ and $Ag_3(dpa)_4Cl_2$ in their corresponding ground states using the Gaussian03 program.[29] The unrestricted formalism of density functional theory (DFT) and the hybrid B3LYP exchange-correlation functional were used for this sake. Double-ξ valence basis sets have been used for light atoms (H, C, N). Los Alamos electron-core potentials were used for Cl and metal atoms, and double-ξ functions for valence electrons (LANL2DZ basis sets). Polarization functions have been added for nitrogen (d) and metal atoms (f) to get more accurate and reliable geometries, since small geometrical distortions can have an important impact in the study of magnetic interactions. We used the ground state optimized geometries for $Pd_3(dpa)_4Cl_2$, $[Cu_3(dpa)_4Cl_2]^+$ and $[Ag_3(dpa)_4Cl_2]^+$ as previously published.[3,8] The main structural parameters of the optimized geometries are displayed in Table 3.1. For the three complexes that have been synthesized to

date, namely **1**, **3** and $\mathbf{3}^+$, the calculated interatomic distances compare rather well with the experimental ones, although being slightly longer in general. This is a well-known failure of most functionals.

Table 3.1. Selected interatomic distances (Å) computed at the DFT/B3LYP level for $Ni_3(dpa)_4Cl_2$ (**1**), $Pd_3(dpa)_4Cl_2$ (**2**), $Cu_3(dpa)_4Cl_2$ (**3**), $[Cu_3(dpa)_4Cl_2]^+$ ($\mathbf{3}^+$), $Ag_3(dpa)_4Cl_2$ (**4**) and $[Ag_3(dpa)_4Cl_2]^+$ ($\mathbf{4}^+$) in their ground states.[a]

	1	**2**	**3**	$\mathbf{3}^+$	**4**	$\mathbf{4}^+$
M-M	2.481	2.544	2.531	2.571	2.695	2.695
	(2.42-2.44)		(2.47-2.49)	(2.51)		
M-Cl	2.399	2.564	2.498	2.470	2.639	2.627
	(2.33-2.34)		(2.44-2.49)	(2.39)		
$M\text{-}N_{term}$	2.125	2.258	2.116	2.084	2.323	2.266
	(2.08-2.10)		(2.06-2.09)	(2.06)		
$M\text{-}N_{cent}$	1.922	2.062	2.004	1.922	2.184	2.093
	(1.88-1.89)		(1.96-1.98)	(1.89)		

(a) The experimental distances of **1**, **3** and $\mathbf{3}^+$, in parentheses, are taken from references 30, 31 and 32, respectively.

All CASSCF/CASPT2 calculations were carried out with the MOLCAS 7 suite of programs.[33] Atomic Natural Orbitals of ANO-RCC types were employed as the basis set for all atoms.[34-35] For Ni and Cu atoms we employed (5s,4p,3d) basis sets, for Ag and Pd atoms (6s,5p,4d), for the bridging N atoms (3s,2p) and for axial Cl ligands (4s,3p). Also, C and H atoms were assigned (3s,2p) and (2s) basis sets, respectively. One prerequisite for working with MOLCAS is decreasing the full symmetry point group of the molecule to the largest symmetry subgroup that does not contain degenerate irreducible representations. For this reason, the original full symmetry has been reduced from D_4 to D_2 and the molecular orbitals in this new symmetry belong to a, b_1, b_2 and b_3 symmetries.

In all CASPT2 calculations, a low reference weight (RW = 0.29) has been observed. Low RWs can either be caused by the presence of undesired intruder states or to the large number of correlated electrons. To fix this shortcut, removal

of the intruder states is performed introducing a level shift (LS) to the CASPT2 calculation. The present calculations always give RWs ~ 0.29–0.30 for level shifts ranging from 0.0 to 0.2, indicating that the intruder states are not the cause of such low RWs, but the large amount of correlated electrons. The criteria that guarantee the reliability and accuracy of the calculations are the energy differences between different states as long as they are calculated with an as similar as possible active spaces in CASSCF calculations and with the similar reference weights in CASPT2 calculations.

For a molecule with only two magnetic centers, the Heisenberg Hamiltonian, which is the summation over all the nearest spin-carrying neighboring interactions,[36-38] takes this simple form:

$$\hat{H} = -J\,\hat{S}_1 \cdot \hat{S}_2$$

where J is the exchange coupling constant, and S_1 and S_2 are the spin moments localized on each magnetic center. Since EMACs are antiferromagnetic in nature, the following discussions are based on the fact that the ground state is an open-shell singlet. For two S = ½ magnetic centers, the two possible eigenfunctions (the singlet ground state and the triplet) have associated energies $\frac{3}{4}J$ and $-\frac{1}{4}J_1$, respectively, as shown in Figure 3.2.b. In this case, J is exactly the energy gap between states. When each interacting center bears a maximal S =1 spin moment, a quintet state appears in addition to the triplet and singlet states. The eigenvalue of the singlet ground state is equal to 2J and those of the excited triplet and quintet states are J and –J, respectively (Figure 3.2.a).

The energy spectrum normally follows the so-called Landé pattern predicted by the Heisenberg Hamiltonian: E(S–1) – E(S) = SJ. Deviations may however be observed when the number of energy levels increase. In these cases, the Heisenberg Hamiltonian can be extended with extra terms such as the isotropic biquadratic exchange or anisotropy (zero-field splitting) terms. It was recently found that the intrinsic precision of CASPT2 does not allow studying the deviations to the Heisenberg Hamiltonian.[39] In the next chapter we discuss in detail how the isotropic deviation can be estimated by the DFT method. For the moment, we ignore the deviations and report effective magnetic couplings

obtained by taking the average of the different J values that can be extracted from the full spectrum.

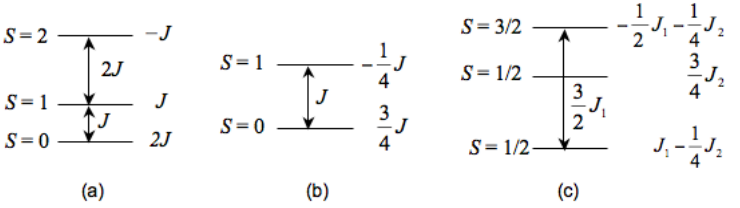

Figure 3.2. Schematic representation of the energy spectrum of (a) **1** and **2**, (b) $\mathbf{3}^{+}$ and $\mathbf{4}^{+}$, and (c) **3** and **4** EMAC string complexes, according to the Heisenberg Hamiltonian.

For linear systems with three magnetic centers, the spin Hamiltonian describing the low-lying states is defined as:

$$\hat{H} = -J_1(\hat{S}_1 \cdot \hat{S}_2 + \hat{S}_2 \cdot \hat{S}_3) - J_2\,\hat{S}_1 \cdot \hat{S}_3$$

in which J_1 and J_2 represent the exchange parameter between nearest neighbors and next-nearest neighbors, respectively. The eigenfunctions of this Hamiltonian for S = ½ magnetic centers are two doublet states and one quartet state with energies:

Doublets: $\quad E(\tfrac{1}{2},A) = J_1 - \frac{1}{4}J_2 \;\; ; \quad E(\tfrac{1}{2},B) = \frac{3}{4}J_2$

Quartet: $\quad E(\tfrac{3}{2}) = -\frac{1}{2}J_1 - \frac{1}{4}J_2$

Thus, the excited quartet state is found at $-\tfrac{3}{2}J_1$ from the doublet ground state (Figure 3.2.c). The interaction between next-nearest neighbors (J_2) in molecules with three magnetic centers is much weaker than that between neighboring metals (J_1), as we will show in the Results section. Therefore, the last term in the Heisenberg Hamiltonian can be ignored without altering the main conclusions of the study.

The CASDI[40] and the NATURAL[41,42] programs have been used in the CI calculations and in the determination of the dedicated orbitals in **3**.

3.3. Results and Discussion

3.3.1. Molecules with Two Magnetic Centers

$Ni_3(dpa)_4Cl_2$ (1) and $Pd_3(dpa)_4Cl_2$ (2). The distribution of the 24 d electrons of the $(Ni^{II})_3$ and $(Pd^{II})_3$ systems over the MOs shown in Fig. 1.2 leads to a $(\sigma^*)^1(\sigma^{nb})^1(\delta_{M(terminal)\text{-}N}{}^*)^1(\delta_{M(terminal)\text{-}N}{}^*)^1$ electronic configuration, four unpaired electrons in four molecular orbitals (Figure 3.2). These orbitals have major contributions from the terminal metal atoms and, hence, the magnetic interaction occurs between electrons localized at both ends of the string. In contrast, the central metal presents a diamagnetic configuration induced by the four amino groups to which it is coordinated. In these complexes with two $S = 1$ centers, the magnetic coupling takes place by two main mechanisms. The first one originates in the electrons occupying σ orbitals. The second one is a consequence of an indirect coupling of the δ electrons involving the bridging ligand orbitals and the x^2-y^2 orbital of the central metal which lies at the crossing point of four equivalent magnetic interaction pathways.[4] The part of the magnetic coupling associated to the σ interaction is the leading interaction as it takes place through the central Ni atom only and by a very effective overlap of d_{z^2} orbitals. In $Ni_3(dpa)_4Cl_2$, the interaction between the two terminal Ni(II) atoms is antiferromagnetic, with experimental J between –198 and –216 cm^{-1} (Peng's group[43] and Cotton's group[30] data, respectively). The Pd homologue, **2**, has not been reported experimentally but a DFT study was recently performed.[8]

To describe the magnetic behavior of **1** and **2** with *ab initio* methods, we first construct a wave function in the minimal active space with the orbitals involved in the magnetic interaction (Figure 3.3) and the four unpaired electrons, i.e., a CAS(4,4). Taking the minimal CAS, the J value (average J) in **1** and **2** complexes have been computed to be –6.64 and –272 cm^{-1}, respectively. The huge increase ($J_{Pd}/J_{Ni} \approx 41$) of the antiferromagnetic coupling strength in **2** with respect to **1** is ascribed to the increase of the size of the interacting orbitals.[8] Adding the dynamical correlation to the CASSCF wave functions, CASPT2 calculations augment these energy differences up to –39.2 and –999 cm^{-1} in **1**

and **2**, respectively. The relative increase in **1** is somewhat more significant than in **2**.

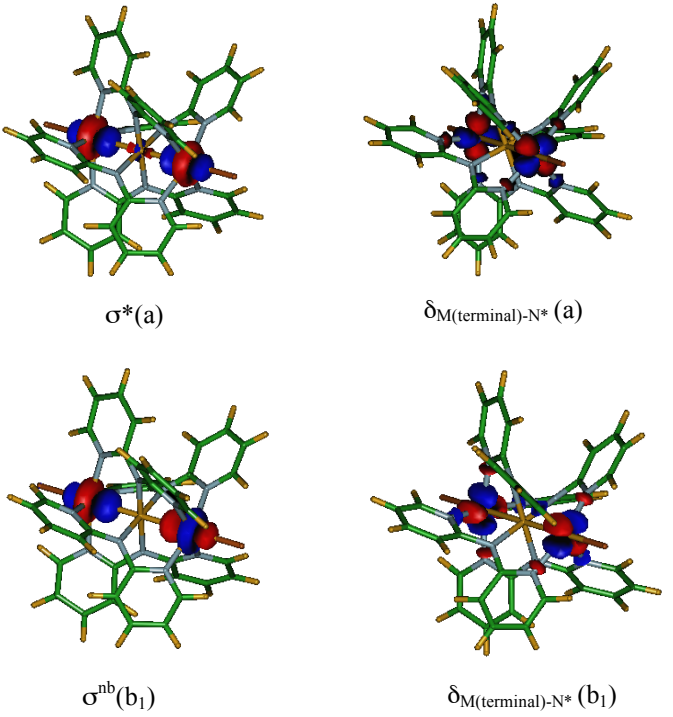

Figure 3.3. Magnetic orbitals involved in CAS(4,4) in **1** and **2**. The symmetry of each orbital is given in parentheses.

The occupation numbers computed for σ- and δ-like active orbitals, shown in Table 3.2, present important differences. The former are considerably different from 1, indicating their strong engagement in magnetic interactions. Oppositely, δ orbitals do not participate so actively in the magnetism. This fact gets especially significant in the Pd complex, implying the existence of a very strong coupling between σ electrons such that some covalent bond is generated in the metal-metal region.

Table 3.2. Occupation numbers of active orbitals in the CAS(4,4) in singlet ground state for compounds **1** and **2**.

	$\delta_{M(terminal)\text{-}N}{}^{*}(a)$	$\delta_{M(terminal)\text{-}N}{}^{*}(b_1)$	$\sigma^{nb}(b_1)$	$\sigma^{*}(a)$
1	1.0006	0.9994	1.0224	0.9776
2	1.0032	0.9968	1.1789	0.8211

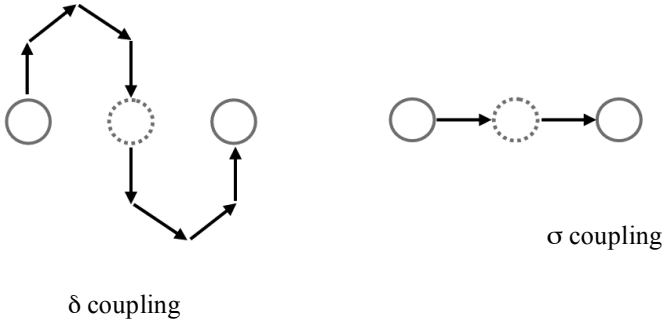

Figure 3.4. Schematic view of δ and σ magnetic coupling paths in **1** and **2** through dpa ligands (left) and through central nickel (right). Dashed circles represent the central, diamagnetic metal atoms.

In systems with antiferromagnetic nature, the *J* parameters obtained at the CASPT2 level with the minimal CAS, despite being qualitatively correct, are typically far from being accurate values since the coupling occurs through the ligand orbitals and they play an important role in the accurate evaluation of the energy differences. In **1** and **2**, the electron coupling happens via two paths: σ-coupling in which the central diamagnetic metal atom acts as a bridge atom between two magnetic centers and δ-coupling where the many ligand orbitals as well as central metal atom are involved in magnetic interactions (Figure 3.4). For compound **1** the CASPT2 value of *J* is about 20% of the experimental value with a minimal CAS. This means that a rational enlargement of the CAS space is necessary. But its dimension may become prohibitive before giving an accurate value of the magnetic exchange. Which orbitals are actually the most important in the present magnetic problem? Knowing that the coupling mechanism between terminal metals occurs via the central metal in both pathways, we extend the active space with those orbitals that are mainly localized on the central metal. This central metal can be considered to play the role of the

diamagnetic bridge in the standard Anderson superexchange model. Three doubly occupied orbitals, $\delta_{Ni(central)-N}$, σ, $\delta_{Ni(central)}$ are included in active space (see Figure 3.5a). Large fluctuations are observed in their occupation numbers (1.9671, 1.9471 and 1.9781, respectively) in the case of compound **1**. By including also their corresponding virtual orbitals, the CAS(10,13), as shown in Figure A1 in Appendix A, the magnitude of the antiferromagnetic interaction augments up to –28.5 cm^{-1} at the CASSCF level. Including the dynamic effects to the reference wave function leads to J = –119 cm^{-1}, still far from the experimental value. The significant contribution of amido- and pyridylic-N atoms in structure of δ orbitals can be noticed.

Table 3.3. Calculated $-J$ (in cm^{-1}) for minimal and extended spaces at CASSCF and CASPT2 levels for compounds **1** and **2**.

	CAS(4,4)	CASPT2	CAS(10,13)	CASPT2	DFT[a]	exp.[d]
1	6.64	39.2	28.5	119[e]	91[b]	198−216
2	272	999	612	1435	1393[c]	–

(a) B3LYP functional. (b) Ref 10. (c) Ref 8. (d) Refs 43 and 30. (e) Level Shift = 0.1

Figure 3.5b displays the doubly occupied orbitals added to the minimal active space in complex **2**. We observe that the active orbitals are not exactly equivalent to those of the extended CAS for **1**. The $4p_z$ orbital of the central Pd automatically enters rather than the $\delta_{Pd(central)}$ of b_1 symmetry. This confirms that the σ magnetic interaction, which takes place along the *z*-axis, is stronger in **2** than in **1** (Table 3.3). Extending the active space (Figure A2 in Appendix A) in **2** mainly affects the CASSCF result. One may conclude that, in **2**, a minimal CAS can quantitatively describe the magnetic interaction since it fully contains the magnetic region. In other words, given that the magnetic orbitals localized on terminal Pd atoms are very voluminous (and the σ interaction is the dominant one), the role of the central metal orbitals is not so crucial and a minimal CAS reproduces the major part of the magnetic coupling. The occupation numbers of $\delta_{Pd(central)-N}$ (a), σ (a), $4p_z$ (b_1) orbitals (1.9722, 1.9649 and 1.9976, respectively) show smaller deviations from 2.0 with respect to the same analysis made on the

Ni complex. Here we report a magnitude of $J = -1435$ cm^{-1} for the exchange parameter in **2** which is of the same order as obtained by López et al. using DFT.[8]

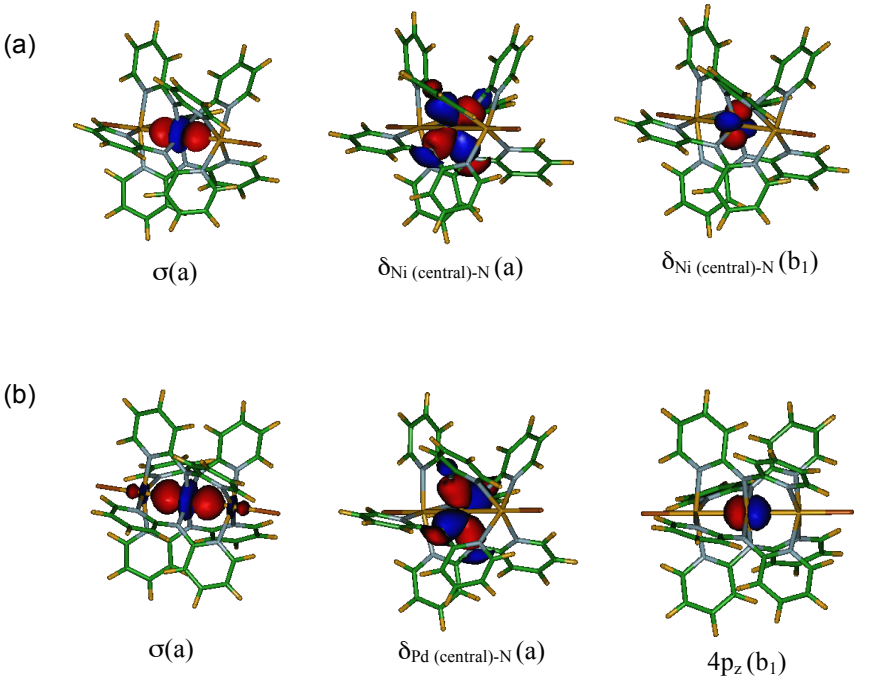

Figure 3.5. Doubly occupied orbitals added to the minimal CAS in (a) Ni and (b) Pd complexes. The symmetry of each orbital is given in parentheses.

To see the effect of distance between magnetic centers upon *J*, the same calculations have been performed using the geometry of the molecule optimized in the quintet state with terminal Ni-Ni distances stretched to 4.976 Å (the previous Ni_{term}-Ni_{term} distance was 4.962 Å, corresponding to the ground state). The magnitude of *J* at the new distance is computed to be –114 cm^{-1}, smaller than the ground state one, –119 cm^{-1}. If we now perform these calculations with shorter Ni_{term}-Ni_{term} distances, like the experimental one (4.86 Å)[44] and some other distances, a magnetostructural correlation can be obtained (see Figure 3.6). At the experimental distance $J = -150$ cm^{-1}, being quite close to the measured value. We observe that a shortening of ~0.1 Å (from 4.976 to 4.86 Å) in the Ni-

Ni distance causes a considerable increase in *J* suggesting that the σ interaction, which takes place directly through the Ni-Ni axis, dominates the overall magnetic interaction.

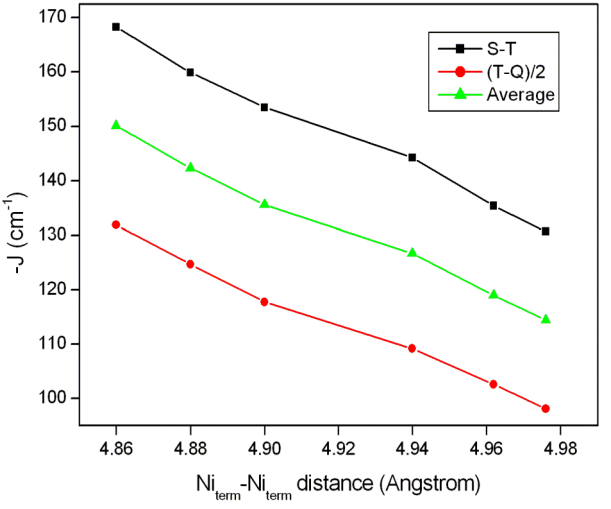

Figure 3.6. CASPT2 (Level Shift = 0.1) value of magnetic coupling, –*J*, as a function of the distance between the two terminal nickel atoms. S, T and Q stand for singlet, triplet and quintet, respectively.

$[Cu_3(dpa)_4Cl_2]^+$ (3^+) and $[Ag_3(dpa)_4Cl_2]^+$ (4^+). The distribution of 26 d electrons over the MOs shown in Fig. 1.2 leads to a $(\sigma^*)^2(\sigma^{nb})^2(\delta_{M(terminal)\text{-}N}^*)^1(\delta_{M(terminal)\text{-}N}^*)^1$ electronic configuration. In compounds $\mathbf{3}^+$ and $\mathbf{4}^+$, the magnetic coupling takes place between two unpaired electrons localized on the terminal atoms as in compounds **1** and **2** (Figure 3.1b). However, the magnetic interaction takes place via δ-like orbitals only, while the σ orbitals are inactive, doubly occupied orbitals. The unpaired electrons in the δ-system interact by a superexchange pathway involving the dpa ligands and the central metal ion, as demonstrated with DFT calculations.[3] Considering the two singly-occupied $\delta_{M(terminal)\text{-}N}^*$ orbitals we get a minimal CAS(2,2). The exchange parameter computed for $\mathbf{3}^+$ is close to zero (Table 3.4). It has been demonstrated that the

central metal, despite being diamagnetic, plays a key role in the superexchange coupling, lying at the crossing point of the magnetic interaction pathways.[3] So, for a better performance of the calculations, an extended CAS must contain δ-type orbitals of the central copper. Nevertheless, extending the CAS with only these δ-type orbitals does not lead to a stable situation. The combined orbital and CI optimization process leads to a lower energy when the δ-functions on the central metal atom are changed to σ-type orbitals of this metal. Then, the tentative quest for increasing the number of magnetic electrons leads to adding six doubly occupied orbitals, i.e., $\delta_{M(terminal)}(a)$, $\delta_{M(central)-N}(a)$, $\sigma^*(a)$, $\delta_{N(terminal)-M}(b_1)$, $\delta_{M(terminal)}(b_1)$ and $\sigma^{nb}(b_1)$ (Figure 3.7 and Figure A3 in Appendix A) and their corresponding virtual orbitals to form a CAS(14,13). The magnitude of *J* significantly increases with this new active space. Among the added orbitals, the appearance of an orbital with mainly ligand character, $\delta_{N(terminal)-M}$ (b_1), is of interest since removal of this orbital leads to disordered states and makes the calculations fail. The presence of doubly occupied $\delta_{M(central)-N}$ and virtual $\delta_{M(central)-N*}$ orbitals in the active space emphasizes the importance of the central metal atom in the coupling. As a matter of fact the considerable fluctuation observed in the occupation number of the mentioned orbitals (1.840 and 0.160 respectively) might be an evidence for this conclusion. Other theoretical works focused on this kind of systems have shown that the central metal atom plays a fundamental role in the magnetic coupling.[3] Eventually, taking into account the dynamic correlation energy, $J = -34.8$ cm^{-1} for $\mathbf{3}^+$, in full agreement with the experimental value of -34 cm^{-1}.[32] The present calculations solve the overestimation by a factor of 2 obtained by DFT method.[3]

The strength of the magnetic coupling in the hypothetical monocationic silver complex, $\mathbf{4}^+$, is expected to be larger than in $\mathbf{3}^+$, as DFT has predicted.[3] This statement is based on the larger overlap of x^2-y^2 orbitals of terminal silver atoms with the ligand orbitals. The triplet-singlet energy splitting obtained with a minimal CAS calculation is small, but already one order of magnitude larger than in $\mathbf{3}^+$, as shown in Table 3.4. Guided by the calculations on $\mathbf{3}^+$, we extend the CAS with both σ and δ orbitals as before to obtain a CAS(14,15) wave

function (Figure A4 in Appendix A). The corresponding *J*-value is more than 3.5 times larger than for the minimal CAS. Finally, $J = -138$ cm^{-1} at the CASPT2 level. The occupation numbers of the formally doubly occupied $\delta_{M(central)-N}$ and virtual $\delta_{M(central)-N}^{*}$ orbitals included in the extended CAS are larger/smaller than in $\mathbf{3}^{+}$ but still significantly far from 2 and 0 (1.938 and 0.063, respectively). The formerly DFT calculated value of *J* is again two times larger than the present CASPT2 result,[3] which is the expected trend. So, the current CASPT2 value can be considered good despite no comparison can be performed with experiment.

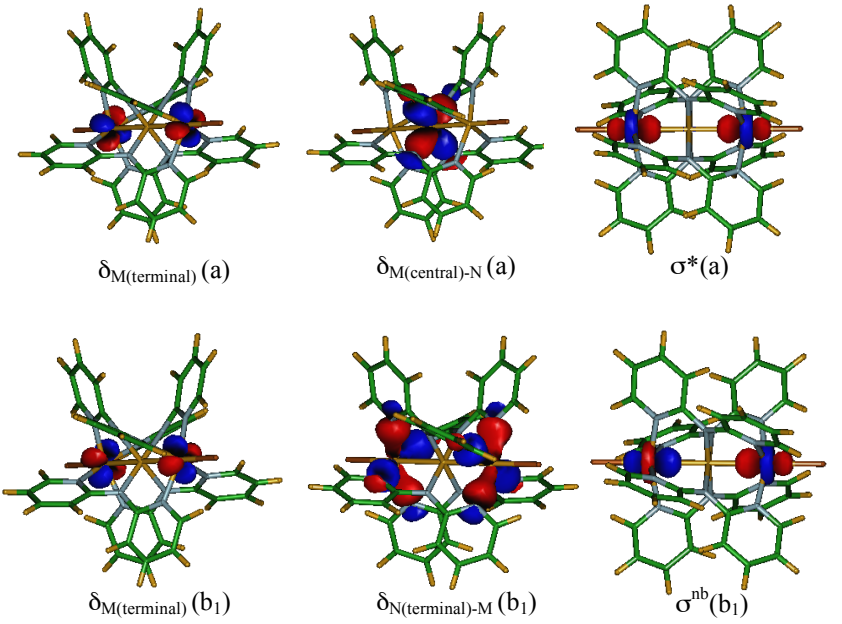

Figure 3.7. Doubly occupied orbitals added to the CAS(2,2) in $\mathbf{3}^{+}$ and $\mathbf{4}^{+}$. The symmetry of each orbital is given in parentheses.

The role of the dynamical correlation becomes evident when we compare the *J*-values of $\mathbf{3}^{+}$ and $\mathbf{4}^{+}$ at the different stages of the calculation. The magnetic coupling calculated with a CAS(2,2)SCF wave function is extremely small for both molecules. CASPT2 enhances the coupling in a similar fashion. The enlargement of the active space leads to a modest increase of the coupling at the

CASSCF level (notice that the J of extended CAS in $\mathbf{3}^+$ is larger than $\mathbf{4}^+$), but the inclusion of the dynamical electron correlation makes the difference: J increased by a factor of 4 in $\mathbf{3}^+$, while this increase is much more pronounced in $\mathbf{4}^+$. We stress that, in the final CASPT2 result for this latter molecule, no indications were found for intruder states. Reference weights do not differ by more than 0.001 and no configurations external to the CAS were found with small expectation values of H^0 or large interaction matrix elements.

Table 3.4. Calculated $-J$ (cm^{-1}) for minimal and extended spaces at CASSCF and CASPT2 levels for the cationic species $\mathbf{3}^+$ and $\mathbf{4}^+$.

	CAS(2,2)	CASPT2	Ext. CAS	CASPT2	DFT[a]	exp. [b]
$\mathbf{3}^+$	0.12	8.3	9.1[c]	34.8	64	34
$\mathbf{4}^+$	1.8	9.1	6.7[d]	138	265	–

(a) B3LYP functional, ref 3. (b) Ref 32. (c) CAS(14,13). (d) CAS(14,15).

3.3.2. Molecules with Three Magnetic Centers

$Cu_3(dpa)_4Cl_2$ (3) and $Ag_3(dpa)_4Cl_2$ (4). The $(M_3)^{6+}$ (M = Cu or Ag) backbone of the neutral complexes **3** and **4** contains three unpaired electrons, one more than the cationic $\mathbf{3}^+$ and $\mathbf{4}^+$ species. The extra electron in **3** and **4** is formally localized on the central metal atom, therefore becoming three-magnetic-center strings with S = ½ each. The highest δ orbitals, i.e., two $\delta_{Ni(terminal)\text{-}N}^*$ and one $\delta_{Ni(central)\text{-}N}^*$, are singly-occupied (see Figure 3.1c). The three unpaired electrons are magnetically coupled. The magnetic exchange parameter in **3** and **4** originates, as in $\mathbf{3}^+$ and $\mathbf{4}^+$, from the interaction of δ-like magnetic electrons via the bridging dpa ligands. As mentioned above, the nearest-neighbors and next-nearest-neighbors interactions (J_1 and J_2, respectively) can be obtained from the eigenvalues of the spin Hamiltonian. In all hereafter calculations, $J_1 = J$ represents by far the strongest interaction, although the next-nearest neighbors parameter, J_2, is not always negligible (see the case of **4** in Table 3.5). The spectrum obtained by considering J_1 only or both J_1 and J_2 remains practically unchanged in **3**,[45] but it is slightly different in **4**. However, neglecting J_2 does not

change the general magnetism of these systems and, for the purpose of the present work we just focus on the largest contribution, J_1.

A primary description of the antiferromagnetic interaction between metal atoms at the CASSCF level can be given by choosing the three singly-occupied δ orbitals (shown in Figure 3.8), as active orbitals; CAS(3,3). The calculations give J = –9.8 and –90.7 cm^{-1} for **3** and **4**, respectively (Table 3.5). The replacement of copper by silver in $M_3(dpa)_4Cl_2$ induces a tremendous increase of the coupling due to more effective overlap between δ orbitals of Ag atoms and p atomic orbitals of nitrogen atoms. This trend is reproduced in CASPT2 calculations.

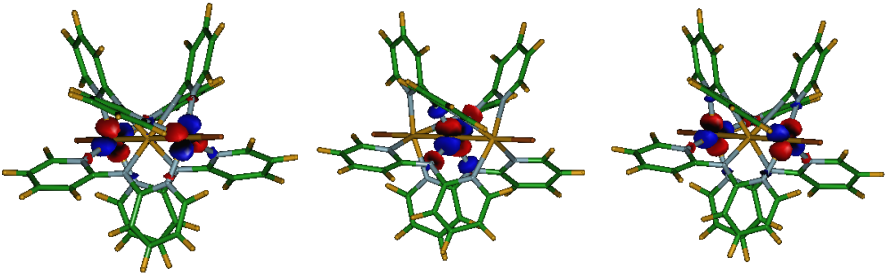

Figure 3.8. Orbitals involved in the CAS(3,3) in **3** and **4**. The symmetry of each orbital is given in parentheses.

We tried to enlarge the active space with δ type orbitals only, that is, with $\delta_{Cu(central)-N}$ (a) and $\delta_{Cu(terminal)}$ (a, b_1), but we faced similar problems as in the cationic species mentioned before. In all the states, σ-type orbitals enter inevitably the active space, although they are not directly involved in magnetic interactions. Hence, the enlargement of the active space in **3** is carried out by entering the five doubly occupied orbitals σ(a), $\sigma^{nb}(b_1)$, $\delta_{Cu(central)-N}$(a), σ^{*}(a) and $\delta_{Cu(terminal)}$(a), and their corresponding virtual orbitals to obtain a CAS(13,14), as shown in Figure 3.9 (and Figure A5 in Appendix A). The same doubly occupied orbitals were used to construct the extended CAS (CAS(13,13)) for compound **4**

(Figure A6 in Appendix A). The only difference is that the $\delta_{Ag(terminal)}$ orbital belongs to b_1 symmetry. The occupation numbers of the added doubly occupied σ-type orbitals do not differ more than 0.01 from 2 in both **3** and **4**. The expansion of the active space enhances *J* at the CASSCF level for **3** and **4** up to –33 and –130 cm^{-1}, respectively. The increase of *J* is thus more important in the Cu_3 complex.

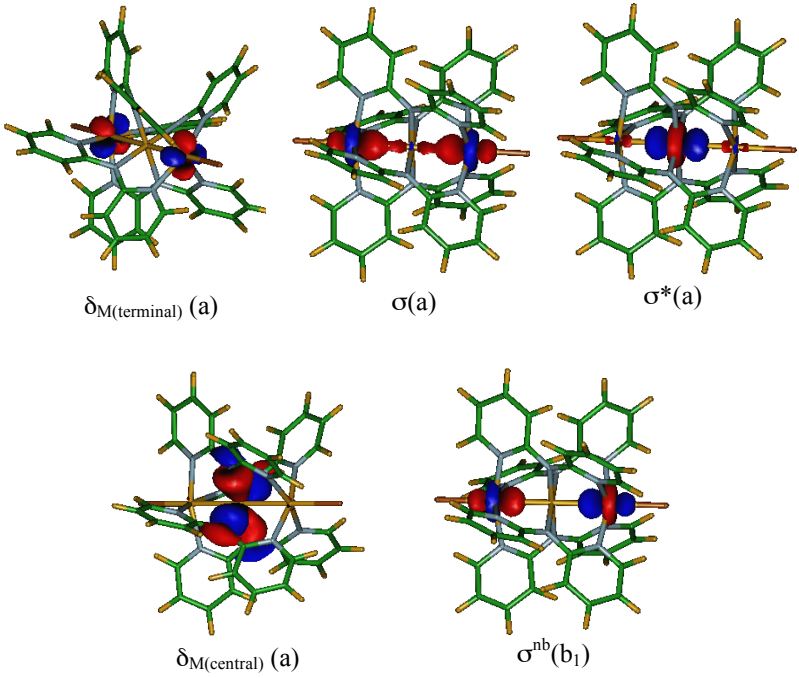

Figure 3.9. Doubly occupied orbitals added to CAS(3,3) in **3** and **4** complexes. The symmetry of each orbital is given in parenthesis.

The value of *J* at the CASPT2 level reaches to –122 cm^{-1} for **3**, which is about a factor of three smaller than the experimental value of –373 cm^{-1}.[31] This is a rather unexpected result. Experience shows that CASPT2 based on a minimal CAS reproduces 50-70% of the experimental coupling, and after extending the active space even better agreement is usually obtained. Therefore,

we explored possible sources for this notable discrepancy. The δ interaction occurs between adjacent metal atoms through some ligand bonds. Hence, not considering the ligand orbitals explicitly could be important in superexchange mechanism influencing the final result. Accordingly, we intended to put additional ligand orbitals to the active space. Nevertheless, these ligand orbitals are transformed to Cu-d orbitals with extra radial nodes (so-called 3d′ orbitals) during the orbital optimization. These d orbitals significantly lower the total CASSCF energy but have no differential effect on the electronic states involved in the magnetic coupling process. The importance of introducing the ligand orbitals in the active space can be assessed by performing RASSCF calculations in which all fifteen Cu-3d orbitals are in the active space and additional configurations that involve single and double replacements in the occupied ligand orbitals and virtual Cu-3d′ orbitals are added to the wave function. Dynamical electron correlation can be introduced by means of the recently presented RASPT2 method.[46] This choice of active space gives the desired orbitals but does no affect the magnetic coupling parameter, $J = -92$ cm^{-1} for RASPT2, the same order of magnitude as our final CASPT2 estimate.

Table 3.5. Calculated $-J$ (cm^{-1}) for the minimal and extended spaces at CASSCF and CASPT2 levels for the neutral species **3** and **4**.

	CAS(3,3)	CASPT2	Ext. CAS	CASPT2	DFT[a]	exp.[b]
3	9.8	53	33[c]	$J_1 = 122$ ($J_2 = 4.8$)	436	373
4	91	435	130[d]	$J_1 = 521$ ($J_2 = -37.6$)[e]	1270	–

(a) B3LYP functional, ref 3. (b) ref 31. (c) CAS(13,14). (d) CAS(13,13). (e) Level Shift = 0.1

Similar conclusions have been derived from DDCI calculations on **3**. The full DDCI calculation is too large to be completed, but the configuration space can be reduced by performing a dedicated orbital transformation on the molecular orbitals,[47] which orders the orbitals by increasing importance to the energy difference of the states of interest. After removing the less important orbitals, a

DDCI calculation can be performed on **3**, resulting in an approximate $J = -75$ cm^{-1}, depending on the number of molecular orbitals considered in the calculation. The full DDCI value would probably be somewhat higher, but other DDCI calculations with dedicated molecular orbitals show that a reasonable estimate of J can be obtained with approximately 50% of the molecular orbitals,[47] exactly the range where the DDCI calculations for **3** have been performed. At present, we lack information to rationalize the anomalous large discrepancy between CASPT2 and experiment. Neither the perturbative approach nor the choice of active space can be the origin.

In order to rationalize the size of the coupling between the nearest neighbor Cu ions, we compare the EMAC system to the well-known benchmark molecule $Cu_2(ac)_4$ (ac = acetate) ($Cu_2(\mu\text{-}CH_3COO)_4(H_2O)_2$), which shows a magnetic coupling constant of ~ –300 cm^{-1},[48-50] similar to what has been reported for **3**. The magnetic interaction path is similar for $Cu_2(ac)_4$ and **3**, but two important differences can be observed. In the first place, the Cu atoms in $Cu_2(ac)_4$ are coordinated by more electronegative atoms than in **3**, and second, the dihedral angle L-Cu-Cu-L (the twist angle) is zero in the acetate compound while it is as large as 21º in **3**. We know that the magnetic coupling has two parts: the direct exchange between the magnetic orbitals, which is a ferromagnetic contribution (positive) and occurs through space, and the kinetic exchange, which is an antiferromagnetic contribution (negative) and happens through the bridging ligands. When the twist angle is zero, both contributions are at their maximum value. Small twist angles tend to increase the magnetic coupling as the direct exchange integral is reduced (less overlap). However, for larger twist angles the magnetic interaction path over the ligand becomes more distorted and less favorable, causing a reduction of the magnetic coupling constant (Figure 3.10). We have reduced the mentioned dihedral angle from an initial value of 21.3º to 16.3º and then to 13.3º. For smaller angles, the two hydrogens of neighboring pyridine rings become too close and bonding interactions appear. The quantities of J for the two new dihedral angles have been calculated –69 cm^{-1} and –78 cm^{-1}, respectively, at the minimal CASPT2 level, which suffices for this qualitative analysis. The initial value was $J = -53$ cm^{-1}. This confirms that the large dihedral

angle makes the coupling weaker. On the other hand, the weaker electronegativity of the N atoms coordinating the Cu ions in **3** favors a stronger coupling in comparison to $Cu_2(ac)_4$, where the first coordination sphere is formed by oxygens. The net effect of these opposite effects is difficult to estimate but it seems reasonable that the magnetic coupling between nearest neighbors in **3** is approximately the same as in $Cu_2(ac)_4$. The slightly smaller Cu–Cu distance in **3** (2.53 Å versus 2.61 Å in $Cu_2(ac)_4$) can increase the importance of the direct exchange somewhat, but not to such an extent that the magnetic coupling is much smaller than in $Cu_2(ac)_4$ as predicted by our calculations.

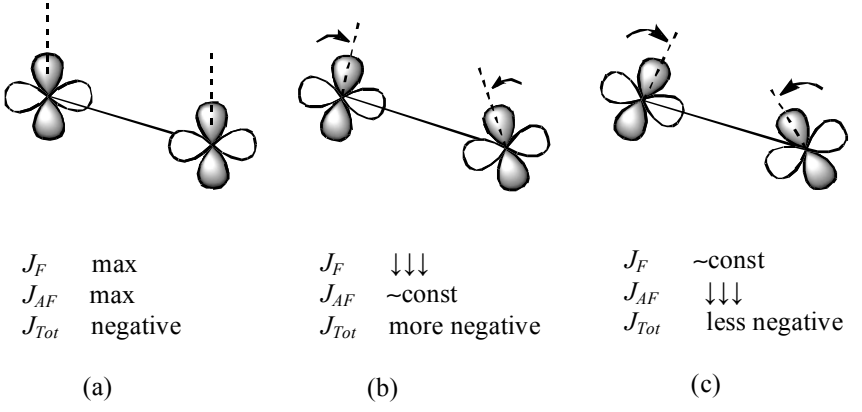

Figure 3.10. Variation of total magnetic coupling with different twist angles; (a) zero (b) small (c) large.

One may looks for the origin of this large discrepancy in **3** in the geometry. For this reason we have done the same calculations with the main experimental distances (like **1**). As expected, the *J* value hardly varies and just reaches to −124 cm^{-1}. We did not expect to restore ~200 cm^{-1} just by small changes in the geometry, especially knowing that the magnetic coupling occurs through the δ-path.

For complex **4**, we report $J = –521$ cm^{-1}, which is less than half of the DFT value. The increase of magnitude of *J* in CASPT2 calculations in both

complexes is similar so the $J_{Ag}/J_{Cu} \approx 4$ remains the same as for the extended CAS. In **4**, the effect of extending the CAS is not so considerable in CASPT2 calculations and the *J* values of CASPT2 of minimal and extended CAS are similar.

3.4. Conclusions

The magnetic coupling parameter in a series of relatively large molecules (89 atoms) containing three TM atoms has been calculated with the CASPT2 method. Three sets of $M_3(dpa)_4Cl_2$ complexes have been studied in this work, each containing one real and one hypothetical molecule. To facilitate the comparison of the results between real and hypothetic molecules, we tried to use the same active space within each set. Moreover, all molecules have been studied with their optimized geometries. The most relevant conclusions are the following:

The calculated magnetic coupling constants *J* for real system $\mathbf{3}^+$ containing two magnetic centers is in excellent agreement with the experimental values, while for **1** the calculated *J* is quite far from its experimental value. An important variation in the strength of *J* is found in $Ni_3(dpa)_4Cl_2$ when the distance between magnetic centers changes. This strong dependence of *J* on the metal-metal distance brings the conclusion that the interaction existing inline with the Ni_3 axis is the dominant part of the total magnetic coupling. That is, the magnetic interaction that occurs by means of the σ orbitals is much stronger than that coming from the δ orbitals. This particular issue is explored in depth in the next chapter to get quantitative information. It is worth mentioning that when the experimental Ni-Ni distance is used, the calculated *J* becomes closer to the measured value.

On the other hand, calculations performed on compound **3**, a system with three magnetic centers, only provide ~33% of the experimental *J*. Knowing that neither the perturbative approach nor the choice of active space can be the origin of such an anomalous large discrepancy between the computed and experimental *J*, it might be interesting in the near future to look closer into the source of error. In the hypothetical systems **4** and $\mathbf{4}^+$, the predicted values for *J* are always

smaller than those obtained by DFT. This behavior was expected beforehand. Nevertheless, for **2**, the *ab initio* method predicts a larger value for *J* than the DFT method, the same trend as **1**.

Since the minimal CAS is not sufficient to obtain quantitatively correct *J* values, extended active spaces have been used for all the complexes. These calculations reveal that the magnitude of *J* is very sensitive to the type and number of active orbitals. Indeed, a broad range of *J*-values is obtained as different orbitals are considered, especially in complexes in which *J* originates in δ interactions only, namely **3**, **4**, $\mathbf{3}^+$ and $\mathbf{4}^+$. In contrast, the tentative determination of the most important orbitals in compounds of the $S = 1$ family, namely **1** and **2**, is straightforward. As the magnetic interactions in the latter complexes are governed by σ and δ orbitals, selecting the orbitals necessary to obtain quantitatively correct *J* is undeviating and just needs to describe properly the σ part. This fact, although not proved here, may imply that the part of *J* coming from the coupling of electrons occupying σ orbitals is much stronger that that coming from δ electrons.

Despite the fact that the *J* parameters of compounds **3**, **4**, $\mathbf{3}^+$ and $\mathbf{4}^+$ are attributed to a mechanism based on δ-like interactions, the existence of σ orbitals in an extended CAS is important to obtain parameters with a quantitative accuracy. In other words, these calculations do not provide precise *J* parameters if just δ orbitals are included in the CAS. The exact character of the active orbitals in these extended CAS calculations is the result of a delicate balance between effects that mainly affect the magnetic interaction and other correlation effects that lower the total energy but do not contribute to the energy difference between the states of interest. In some cases, it might not be possible to introduce the desired orbitals in the CAS. Then the RASSCF approach may be an interesting option.

The CASPT2 method is an alternative to DFT in the calculation of magnetic parameters in large systems as EMACs, giving results with semi-quantitative precision. In all molecules discussed here, the dynamical electron correlation provides the main part of *J*.

References

[1] M. M. Rohmer, M. Bénard, *J. Am. Chem. Soc*. 120 (1998) 9372.

[2] M. M. Rohmer, A. Strich, M. Bénard, J. P. Malrieu, *J. Am. Chem. Soc*. 123 (2001) 9126.

[3] M. Bénard, J. F. Berry, F. A. Cotton, C. Gaudin, X. López, C. A. Murillo, M. M. Rohmer, *Inorg. Chem*. 45 (2006) 3932.

[4] X. López, M. Bénard, M. M. Rohmer, *J. Mol. Struct. THEOCHEM* 777 (2006) 53.

[5] X. López, M. Bénard, M. M. Rohmer, *Inorg. Chem*. 46 (2007) 5.

[6] M. M. Rohmer, I. P. C. Liu, J. C. Lin, M. J. Chiu, C. H. Lee, G. S. Lee, M. Bénard, X. López, S. M. Peng, *Angew. Chem., Int. Ed*. 46 (2007) 3533.

[7] I. P. C. Liu, G. H. Lee, S. M. Peng, M. Bénard, M. M. Rohmer, *Inorg. Chem*. 46 (2007) 9602.

[8] X. López, M. M. Rohmer, M. Bénard, *J. Mol. Struct.* 890 (2008) 18.

[9] M. M. Rohmer, M. Bénard, *Chem. Soc. Rev*. 30 (2001) 340.

[10] P. Kiehl, M. M. Rohmer, M. Bénard, *Inorg. Chem*. 43 (2004) 3151.

[11] K. Andersson, P.-Å. Malmqvist, B. O. Roos, A. J. Sadlej, K. Wolinski, *J. Phys. Chem*. 94 (1990) 5483.

[12] K. Andersson, P. Å. Malmqvist, B. O. Roos, *J. Chem. Phys*. 96 (1992) 1218.

[13] J. Miralles, J. P. Daudey, R. Caballol, *Chem. Phys. Lett*. 198 (1992) 555.

[14] N. H. F. Beebe, J. Linderberg, *Int. J. Quantum Chem*. 7 (1997) 683.

[15] H. Koch, A. Sánchez de Merás, T. B. Pedersen, *J. Chem. Phys*. 118 (2003) 9481.

[16] F. Aquilante, P.-Å. Malmqvist, T. B. Pedersen, A. Ghosh, B. O. Roos, *J. Chem. Theory. Comput*. 4 (2008) 694.

[17] S. Saebo, P. Pulay, *Annu. Rev. Phys. Chem*. 44 (1993) 213.

[18] M. Schütz, H. J. Werner, *J. Chem. Phys.* 114 (2001) 661.

[19] J. E. Subotnik, A. Sodt, M. Head-Gordon, *J. Chem. Phys.* 128 (2008) 034103.

[20] F. Bessac, S. Hoyau, D. Maynau, *J. Chem. Phys*. 123 (2005) 104105.

[21] T. Ayed, N. Guihéry, B. Tangour, J. C. Barthelat, *Theor. Chem. Acc*. 116 (2006) 497.

[22] C. de Graaf, R. Broer, W. C. Nieuwpoort, *Chem. Phys. Lett*. 271 (1997) 372.

[23] S. Yamanaka, M. Okumura, H. Nagao, K. Yamaguchi, *Chem. Phys. Lett*. 233 (1995) 88.

[24] C. de Graaf, F. Illas, *Phys. Rev. B* 63 (2001) 014404.

[25] C. Sousa, C. de Graaf, F. Illas, G. Pacchioni, *Prog. Theor. Chem. Phys*. 7 (2000) 227.

[26] C. de Graaf, C. Sousa, I. de P. R. Moreira, F. Illas, *J. Phys. Chem. A* 105 (2001) 11371.

[27] A. Ceulemans, G. A. Heylen, L. F. Chiboatru, T. L. Maes, K. Pierloot, C. Ribbing, L. G. Vanquickenborne, *Inorg. Chim. Acta*. 251 (1996) 15.

[28] M. F. A. Hendrickx, S. Clima, L. Chibotaru, A. Ceulemans, *J. Phys. Chem. A* 109 (2005) 8857.

[29] Gaussian 03, Revision C.01, M. J. Frisch, G. W. Trucks, H. B. Schlegel, G. E. Scuseria, M. A. Robb, J. R. Cheeseman, J. A. Montgomery, Jr., T. Vreven, K. N. Kudin, J. C. Burant, J. M. Millam, S. S. Iyengar, J. Tomasi, V. Barone, B. Mennucci, M. Cossi, G. Scalmani, N. Rega, G. A. Petersson, H. Nakatsuji, M. Hada, M. Ehara, K. Toyota, R. Fukuda, J. Hasegawa, M. Ishida, T. Nakajima, Y. Honda, O. Kitao, H. Nakai, M. Klene, X. Li, J. E. Knox, H. P. Hratchian, J. B. Cross, V. Bakken, C. Adamo, J. Jaramillo, R. Gomperts, R. E. Stratmann, O. Yazyev, A. J. Austin, R. Cammi, C. Pomelli, J. W. Ochterski, P. Y. Ayala, K. Morokuma, G. A. Voth, P. Salvador, J. J. Dannenberg, V. G. Zakrzewski, S. Dapprich, A. D. Daniels, M. C. Strain, O. Farkas, D. K. Malick, A. D. Rabuck, K. Raghavachari, J. B. Foresman, J. V. Ortiz, Q. Cui, A. G. Baboul, S. Clifford, J. Cioslowski, B. B. Stefanov, G. Liu, A. Liashenko, P. Piskorz, I. Komaromi, R. L. Martin, D. J. Fox, T. Keith, M. A. Al-Laham, C. Y. Peng, A. Nanayakkara, M. Challacombe, P. M. W. Gill, B. Johnson, W. Chen, M. W. Wong, C. Gonzalez, and J. A. Pople, Gaussian, Inc., Wallingford CT, 2003.

[30] R. Clérac, F. A. Cotton, K. R. Dunbar, C. A. Murillo, I. Pascual, X. Wang, *Inorg. Chem*. 38 (1999) 2655.

[31] J. F. Berry, F. A. Cotton, L. Peng, C. A. Murillo, *Inorg. Chem*. 42 (2003) 377.

[32] J. F. Berry, F. A. Cotton, L. M. Daniels, C. A. Murillo, X. Wang, *Inorg. Chem*. 42 (2003) 2418.

[33] G. Karlström, R. Lindh, P. Å. Malmqvist, B. O. Roos, U. Ryde, V. Veryazov, P. O. Widmark, M. Cossi, B. Schimmelpfennig, P. Neogrady, L. Seijo, *Comput. Mater. Sci*. 28 (2003) 222. *MOLCAS* Version 7.0. Department of Theoretical Chemistry, University of Lund.

[34] B. O. Roos, R. Lindh, P.- Å. Malmqvist, V. Veryazov, P. O. Widmark, *J. Phys. Chem. A* 109 (2005) 6575.

[35] B. O. Roos, R. Lindh, P.-Å. Malmqvist, V. Veryazov, P. O. Widmark, *J. Phys. Chem. A* 108 (2004) 2851.

[36] P. A. M. Dirac, *Proc. R. Soc. London, Ser. A* 112 (1926) 661.

[37] W. Heisenberg, *Z. Phys*. 38 (1926) 411.

[38] J. H. van Vleck, *Theory of electric and Magnetic Susceptibilities,* Oxford University Press, London, 1932.

[39] N. Queralt, D. Taratiel, C. de Graaf, R. Caballol, R. Cimiraglia, C. Angeli, *J. Comput. Chem.* 29 (2008) 994.

[40] N. Ben Amor, D. Maynau, *Chem. Phys. Lett*. 286 (1998) 211.

[41] R. Caballol, J. P. Malrieu, *Chem. Phys. Lett*. 188 (1992) 543.

[42] R. Caballol, J. P. Malrieu, J. P. Daudey, O. Castell, SCIEL program, Rovira i Virgili University, Tarragona, Spain, 1998.

[43] S. M. Peng, C. C. Wang, Y. L. Jang, Y. H. Chen, F. Y. Li, C. Y. Mou, M. K. Leung, *J. Magn. Magn, Mater*. 209 (2000) 80.

[44] The geometry of molecule **1** with experimental Ni-Ni distance has been obtained by keeping the Cl-Ni-Ni-Ni-Cl chain frozen and optimizing the rest of the molecule with DFT.

[45] We simulated the magnetic susceptibility curve (χT vs. T) for the Cu_3 complex with $J_2 = 0$ and -4.8 cm^{-1} resulting in two perfectly superimposed curves up to 300 K.

[46] P. Å. Malmqvist, K. Pierloot, A. Rehaman, M. Shahi, C. J. Cramer, L. Gagliardi, *J. Chem. Phys.* 128 (2008) 204109.

[47] C. J. Calzado, J. P. Malrieu, J. Cabrero, R. Caballol, *J. Phys. Chem. A* 104 (2000) 11636.

[48] B. N. Figgis, R. L. Martin, *J. Chem. Soc*. (1956) 3837.

[49] H. U. Güdel, A. Stebler, A. Furrer, *Inorg. Chem*. 18 (1979) 1021.

[50] P. de Loth, P. Cassoux, J. P. Daudey, J. P. Malrieu, *J. Am. Chem. Soc*. 103 (1981) 4007.

Chapter 4

Magnetic Properties of $M_3(dpa)_4Cl_2$ Systems with S = 1 Centers with DFT: Beyond the Heisenberg Behaviour or Beyond Hybrid Functionals

4.1. Introduction and Objectives

In the previous chapter we have reported the J values of $Ni_3(dpa)_4Cl_2$ and $Pd_3(dpa)_4Cl_2$ complexes (magnetic systems with two S = 1 sites) as the mean value of the $E(S)–E(T)$ and $\frac{1}{2}[E(T) –E(Q)]$ energy differences. We have seen that, in Ni_3, the J obtained from the two lowest states is quite different (by ~35 cm^{-1}) to that obtained from the two highest ones (see Figure 3.6). In the Pd_3 complex, the difference between the calculated magnetic couplings in both ways reaches to 700cm^{-1}. This large difference can possibly be related to the use of the simple form of the Heisenberg Hamiltonian for describing the magnetic interactions in these systems. This is a motivation to the study of deviations from the Heisenberg Hamiltonian in systems with S = 1 magnetic sites in this chapter.

In chapter 3 we have also seen that CASPT2 does not fully reproduce the magnetic exchange parameter of the $Ni_3(dpa)_4Cl_2$ complex, not even taking the experimental Ni-Ni distances ($-150cm^{-1}$). With DFT/B3LYP, an unusual underestimation of J is also observed. To clarify this behavior, we decided to go beyond the hybrid functionals and examine the performance of other ones.

Magnetic interactions are usually described by the simple phenomenological Heisenberg Hamiltonian:[1-2]

$$\hat{H} = \sum_{i<j} J_{ij} S_i \cdot S_j \qquad (1)$$

that contains the bilinear exchange integral J_{ij} accounting for the magnetic coupling between centers i and j. If the magnetic behavior of a molecule can be properly fitted to eq. (1), it can be considered as an isotropic Heisenberg system. The application of this Hamiltonian to compounds with high spin moments is done routinely, although it should be performed with care, since the electronic nature of magnetic centers may affect the applicability of this simple spin Hamiltonian. For this reason, in some cases, a more general form of the spin Hamiltonian must be applied to account for deviations to the Heisenberg behavior for compounds with local $S > 1/2$. What are the principal sources of deviation? For $S = 1$ systems,[3] the model space of the Heisenberg Hamiltonian is spanned by the linear combinations of products of the local ground state spin functions of each magnetic center, i.e., the local triplets. It has been pointed out that the existence of low-lying atomic non-Hund states (local singlet excited states) can be important in some cases.[4] The interaction of these excited states with the model space configurations can lead to deviations from the regular Landé pattern. These so-called isotropic deviations contrast with the anisotropic deviations to the standard magnetic behavior. The latter find their origin in spin-orbit interactions of the unpaired electrons and lead to a zero-field splitting of the different $M_{s,tot}$ components of the spin functions ($M_{s,tot}$ being the sum of local M_s values) even in the absence of an external magnetic field. In the herein studied complexes, these effects are not considered since they are expected to be small. The $S = 1$ magnetic centers have a nearly octahedral coordination and the

zero-field splitting is strictly zero in perfect octahedral symmetry. Anyhow, anisotropic effects do not influence the extraction of the isotropic interactions. The complexes studied here are in the strong-exchange limit (as shown below) implying that there is no appreciable spin-orbit interaction between the fundamental quintet, triplet and singlet states. In these cases, the isotropic part of the interactions can be determined independently of the anisotropic part.[5,6] To proof that the systems we are dealing with in the present work are indeed in the strong exchange limit, we performed a preliminary calculation on the single ion anisotropy of the Ni^{2+} ion in $[Ni_2(napy)_4Cl_2]^{2+}$ since its magnetic sites and also the arrangement of organic ligands around the metal chain are very similar to those in trimetallic complexes . Following the computational strategy outlined in ref. 6, the isotropic interaction was found to be about 20 times larger than the single ion anisotropy, i.e., a clear case of the strong exchange limit.

Considering a system with two magnetic centers with $S = 1$ each, there are three different electronic configurations that should be taken into account to obtain an accurate first-order description of the magnetic coupling. In the first place, there are the so-called neutral determinants. The magnetic centers stay in their formal oxidation state and the local triplet couplings are maintained, leading to singlet, triplet and quintet states for the whole molecule. In the second place, one should consider the ionic determinants in which one electron is transferred from site i to site j or vice-versa. The ionic determinants largely enhance the magnetic coupling but do not lead to deviations from the standard magnetic behavior.[4] Finally, the non-Hund states in which the number of electrons per magnetic site remains as in the neutral determinants, but the local triplets are changed to singlet on one (or both) site(s). These non-Hund states interact in a non-uniform manner with the states contained in the Heisenberg model space.[4] The coupling of the ionic and the neutral configurations is essential in the description of the magnetic interactions and is usually identified as a hopping integral t, as described by the Hubbard Hamiltonian.[7] The energy of the ionic configuration with respect to the neutral one is U. The magnetic coupling constant depends on these two parameters through the second-order perturbative expression $J \propto -t^2/U$. The hopping integral between centers i and j

strongly depends on the nature of the orbitals involved in such a process. In the present case, as will be discussed later, there are two possible hopping integrals (t_σ and t_δ), which relate to two different magnetic interaction paths denoted by J_σ and J_δ.

In a series of recent works, Guihéry and collaborators have developed,[4,8-9] explained and tested[10] a more general form for the Spin Hamiltonian that can be applied to S = 1 compounds. The spin Hamiltonian, called non-Heisenberg in short from now on, contains the well-known biquadratic interaction (second term) and a three-body operator (third term):

$$\hat{H} = \sum_{\langle i,j \rangle} J_{ij}^{eff}\, \hat{S}_i \cdot \hat{S}_j + \lambda_{i,j} (\hat{S}_i \cdot \hat{S}_j)^2$$

$$+ \sum_{i,\langle j,k \rangle} \frac{B_{ji}\, B_{ik}}{2K} \left[(\hat{S}_i \cdot \hat{S}_j) \cdot (\hat{S}_i \cdot \hat{S}_k) + (\hat{S}_i \cdot \hat{S}_k) \cdot (\hat{S}_i \cdot \hat{S}_j) - (\hat{S}_i \cdot \hat{S}_i) \cdot (\hat{S}_j \cdot \hat{S}_k) \right] \qquad (2)$$

These additional interactions arise from contributions of the locally excited states (non-Hund states) to the N-electron wave function. The three-body interaction was found to be as important as the biquadratic exchange interactions in the magnetic coupling between Ni^{2+} ions along a linear Ni–O–Ni–O–Ni exchange path.[9]

To the fourth order of perturbation, and considering the local singlets S^0 as the only accessible non-Hund states, the magnitude of mentioned interactions can be obtained from eqs. (3-6), where $(t_\sigma)_{ij}$ is the hopping integral between two σ orbitals and $(t_\delta)_{ij}$ is the hopping integral between two δ orbitals. U and K are the on-site repulsion integral and intrasite exchange integral, respectively.

We herein deal with n = 3 homo- and heterometallic symmetric systems, $[Ni_3(dpa)_4Cl_2]$, $[NiPdNi(dpa)_4Cl_2]$ and $[Pd_3(dpa)_4Cl_2]$ (dpa: dipyridylamido). The central metal atom is diamagnetic and each terminal metal is paramagnetic with S = 1. Thus, four unpaired electrons interact, two of them occupy σ-type orbitals and the other two are in δ-type orbitals. Our purpose is to gain some more insight into the magnetic properties of such EMACs by means of density functional calculations. The main goals of the present work are: (i) to establish

the importance of the terms that introduce deviations to the standard Heisenberg Hamiltonian in compounds with S = 1 centers, (ii) to compute the magnetic parameters of the general form of Spin Hamiltonian in eq. (2) and (iii) to determine the relative contribution of the σ- and δ-type interactions to the total magnetic coupling. In this study we also tackle a smaller bimetallic Ni model compound, $[Ni_2(napy)_4Cl_2]^{2+}$ (napy = naphtyridine), to check the validity of the DFT results against the more accurate Difference Dedicated Configuration Interaction (DDCI) method.[11-13]

$$J_{ij} = \frac{(t_\sigma)_{ij}^2}{U} + \frac{(t_\delta)_{ij}^2}{U} \tag{3}$$

$$B_{ij} = \frac{(t_\sigma)_{ij}^2}{U} - \frac{(t_\delta)_{ij}^2}{U} \tag{4}$$

$$J_{eff} = \frac{(t_\sigma)_{ij}^2}{U} + \frac{(t_\delta)_{ij}^2}{U} + \frac{B_{ij}^2}{K} = J_{ij} + \frac{B_{ij}^2}{K} \tag{5}$$

$$\lambda_{i,j} = \frac{B_{ij}^2}{K} - \frac{J_{ij}^2}{4K} \tag{6}$$

Figure 4.1 shows the structure of bi- and trimetallic systems. At the end of this chapter we explore the origin of underestimation of J encountered in the previous DFT-based works in $Ni_3(dpa)_4Cl_2$ complex.

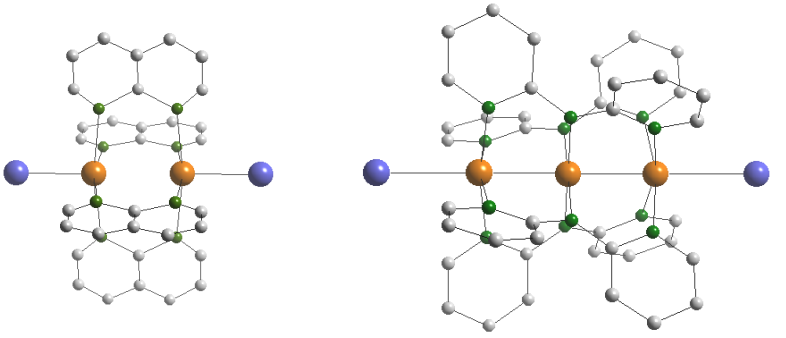

Figure 4.1. The bimetallic $[Ni_2(napy)_4Cl_2]^{2+}$ model system (left) and the trimetallic $[M_3(dpa)_4Cl_2]$ EMAC (right). Color-coding: orange-metal; green-nitrogen; blue-chlorine; light gray-carbon. Hydrogen atoms are not drawn for clarity.

4.2. DFT-KS Description of the Magnetic Interactions between Two *S* = 1 Centers

DDCI is considered as one of the most accurate computational methods to obtain magnetic coupling constants. The method has been applied to many systems ever since its introduction in 1992. In general, DDCI estimates are in good agreement with experimental data; see, for example, refs 14-16 among many others. This method is, however, computationally expensive and virtually impossible to be applied to medium- and large-sized systems. Reasonably accurate and computationally less expensive solutions are achieved by means of the DFT. In this methodology, the most widely used Kohn-Sham (KS) version is based on a monodeterminantal assumption, which is the main limitation of this methodology. This implies that, for spin-coupled open-shell systems (such as magnetic systems), the DFT description of the electronic structure is severely limited. However, this shortcoming can be pragmatically bypassed with the broken symmetry approach, which provides helpful solutions and have amply shown their usefulness in the description of isotropic Heisenberg systems.[17-24]

Table 4.1. Monodeterminantal solutions and associated second-order perturbative energy expressions for $M_{s,tot}$ = 2, 1 and 0.

$M_{s,tot}$	Configuration	Atom 1	Atom 2	$E^{(2)\,a,b}$
2	D^1D^1	$\lvert\sigma_1\delta_1\rvert$	$\lvert\sigma_2\delta_2\rvert$	$-2K$
0	D^1D^{-1}	$\lvert\sigma_1\delta_1\rvert$	$\lvert\bar{\sigma}_2\bar{\delta}_2\rvert$	$-2K-2\frac{(t_\sigma)^2}{U}-2\frac{(t_\delta)^2}{U}$
1	D^1D^0	$\lvert\sigma_1\delta_1\rvert$	$\lvert\bar{\sigma}_2\delta_2\rvert$	$-K-2\frac{(t_\sigma)^2}{U}$
0	D^0D^0	$\lvert\sigma_1\bar{\delta}_1\rvert$	$\lvert\bar{\sigma}_2\delta_2\rvert$	$-2\frac{(t_\sigma)^2}{U}-2\frac{(t_\delta)^2}{U}$

(a) The denominators in the energy expressions have been simplified from ($U - K$) to U under the assumption $U >> K$ throughout this work. See ref. 10 for details. (b) As we deal with systems with only two magnetic centers, λ_{ij}, B_{ji} (B_{ik}) and J_{ij}^{eff} are simplified to λ, B and J_{eff} respectively.

A strategy that goes beyond the usual broken symmetry approximation and gives access to non-Heisenberg terms was reported by Labèguerie et al.[10] They have used the other broken symmetry solutions of intermediate values of $M_{s,tot}$, as well as $M_{s,tot}^{max} = 2$ and $M_{s,tot}^{min} = 0$. [25] Let us denote D^{M_s} an atomic determinant with a given M_s value. Within this notation, the previous solutions can be written as D^1D^1 and D^1D^{-1} (or $D^{-1}D^1$), respectively. The other neutral monodeterminantal solutions are: D^0D^1 and D^1D^0 for $M_s = 1$, and D^0D^0 for $M_s = 0$. At the zeroth-order of perturbation, the energies $E^{(0)}$ of all solutions arise from the intrasite exchange integral K, which always favors the maximal local M_s. $E^{(0)} = -2K$ for D^1D^1, D^1D^{-1} and $D^{-1}D^1$). For D^0D^1 (or D^1D^0) and D^0D^0, the energies are $-K$ and 0, respectively. The ionic configurations that are treated at the second order of perturbation in the Heisenberg Hamiltonian incorporate the interatomic kinetic exchange contributions to the zeroth order energies. The energy expression of each solution at the second order of perturbation, $E^{(2)}$, is shown in Table 4.1. Each magnetic center contains one σ and one δ localized orbital. By calculating the energy of these four solutions, one may determine the magnitude of K, $(t_\sigma)^2/U$ and $(t_\delta)^2/U$ and then obtain the J, J_{eff}, B and λ parameters by eqs. 3-6. The most stable solution in antiferromagnetic systems is D^1D^{-1}, corresponding to an open-shell with $M_s = 0$, followed by the $M_{s,tot} = 2$ determinant D^1D^1. These two solutions are based on local Hund states. Determinants D^1D^0 and D^0D^0 are products of local non-Hund states, and hence, much higher in energy.

4.3. Computational Details

Geometry optimizations and energy calculations in this work have been performed with the DFT methodology using the B3LYP hybrid exchange-correlation functional (20% exact Fock exchange) implemented in the Gaussian03 package.[26] Variations in the percent of exact Fock exchange have been utilized where indicated. The optimized geometries of the hypothetical trimetallic complexes $[NiPdNi(dpa)_4Cl_2]$ and $[Pd_3(dpa)_4Cl_2]$ have been taken from ref. 27. Concerning the $[Ni_2(napy)_4Cl_2]^{2+}$ model system, a Ni-Ni distance of

2.912 Å has been assumed for reasons discussed below and the rest of the molecular geometry has been optimized in its ground state. The geometry of $[Ni_3(dpa)_4Cl_2]$ has been optimized with the fixed Ni-Ni, Ni-N and Ni-Cl experimental distances.[28] Table 4.2 shows some important geometrical parameters for the mentioned molecules in their ground states. Single point energy calculations of all electronic configurations were performed at the geometry of the ground state. We used the unrestricted formalism for all the open shell configurations. All-electron valence double-ζ basis sets (D95V) were used to describe C, and H atoms, and a full double-ζ (D95) basis set supplemented with one d polarization function for N, and a double-ζ (LANL2DZ basis) for Cl. For the metal atoms, the valence shells were described with LANL2DZ basis supplemented with one *f*-type polarization function with exponent 3.13 for Ni and 1.472 for Pd. For the heavy atoms (Cl, Ni and Pd), the core electrons were modeled with a Los Alamos core potential.

Table 4.2. Selected interatomic distances (Å) for $[Ni_2(napy)_4Cl_2]^{2+}$, $Ni_3(dpa)_4Cl_2$, $NiPdNi(dpa)_4Cl_2$ and $Pd_3(dpa)_4Cl_2$.

	Ni_2	Ni_3[a]	NiPdNi[b]	Pd_3[b]
M–M	2.912	2.43	2.513	2.544
M–Cl	1.856	2.33	2.398	2.564
$M–N_{term}$	1.995	2.09	2.162	2.258
$M–N_{cent}$		1.89	2.040	2.062

(a) The experimental distances reported in ref. 29. (b) DFT optimized geometries taken from ref. 27.

For $[Ni_2(napy)_4Cl_2]^{2+}$, DDCI calculations were carried out to check the validity of the DFT extracted parameters to address the deviations from the Heisenberg Hamiltonian. The DDCI expansion of the wave function includes all single and double replacements from a CASSCF reference wave function, excluding the double replacements from inactive to virtual orbitals. These configurations contribute in the quasi-degenerate second-order perturbation theory equally to the energy of the different states, and hence, can be omitted in the calculation of vertical energy differences.[30] The active space in the CASSCF

calculation contains the four magnetic orbitals with mainly Ni-3d character and the four unpaired electrons present in the molecule. The CASSCF calculations have been performed with the MOLCAS 7 package.[31] The one-electron basis set used to expand the MOs is of the atomic natural orbital type for all atoms. We have employed ANO-RCC type for Ni atoms (5s,4p,3d), for the bridging N atoms (3s,2p) and for axial Cl ligands (4s,3p). For C and H atoms, we used (3s,2p) and (2s) basis sets, respectively.[32]

The DDCI formalism requires the use of a common set of orbitals for the states of interest. Therefore, average natural orbitals have been constructed by diagonalizing the average of the singlet, triplet and quintet CASSCF density matrices. To reduce the computational cost of the DDCI calculation, these average MOs were transformed to so-called dedicated orbitals.[33] This unitary transformation consists in a block diagonalization of the inactive and virtual part of the DDCI2 difference density matrix $\rho_{diff} = (2\rho_Q - \rho_T - \rho_S)$, where Q, T and S stand for quintet, triplet and singlet, respectively. The resulting dedicated orbitals are ordered by increasing relevance to the energy difference between the states and the less relevant orbitals were not used in the generation of the CI expansion. It has been shown that this procedure reproduces the DDCI results obtained with the full MO space at a much lower computational cost.[33-34] The maximum number of dedicated orbitals that we managed to include in present DDCI calculations is 217 over a total of 349 molecular orbitals. As will be shown below this number of MOs is enough to converge to the DDCI result of the complete MO space. DDCI calculations have been performed with the CASDI program.[35]

4.4. Results and Discussion

4.4.1. $[Ni_2(napy)_4Cl_2]^{2+}$ Model System (Ni_2)

In the first part of the study we present a model system with the following characteristics: (1) it contains two S = 1 magnetic centers (Ni atoms), (2) the ligands are as similar as possible to the dpa ligand of real EMACs to make the magnetic coupling comparable, and (3) it is smaller than the 89-atom

$M_3(dpa)_4Cl_2$ nanowires. We found that a naphtyridyl (napy) based molecule accomplishes this list fairly well, although it cannot be considered to be really small for DDCI standards. However, smaller ligands that could mimic the role of polypyridylamides in EMACS are rather crude models since the pyridine rings are mandatory to reproduce (i) the correct difference of basicities between the two types of nitrogen donors, and (ii) the flexibility of the ligand molecules, and more specifically the characteristic twist of dpa and related molecules around the metal chain. The geometry of the $[Ni_2(napy)_4Cl_2]^{2+}$ model system was optimized with DFT, getting to a structure with a σ covalent Ni-Ni bond. Since we needed four unpaired electrons to deal with S = 1 magnetic centers, such σ bond is inadequate and must be removed. To this end, we performed a Ni-Ni distance scan, where at each step the rest of the molecule was optimized. We found an electronic structure convenient for our goal at d(Ni-Ni) = 2.912 Å (significantly longer than the B3LYP equilibrium distance of ~2.5 Å).

DFT calculations: We have computed the energy of the solutions listed in Table 4.1. It is important to note that the $\{\sigma_1, \sigma_2, \delta_1, \delta_2\}$ set of localized orbitals are not exactly the same in all the solutions considered since the process of convergence of each broken symmetry solution has produced new orbitals adapted to the particular spin orientations. That is, each broken symmetry solution contains a particular degree of electron delocalization and thus a slightly different amount of ionic character. Specifically, the ionic contribution is strictly zero in the quintet determinant. For simplicity, we have used the same orbital labeling for all the local magnetic orbitals present in the determinants.

Using the second-order perturbative energy expressions of Table 4.1 in combination with equations (3-6), one can obtain the parameters shown in Table 4.3. The corresponding J_{eff} = 550 cm^{-1} is very large, as expected, since it arises from the coupling between two neighboring S = 1 nickel atoms instead of the next-nearest interaction of the typical Ni_3 EMAC. The relative magnitude of J_σ and J_δ reveals a dominating magnetic exchange of σ nature (~80% of total J_{eff}). The calculated λ is 12.7 cm^{-1}, to be compared to the effective coupling, J_{eff} = 550 cm^{-1}, is quite large in comparison with previously reported deviations, which never exceeded 1% of the total coupling.[4,8]

Table 4.3. DFT/B3LYP based electronic and magnetic interaction parameters (cm^{-1}) for $[Ni_2(napy)_4Cl_2]^{2+}$ model complex.

K	J_δ	J_σ	$\%J_\delta$	$\%J_\sigma$	J	B	J_{eff}	λ
4057	87.9	433	16.8	83.2	520	345	550	12.7

DDCI calculations: The same geometry as for DFT energy calculations has been used in DDCI calculations. The magnetic parameters related to non-Heisenberg terms obtained with DDCI are based on the minimal CAS(4,4). This set of orbitals is composed of two linear combinations of δ character and two of σ character, shown in Figure 4.2.

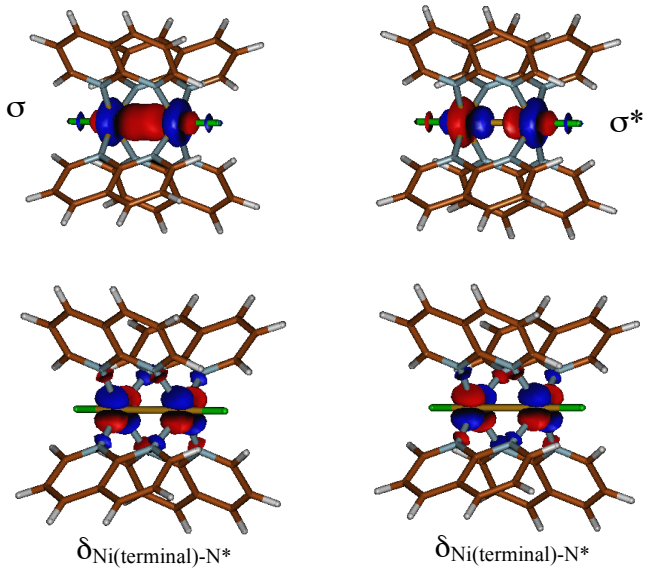

Figure 4.2. Symmetry-adapted orbitals of the CAS(4,4) for the Ni_2 model system.

To extract the magnitude of the biquadratic term from the non-Heisenberg Hamiltonian, equation (2), we have calculated J_1, J_2 and λ using equations (7-9). $E(S)$, $E(T)$ and $E(Q)$ indicate the energy of singlet, triplet and quintet states, respectively.[8]

$$J_1 = \frac{E(S) - E(Q)}{3} \tag{7}$$

$$J_2 = \frac{E(T) - E(Q)}{3} \tag{8}$$

$$\lambda = J_2 - J_1 \tag{9}$$

At this point, we are interested in comparing the DFT and DDCI values of J and λ to validate the DFT method. The DDCI values of J_1 and J_2 hardly depend on the number of dedicated orbitals included, as observed in Table 4.4. We can thus take the DDCI results as accurate enough and a benchmark for the rest of the discussions. From the whole series of DDCI calculations (38 to 217 dedicated orbitals), the values of J_1 and J_2 tend to converge to ~366 and ~392 cm^{-1}, respectively. Also, λ gets larger when more dedicated orbitals are considered as the difference between J_1 and J_2 increases. For DDCI (217), λ is 26.5 cm^{-1} which is a rather large value and our *best* estimate for the Ni_2 model system. Comparing Tables 4.3 and 4.4, it can be seen at a qualitative level that the J and λ parameters are, in general, comparable for DDCI and DFT methods, although the B3LYP functional overestimates the values of J, as expected. In this particular case, the best coincidence of J between the two methodologies would occur at a higher percentage of Fock exchange than the one herein considered. This behavior has also been found in other systems[10] but this cannot be taken as a general fact.

Here, we come shortly back to the question of the magnetic anisotropy in compounds studied here. To demonstrate the assumption that the complexes are in the strong exchange limit, we calculated the single ion anisotropy of the Ni^{2+} ion in the Ni_2 model complex. For this purpose, we followed the strategy described in ref. 6. The calculated value is less than 20 cm^{-1}, which is about twenty times smaller than the estimated isotropic exchange, confirming the complex is in the strong exchange limit, and consequently, no interference of the anisotropy and the isotropic interactions is expected.

Table 4.4. Magnetic interaction parameters (in cm^{-1}) at different approximations to the exact *N*-electron wave function.

	J_1	J_2	$\lambda = J_2 - J_1$
CAS(4,4)	129	122	–6.77
DDCI2	438	458	20.0
DDCI(38)[a]	356	369	13.0
DDCI(87)	365	381	15.5
DDCI(203)	370	393	23.1
DDCI(217)	366	392	26.5

(a) Number of dedicated orbitals in the DDCI run is given in parentheses.

4.4.2. $Ni_3(dpa)_4Cl_2$ System (Ni_3)

The DFT strategy used in the Ni_2 model system to compute the deviation from the Heisenberg behavior is now applied to trinuclear EMAC systems. We are also interested in the quantitative determination of the relative contributions to the total magnetic coupling (*J*) originating in each coupling pathway, namely, those involving the δ and the σ orbitals. The Ni_3 compound appears as a good candidate for such a study since it has been synthesized and structurally characterized,[36] and its magnetic properties have been previously studied, both experimentally and by means of standard, DFT-based broken symmetry calculations.[29,37-39]

Using Labèguerie's approach,[10] we have obtained the relevant parameters for $Ni_3(dpa)_4Cl_2$ listed in Table 4.5. As for Ni_2, J_σ governs the total *J* due to the more effective overlap of σ orbitals, accounting for 95% of the total magnetic coupling. The magnitude of *K* appears similar for the Ni_3 and Ni_2 complexes, and also for the Ni^{2+} ion embedded in the La_2NiO_4 crystal.[10] This confirms that the intrasite exchange integral is essentially an atomic parameter moderately sensitive to the ligand field. In the present case, the difference between the *K* values computed for Ni_2 (~ 4000 cm^{-1}) and Ni_3 (~ 5000 cm^{-1}) can be traced to the different interaction strengths between the magnetic metal atoms and the ligands in both cases, as reflected by the Ni-N distances (Table 4.2). As a first

approximation, the variation of the magnetic coupling in the various Ni compounds can be primarily attributed to the differences in the hopping parameters.

Table 4.5. Electronic and magnetic interaction parameters (in cm^{-1}) for $Ni_3(dpa)_4Cl_2$ compound with B3LYP functional at the experimental[a] and the DFT/B3LYP optimized geometry.[b]

Geom.	K	J_δ	J_σ	$\%J_\delta$	$\%J_\sigma$	J	B	J_{eff}	λ
Exp.	4949	6.13	117	5.0	95.0	123	111	126	1.73
DFT	5050	4.91	82.0	5.6	94.4	86.9	77.1	88.1	0.80

(a) The experimental Ni-Ni, Ni-Cl and Ni-N distances have been taken from ref 29. (b) ref. 38.

With the B3LYP functional, the percent deviation from the Heisenberg Hamiltonian calculated for the Ni_3 complex is modest: $(J_{eff} - J)/J_{eff} \cdot 100 = 1.8\%$, validating the experimental extraction of the magnetic interactions through the simple Heisenberg Hamiltonian. Considering now the criterion λ_{ij} defined in equations (3-6), we have to consider for Ni_3 the case where the σ coupling is largely dominant (95%), which means that B and J have the same order of magnitude, and λ can be approached by the positive term B^2/K alone, which is $(J_\sigma)^2/K$. This term remains negligible due to the small value of B combined with large value of K, from which it can be inferred that the validity of the Heisenberg Hamiltonian in this case is due to the σ coupling remaining relatively weak, although largely dominant. In the case of Ni_2, J_σ is about four times of that in Ni_3 with a quite similar value of K leading to a much larger λ. Even though a more important contribution from J_δ (16.8%, Table 4.3) limits the increase of λ, the validity criterion is nevertheless raised to 12.7 cm^{-1} for Ni_2, compared to only 1.73 cm^{-1} for Ni_3.

4.4.3. Hypothetical $Pd_3(dpa)_4Cl_2$ (Pd_3) and $NiPdNi(dpa)_4Cl_2$ (NiPdNi) Systems

Pd_3 and NiPdNi complexes were theoretically studied recently.[27] Despite of being hypothetical compounds, they can provide us with valuable results

concerning the change induced in some magnetic properties by the replacement of one or several metal atoms by heavier homologues, and the associated deviation to the Heisenberg behavior. It is also interesting to extend the analysis of σ and δ contributions to *J* in these derivatives. The set of parameters defined in eqs. (3-6) was therefore computed for these two complexes.

$NiPdNi(dpa)_4Cl_2$. The replacement of the central Ni by Pd induces significant changes specifically in J_σ, which increases almost three times, whereas J_δ remains fairly constant. Therefore, the increase from J_{eff} = 126 cm^{-1} to 342 cm^{-1} from Ni_3 to NiPdNi almost exclusively originates in the σ interaction, which now amounts 97.9% of the total coupling (Table 4.6). This increase of the σ contribution can be assigned to the well-documented trend of the second row transition metals to favor more delocalized and covalent interactions with their neighbors, in comparison with their first row homologues. The interaction along the σ axis is therefore enhanced by a larger overlap between $d(z^2)_{Ni}$ and $d(z^2)_{Pd}$ orbitals. The δ interaction, which relies only for a small part on a direct overlap between metal orbitals, but mostly on the ligand pathway, is also enhanced, but to a much smaller extent. The intrasite exchange integral *K* remains unaltered with respect to Ni_3 since the magnetic centers are kept unchanged emphasizing that *K* is a local, mainly atomic parameter. The raise of the σ interaction strength increases considerably λ to 13.8 cm^{-1}. To summarize, considering the raise of the total J_{eff} by a factor close to 3 and the significant degradation of the Heisenberg model for the heterometallic complex, the role played by the diamagnetic central metal can be eventually qualified as *non-innocent*.

$Pd_3(dpa)_4Cl_2$. For this compound, a previous DFT study carried out with the B3LYP functional and based upon Noodleman's standard broken symmetry approach assuming the validity of the Heisenberg model yielded a large coupling constant of 1393 cm^{-1}.[27] While performing the calculations for Pd_3 with the B3LYP functional, we encountered additional problem, namely, the D^1D^0 broken symmetry solution, with $M_{s,tot}$ = 1, appears to be more stable than the D^1D^1 quintet state, in clear violation of Hund's rule. Such a behavior suggests an *intermediate regime* between the strong antiferromagnetic coupling of the

unpaired σ electrons, and a delocalized 4-electron / 3-center σ bond. The correct ordering between the D^1D^1 and the D^1D^0 solutions have been addressed by a slight increase from 20 to 25% of the exact Fock exchange introduced in the hybrid functional, which do not alter significantly the relative energies of the other solutions. So, the parameters for Pd_3 shown in Table 4.6 have been computed with a 25% Fock exchange allowing us to complete the study. The present results show that both exchange parameters in the tripalladium complex increase sharply with respect to NiPdNi and, *a fortiori*, to Ni_3. Such a strengthening of the couplings is not unexpected since the atomic orbitals at the origin of the magnetic interaction are now diffuse 4d. This explains why the δ interaction, almost unaltered from Ni_3 to NiPdNi, is notably enhanced in Pd_3, due to an increase of both the $Pd_{terminal}$-N and direct Pd-Pd overlap. Another change of major importance with respect to NiPdNi compounds is the collapse of the K value from ~ 5000 cm^{-1} to 1960 cm^{-1}, which implies a much looser correlation between the unpaired electrons on each Pd^{2+}, leading to a less tight application of the Hund principle.[40] As a consequence, the non-Hund local singlet configuration (D^0) appears energetically affordable in this case. As discussed in the previous work,[4] a local D^0 configuration combined with a triplet on the opposite center can provide a significant stabilizing contribution to the molecular triplet wave functions and lower their energy so as to put them in competition with the pure (D^1D^1) state. The discrepancy with respect to the standard model is illustrated by the very different values of J = 1323 and J_{eff} = 2040 cm^{-1}, and by the exceedingly large contribution from the biquadratic exchange (λ = 498 cm^{-1}). Since λ can be approximated by the term $(J_\sigma)^2/K$ when J_σ remains largely dominant, the decrease of K indeed contributes to the important deviation from the Heisenberg model evidenced from the parameters computed for Pd_3. However, the most important factor in determining the magnitude of λ remains in the strength of σ interaction J_σ, which appears at the second power and whose value is almost eleven times that of Ni_3 and still increased by more than 25% with respect to NiPdNi. Finally, it is worth pointing out that the *effective* magnetic coupling computed for Pd_3 is significantly larger than the one resulting from a standard application of the broken symmetry

strategy. Therefore, any attempt to extract magnetic interaction parameters for complexes with $S = 1$ magnetic centers involving 4d orbitals should consider a model Hamiltonian including terms beyond the standard bilinear interactions.

Table 4.6. Electronic and magnetic interaction parameters (in cm^{-1}) for $NiPdNi(dpa)_4Cl_2$ and $Pd_3(dpa)_4Cl_2$ compounds.

	K	J_δ	J_σ	$\%J_\delta$	$\%J_\sigma$	J	B	J_{eff}	λ
NiPdNi	5065	6.69	316	2.1	97.9	323	310	342	13.8
Pd_3[a]	1960	66.0	1258	5.0	95.0	1323	1194	2040	498

(a) Parameters obtained with 25% of exact Fock exchange (see text for details).

Up to this point, we can conclude that the use of the standard Heisenberg Hamiltonian for the well-documented $Ni_3(dpa)_4Cl_2$ system appears as a correct approximation, as evidenced by the small value of λ obtained from density functional calculations. The reliability of the DFT/B3LYP methodology in such compounds with Ni^{2+} magnetic centers has been further tested and validated from comparison with *ab initio* DDCI results carried out on the smaller model system $[Ni_2(napy)_4Cl_2]^{2+}$.

Contrarily, systems for which the unpaired electrons are hosted in diffuse 4d orbitals most probably require a model Hamiltonian including biquadratic interactions. The three-body interactions can possibly play a role in these complexes too. Along the series of the three $MM'M(dpa)_4Cl_2$ complexes investigated in the present work, the σ coupling was always found to be largely dominant. The biquadratic correction to the Heisenberg Hamiltonian, λ, increases upon replacement of Ni by Pd first in the central position, and then, more dramatically, in the terminal ones. Since λ approximately varies as $(J_\sigma)^2/K$ as long as the σ coupling represents more than 90% of J, the importance of the deviation to the Heisenberg model can be correlated to the increase of the σ magnetic interaction induced by the diffuse 4d orbitals of Pd.

The role of the intrasite exchange integral K of the first and second transition metal series should be taken into account, however. This parameter, which should be considered as an atomic property of the magnetic center, is related to

the energy difference between the local high-spin state and the first excited non-Hund state. For many transition metal atoms with 3d valence shell such as Ni, the order of magnitude of *K* is large enough (~5500 cm^{-1} with B3LYP) to exclude any significant interaction between the triplet ground state and the lowest singlet. However, large atoms with diffuse 4d orbitals like Pd feature much smaller *K* values (~1950 cm^{-1}), which contribute to impairment of the quality of the Heisenberg model.

4.5. Underestimation of Magnetic Coupling in Nickel-based Metallic Complexes

The unexpected DFT underestimation of the *J* parameter for $Ni_3(dpa)_4Cl_2$, a well-known system whose magnetic properties have been characterized, contrasts with the typical overestimation of *J* for the other members of the EMAC family, notably $[Cu_3(dpa)_4Cl_2]^+$. The experimental value for *J* pertaining to the copper complex is –34 cm^{-1},[37] and the B3LYP value obtained from broken symmetry calculations is approximately double (–63.9 cm^{-1}).[41] This is the typical trend observed in DFT/B3LYP calculations of *J* applying spin projection. The origin of the theoretical underestimation of the *J* for Ni-derived complexes such as $Ni_3(dpa)_4Cl_2$[38] and $Ni_5(tpda)_4Cl_2$[42,43] (Fig. 4.3) is explored here. As it was seen in previous sections, this underestimation in the Ni_3 complex is not due to the use of the simple form of Heisenberg Hamiltonian since the deviation to the expected energy differences was found to be negligible. One can be sure that the deviation in Ni_5, with much smaller *J*, is even smaller than in Ni_3.

The oxidized copper complex only has the pathway provided by the δ MOs. In the case of the $Ni_3(dpa)_4Cl_2$ complex, two coupling pathways are present, σ and δ. It has been shown before that the σ pathway is the dominant one, and that the contribution from the δ path is tiny in comparison. The method of Labèguerie allows determination of each contribution individually.[10] Hence, it would be interesting and an indicative point studying the behaviour of each path upon changing functional. We herein present the calculations of magnetic coupling on $[Cu_3(dpa)_4Cl_2]^+$, $Ni_3(dpa)_4Cl_2$ and $Ni_5(tpda)_4Cl_2$ (dpa = dipyridylamido; tpda = tripyridyldiamido), varying the amount of Hartree-Fock

exchange (HFX) in a hybrid functional such as B3LYP. The Cu_3^+ complex can be taken as a reference for comparison of the δ part with those of in Ni_3 and Ni_5 complexes. In all three complexes, the magnetic centres are the outermost metal atoms. The Cu_3^+ constitutes a simple two-electron/two orbital-problem whereas the other two are four-electron/four-orbital problem.

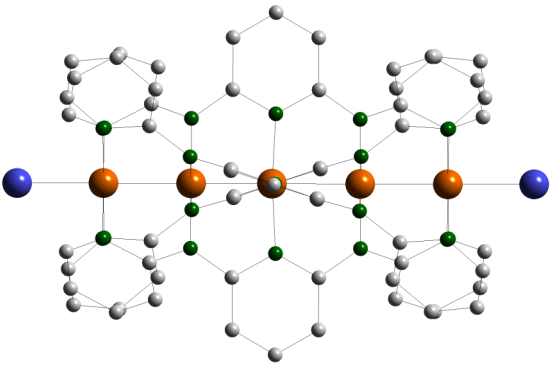

Figure 4.3. Structure of $Ni_5(tpda)_4Cl_2$. The central backbone contains the Ni atoms, in grey. Green spheres represent nitrogens. Hydrogen atoms have been omitted for clarity.

The Becke's gradient corrected three-parameter B3LYP functional,[44] of the form

$$E_{B3LYP} = E_{Slater,x} + c_0(E_{HFx} - E_{Slater,x}) + 0.72E_{Becke88,x} + E_{VWN3,c} + 0.81(E_{LYP,c} - E_{VWN3,c}) \quad (10)$$

built up from Slater's local exchange[45] with Becke's gradient corrections,[46] and the Vosko, Wilk and Nusair[47] local correlation functional with Lee, Yang and Parr's[48] gradient corrections. Conventionally the c_0 coefficient which regulates the amount of HFX is set to 0.2. In this study it was varied between 0.0 and 0.3. The geometries were optimized with constrains on the metal-metal and metal-ligand bond lengths to fix them to their experimental values, taking advantage of the D_4 point group symmetry whenever possible. For $Ni_5(tpda)_4Cl_2$, the energy

of another D^1D^0 solution $\left(|\sigma_1\delta_1| \quad |\sigma_2\bar{\delta}_2|\right)$ with energy $-K-2\frac{(t_\delta)^2}{U}$ is used instead of D^0D^0 since the latter is found at much higher energies for this system.

Figures 4.4, 4.5 and 4.6 show the variation of *J* as a function of HFX in the B3LYP functional in Cu_3^+, Ni_3 and Ni_5 respectively. In the case of the oxidized copper complex the values of *J* vary dramatically along the chosen range of 0-30% in an expected manner, that is, the coupling constant decreases as the amount of HFX grows in the functional (Figure 4.4). The variation of *J* features a smooth exponential decrease reaching a value (–39.0 cm^{-1}) close to the experimental one (–34 cm^{-1}) at 25% HFX. The previously reported overestimation of *J* by DFT/B3LYP (–64 cm^{-1}) is herein reproduced.

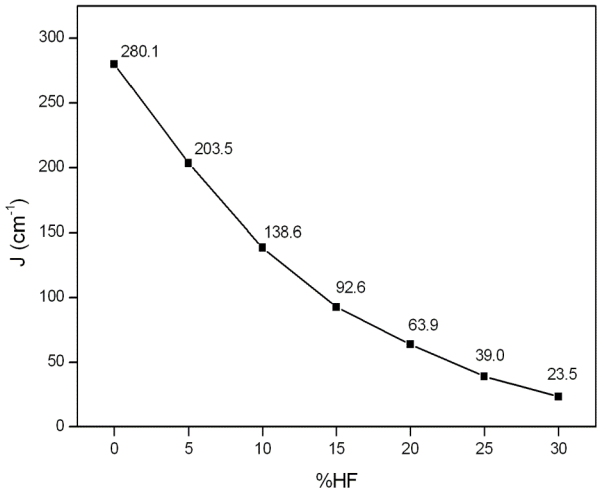

Figure 4.4. Variation of *J* as a function of the amount of exact exchange (%HF) in $[Cu_3(dpa)_4Cl_2]^+$ in experimental geometry.

Supposedly, in the Ni_3 complex the δ coupling is overestimated by generalization of the oxidized tricopper case and many other DFT studies featuring the same type of covalent metal-ligand interaction. Calculation of J_σ and J_δ in $Ni_3(dpa)_4Cl_2$ in different amount of HFX (Figure 4.5) shows that the variation of J_σ is more pronounced than $J_\text{。}$ indicating that the governing J_σ is very sensitive to HFX. At smaller amounts than 20% of HFX, the dominating J_σ

pathway resembles the J_{exp}. It may be deduced that the B3LYP functional overestimates the tiny J_δ but underestimates the largely dominant J_σ, overall underestimating J.

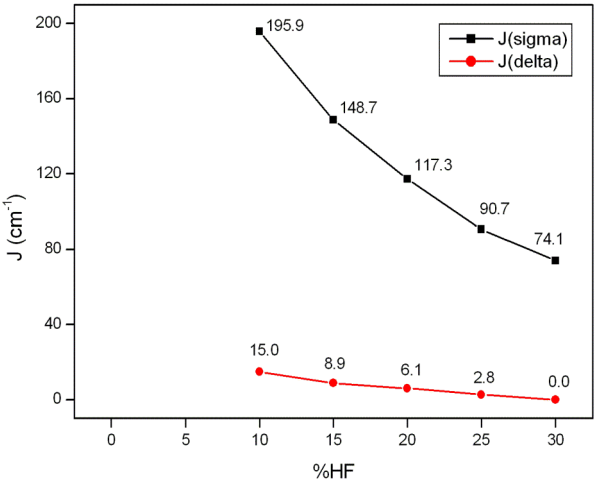

Figure 4.5. Variation of J_σ and J_δ as a function of the amount of exact exchange (%HF) in $Ni_3(dpa)_4Cl_2$ in experimental Ni-Ni, Ni-Cl and Ni-N distances.

The discrepancy found in the $Ni_3(dpa)_4Cl_2$ complex with B3LYP is also observed in the pentanickel complex. The latter compound has J_{exp} = –33.5 cm^{-1} well beyond the spin projected computed value of –8.1 cm^{-1} (B3LYP functional), with J_σ = –7.3 cm^{-1} and J_δ = –0.8 cm^{-1}, following the trend of the $Ni_3(dpa)_4Cl_2$ complex. As Figure 4.6 shows, the optimal amount of HFX has to be reduced to ~10% for Ni_5 to roughly reproduce the experimental data. This establishes a rational trend in the calculation of J values in compounds featuring the J_σ and J_δ coupling parameters, such as the nickel derivatives herein discussed. Since in Ni_3 complex the calculations did not converge at 0 and 5% HFX, the Ni_5 complex provides a complete study of the variation of the magnetic coupling at different percentages of HFX, confirming that at lower HFX the raising behaviour of J_σ and J_δ continues.

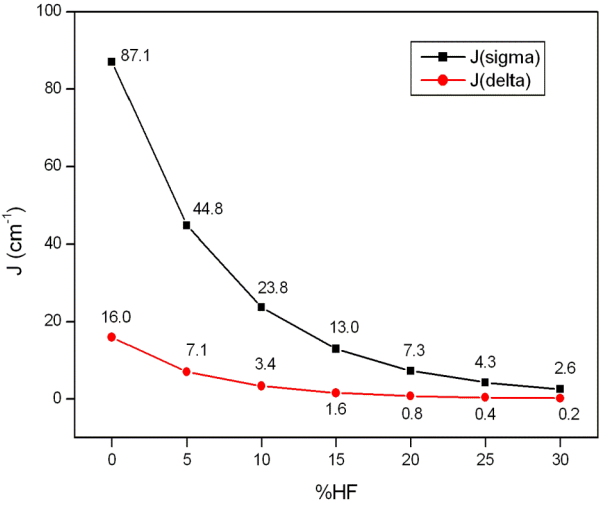

Figure 4.6. Variation of J_σ and J_δ as a function of the amount of exact exchange (%HF) in $Ni_5(tpda)_4Cl_2$ in its experimental geometry.

The present analysis allows obtaining other electronic structure parameters such as the intrasite exchange integral, *K*, the biquadratic exchange constant, λ, and the three-body interaction constant, *B*, presented in eqs. (3-6). *K* amounts the same for both nickel compounds (at the same %HFX), as shown in Table 4.7, confirming again that *K* is an atomic parameter. Its value decreases in parallel with the %HFX, that is, with more diffuse orbitals. This recalls the small *K* value obtained for the voluminous Pd(II) atoms in the hypothetical $Pd_3(dpa)_4Cl_2$ compound. In this case, the smaller intrasite exchange constant associated to the diffuse 4d valence orbitals of palladium allows low-energy local singlet states.

As before, in the case of a largely dominant σ interaction over the δ one, the λ parameter is governed by the term $(J_\sigma)^2/K$. As Table 4.7 shows, λ decreases in both systems as increases %HFX. With the same functional, λ is smaller by one order of magnitude for the Ni_5 compound due to its smaller *J*. As expected, the deviation goes to zero as the %HFX increases, and it is much smaller in the pentanickel system. The three-body term, *B*, although being numerically larger, behaves similarly to the λ parameter. Expectedly, it increases as %HFX

decreases since both J_σ and J_δ decrease and their difference also decreases. Finally, it can be observed that for increasing %HFX, J_{eff} approaches the sum of J_σ and J_δ as λ decreases at large amounts of %HFX.

Table 4.7. Electronic structure parameters (in cm^{-1}) computed for tri- and pentanickel derivatives for different percentages of HF exchange in their experimental geometries.

	%HFX	K	J_σ	J_δ	B	J_{eff}	λ
$Ni_3(dpa)_4Cl_2$	10	4225	196	15.0	181	219	5.11
	15	4651	149	8.94	140	162	2.86
	20	4949	117	6.13	111	126	1.73
	25	5407	90.7	2.83	87.9	95.0	1.02
	30	5748	74.1	0.00	74.1	75.0	0.718
$Ni_5(tpda)_4Cl_2$	0	3398	87.1	16.0	71.1	105	0.705
	5	3829	44.8	7.12	37.7	52.3	0.194
	10	4239	23.8	3.36	20.4	27.3	0.055
	15	4636	13.0	1.62	11.4	14.6	0.016
	20	5017	7.34	0.76	6.61	8.11	0.0056
	25	5381	4.32	0.42	3.87	4.74	0.0016
	30	5724	2.63	0.24	2.42	2.87	0.0008

Decomposition of J in $Ni_3(dpa)_4Cl_2$ and $Ni_5(tpda)_4Cl_2$ using the method of Labèguerie[10] and analyzing the behaviour of its components upon variation of %HFX in B3LYP functional helps understanding the origin of the underestimation of J in Ni-based EMACs. We have deduced that the DFT/B3LYP underestimation of the total J in tri- and pentanickel complexes originates in the dominant J_σ component. The theoretical decomposition of $J = J_\sigma + J_\delta$ shows that the former component is poorly described. Apparently, B3LYP fails to describe the interaction along the σ path, characterized by a weaker overlap of the atomic functions $3d(z^2)_{Ni}$ than the overlaps of the relevant

basis functions along the δ path , namely, $3d(x^2–y^2)_{Ni}$ / $2p_N$. On the other hand, we assume (there is no strong evidence) that J_s is overestimated in both nickel complexes by generalization of the findings made for $[Cu_3(dpa)_4Cl_2]^+$ in the present and previous reports. For the $Ni_5(tpda)_4Cl_2$ complex, B3LYP also underestimates the total J with regards to the experimental value, thus exhibiting the same trend as its trinuclear congener. We have observed that the amount of HFX that comes close to reproducing the experimental values is ~10% for the nickel complexes. From this study we learnt (i) the uniqueness of nickel complexes of the EMAC family from the magnetic point of view due to the presence of a dominating J_σ coupling based on weak metal-metal interactions, and (ii) that the B3LYP functional not always overestimates J, as generally accepted, but it can actually underestimate it when the electron-electron interactions responsible for antiferromagnetism do not take place via covalent bonds but via direct metal-metal contacts ($d_{Ni\text{-}Ni}$ = 2.43 Å) instead. We tentatively propose that range-separated functionals can help understanding this problem if they increase the presently underestimated J_σ and decrease the overestimated J_δ at the same time.

4.6. Range-separated Hybrid Functionals or "*Screened Exchange Functionals*"

According to the previous discussion, looking for a functional which can properly describe the weak interactions of the σ-type (and also covalent interactions of the δ-type), leads us to the use of range-separated functionals such as the long-range corrected version of the PBE functional (LC-ωPBE).[49] The main idea behind these functional is smoothing out the inconvenient physical/numerical behavior of the exact exchange in a given range by defining a way to switch on Fock exchange (in the exchange functional) through a given radius used to discriminate the short- and long-range electron-electron interactions. This may be achieved by using a smooth partitioning function to switch on/off Fock exchange depending on the value of the $u = |\boldsymbol{r}_1 - \boldsymbol{r}_2|$ electron-electron potential. The smooth weight function used in the Gauss error function $erf(\omega u)$ defined as

$$erf(\omega u) = \frac{2}{\sqrt{\pi}} \int_0^{\omega|r_1 - r_2|} e^{-t^2} dt \tag{11}$$

and the complementary error function $erfc(\omega u)$ defined as

$$erfc(\omega u) = 1 - erf(\omega u) = \frac{2}{\sqrt{\pi}} \int_{\omega|r_1 - r_2|}^{0} e^{-t^2} dt \tag{12}$$

This function permits one to discriminate between short (first right hand term in eq. 13) and long (second right hand term in eq. 13) range for u in terms of ω as

$$\frac{1}{u} = \frac{erfc(\omega u)}{u} + \frac{erf(\omega u)}{u} \tag{13}$$

and provides a way to switch on a given percent of the Fock exchange in one or the other domain of u values.

In the LC-ωPBE functional, Fock exchange is used to describe the long-range electron-electron interactions whereas at short distances the interaction is described by a pure GGA functional as follows:

$$E_{xc}^{LC-\omega PBE}(\omega) = E_x^{LR-HF}(\omega) + E_x^{SR-PBE}(\omega) + E_c^{PBE} \tag{14}$$

Electronic structure parameters have been calculated with the LC-ωPBE functional at the experimental Ni-Ni and Ni-ligand distances (Table 4.8). Compared with B3LYP (Table 4.5, exp. distances), the magnitude of the σ exchange parameter increases significantly (from 117.3cm^{-1} to 153cm^{-1}) while the δ one considerably decreases. Due to this notable increase in the σ part of the magnetic exchange the J_σ becomes more dominant and J_{eff} reaches to 160cm^{-1}. It seems that this functional provides significant improvement to the σ-type long-range interaction. Assuming that J_δ is overestimated in B3LYP, one may also take the decrease of J_δ as an indication of better description of δ-type interactions with the LC-ωPBE functional. This suggests that the LC-ωPBE treats both part of J in a more balanced way. Moreover, the deviation from the Heisenberg Hamiltonian (λ) increases by a factor of ~2 is (compared with B3LYP), as a consequence of increase of J. However, one may still use the

simple form of the Heisenberg Hamiltonian for describing the magnetic interactions.

Table 4.8. Electronic and magnetic interaction parameters (in cm^{-1}) for $Ni_3(dpa)_4Cl_2$ complex at its experimental geometry using the LC-ωPBE functional.

	K	J_δ	J_σ	$\%J_\delta$	$\%J_\sigma$	J	B	J_{eff}	λ
LC-ωPBE	5149	3.31	153	2.12	97.9	156	149	160	3.15
B3LYP	4949	6.13	117	5.0	95.0	123	111	126	1.73

The study of the behaviour of J_σ and J_δ with different functionals allows one to pinpoint the computational origin of the uncommon underestimation in computed J in Ni_3 and Ni_5 complexes. The double error made in calculation of J can be partially eliminated by using the range-separated functionals, namely, LC-ωPBE functional.

References

[1] (a) P. A. M. Dirac, *Proc. Roy. Soc. London, Ser. A* 112 (1926) 661; 123 (1929) 714. (b) W. Heisenberg, *Z. Phys*. 38 (1926) 411. (c) J. H. van Vleck, *Theory of Electric and Magnetic Susceptibilities*, Oxford University Press, London, 1932.

[2] O. Kahn, *Molecular Magnetism,* Wiley-VCH, New-York, 1993.

[3] $S = 1$ indicates the maximum spin moment of one magnetic center.

[4] R. Bastardis, N. Guihéry, C. de Graaf, *J. Chem. Phys*. 129 (2008) 104102.

[5] R. Boca, *Theoretical Foundations of Molecular Magnetism*, Elsevier, Amsterdam, 1999.

[6] R. Maurice, N. Guihéry, R. Bastardis, C. de Graaf, *J. Chem. Theory Comput*., 6 (2010) 55.

[7] J. Hubbard, *Proc. Roy. Soc*. A276 (1963) 238.

[8] I. de P. R. Moreira, N. Suaud, N. Guihéry, J. P. Malrieu, R. Caballol, J. M. Bofill, F. Illas, *Phys. Rev. B* 66 (2002) 134430.

[9] R. Bastardis, N. Guihéry, C. de Graaf, *Phys. Rev. B* 76 (2007) 132412.

[10] P. Labèguerie, C. Boilleau, R. Bastardis, N. Suaud, N. Guihéry, J. P. Malrieu, *J. Chem. Phys*. 129 (2008) 154110.

[11] J. Miralles, J. P. Daudey, R. Caballol, *Chem. Phys. Lett*. 198 (1992) 555.

[12] J. Miralles, O. Castell, R. Caballol, J. P. Malrieu, *Chem. Phys*. 172 (1993) 33.

[13] R. Broer, W. J. A. Maaskant, *Chem. Phys*. 102 (1986) 103.

[14] O. Castell, R. Caballol, *Inorg. Chem*. 38 (1999) 668.

[15] I. de P. R. Moreira, F. Illas, C. J. Calzado, J. F. Sanz, J. P. Malrieu, N. Ben Amor, D. Maynau, *Phys. Rev. B* 59 (1999) 6593.

[16] C. J. Calzado, S. Evangelisti, D. Maynau, *J. Phys. Chem. A* 107 (2003) 7581.

[17] D. Dai, M. H. Whangbo, *J. Chem. Phys*. 114 (2001) 2887.

[18] D. Dai, M. H. Whangbo, *J. Chem. Phys*. 118 (2003) 29.

[19] V. Barone, I. Cacelli, P. Cimino, A. Ferretti, S. Monti, G. Prampolini, *J. Phys. Chem. A* 113 (2009) 15150.

[20] E. Ruiz, P. Alemany, S. Alvarez, J. Cano, *J. Am. Chem. Soc*. 119 (1997) 1297.

[21] A. Bencini, F. Totti, C. A. Daul, K. Doclo, P. Fantucci, V. Barone, *Inorg. Chem*. 36 (1997) 5022.

[22] N. N. Nair, E. Schreiner, R. Pollet, V. Staemmler, D. Marx, *J. Chem. Theory Comput*. 4 (2008) 1174.

[23] E. Ruiz, S. Alvarez, J. Cano, V. Polo, *J. Chem. Phys*. 123 (2005) 164110.

[24] E. Ruiz, J. Cano, S. Alvarez, P. Alemany, *J. Comp. Chem*. 20 (1999) 1391.

[25] This corresponds to Method A in ref. 10.

[26] Gaussian 03, Revision C. 01, Gaussian, Inc., Wallingford CT, 2003.

[27] X. López, X.; M. M. Rohmer, M. Bénard, *J. Mol. Struct*. 890 (2008) 18.

[28] The DFT optimized Ni-Ni distances are somewhat overestimated, leading to smaller *J* values.

[29] R. Clérac, F. A. Cotton, K. R. Dunbar, C. A. Murillo, I. Pascual, X. Wang, *Inorg. Chem*. 38 (1999) 2655.

[30] C. J. Calzado, J. Cabrero, J. P. Malrieu, R. Caballol, *J. Chem. Phys*. 116 (2002) 2728.

[31] G. Karlström, R. Lindh, P. Å. Malmqvist, B. O. Roos, U. Ryde, V. Veryazov, P. O. Widmark, M. Cossi, B. Schimmelpfennig, P. Neogrady, L. Seijo, *Comput. Mater. Sci*. 28 (2003) 222. MOLCAS Version 7.0. Department of Theoretical Chemistry, University of Lund.

[32] (a) B. O. Roos, R. Lindh, P. Å. Malmqvist, V. Veryazov, P. O. Widmark, *J. Phys. Chem. A* 109 (2005) 6575. (b) B. O. Roos, R. Lindh, P. Å. Malmqvist, V. Veryazov, P. O. Widmark, *J. Phys. Chem. A* 108 (2004) 2851.

[33] C. J. Calzado, J. P. Malrieu, J. Cabrero, R. Caballol, *J. Phys. Chem. A* 104 (2000) 11636.

[34] V. Barone, I. Cacelli, A. Ferretti, G. Prampolini, *J. Chem. Phys*. 131 (2009) 224103.

[35] (a) CASDI program, N. Benamor, D. Maynau, *Chem. Phys. Lett*. 286 (1998) 211. (b) D. Maynau, N. Benamor, J. Pitarch-Ruiz, CASDI program, Laboratoire de Chimie et de Physique Quantiques, Toulouse University, 1999.

[36] S. Aduldecha, B. Hathaway, *J. Chem. Soc., Dalton Trans*. (1991) 993.

[37] J. F. Berry, F. A. Cotton, L. M. Daniels, C. A. Murillo, X. Wang, *Inorg. Chem*. 42 (2003) 2418.

[38] P. Kiehl, M. M. Rohmer, M. Bénard, *Inorg. Chem*. 43 (2004) 3151.

[39] S. M. Peng, C. C. Wang, Y. L. Jang, Y. H. Chen, F. Y. Li, C. Y. Mou, M. K. Leung, *J. Magn. Magn. Mater*. 209 (2000) 80.

[40] This fact might explain the difficulties encountered to get a correct ordering of the D^1D^1 and D^1D^0 states.

[41] M. Bénard, J. F. Berry, F. A. Cotton, C. Gaudin, X. López, C. A. Murillo, M. M. Rohmer, *Inorg. Chem*. 45 (2006) 3932.

[42] Y. Kitagawa, M. Shoji, K. Koizumi, T. Kawakami, M. Okumura, K. Yamaguchi, *Polyhedron* 24 (2005) 2751.

[43] I. P. C. Liu, M. Bénard, H. Hasanov, I. W. P. Chen, W. H. Tseng, M. D. Fu, M. M. Rohmer, C. H. Chen, G. H. Lee, S. M. Peng, *Chem. Eur. J*. 13 (2007) 8667.

[44] A. D. Becke, *J. Chem. Phys*. 98 (1993) 5648.

[45] J. C. Slater, *Phys. Rev*. 81 (1951) 385.

[46] A. D. Becke, *Phys. Rev. A* 38 (1988) 3098.

[47] S. H. Vosko, L. Wilk, M. Nusair, *Can. J. Phys*. 58 (1980) 1200.

[48] C. Lee, W. Yang, R.G. Parr, *Phys. Rev. B* 37 (1988) 785.

[49] Y. Tawada, T. Tsuneda, S. Yanagisawa, T. Yanai, and K. Hirao, *J. Chem. Phys.* 120 (2004) 8425.

Chapter 5

Toward a Low-Spin Configuration in Extended Metal Atom Chains. Theoretical Study of Trimetallic Systems with 22 Metal Electrons

5.1. Introduction and Objectives

Electron transport along a single molecule is the paradigm of nanoelectronics.[1-7] Some compounds of the family of extended metal atom chains[8] (EMACs) feature electronic conductivity,[9-13] a property that has been recently investigated with theoretical methods.[14-17] So, applications as molecular wires or switches are envisaged.

The structural, electronic and magnetic properties of trimetallic EMAC compounds, $M_3(dpa)_4X_2$, can be rationalised or predicted upon the distribution

of the valence electrons among the fifteen molecular orbitals (shown in Figure 5.1) with mainly metal character of δ, π and σ type. Electron transport and magnetism, the most interesting properties in these systems, can in principle be described in terms of the energy and occupation of a few MOs. Understanding the conductance phenomena in EMACs is not an easy task, but the latest theoretical studies have shown that the orbitals closest to the Fermi level dominate electron transport and, in most cases, these are the σ-like MOs.[14-17] The relative conductance of metal string complexes has been related to various factors, such as the metal-metal bond order[13-15,18] or the degree of electron delocalisation along the chain.[19] Nevertheless, the link between electronic structure and electron transport has not been yet fully clarified. On the other hand, magnetic properties in EMACs have been deeply studied with computational methods to show the nature, pathways and strength of the electron coupling and the MOs involved in such phenomenon.[19-23]

In the present chapter we are aimed at exploring 'uncommon' electronic structures in EMACs. For this goal we focus on hypothetical compounds that can presumably feature low-spin configurations. Chain compounds with localized, magnetically coupled electrons in δ- (or δ- and σ-)type orbitals have been reported (M = Cu, Co, Ni, etc.).[20] All these molecules containing late transition metal atoms feature electron-rich metal chains (21–27 metal valence electrons). In particular, our goal is to explore if compounds with 22 (extensively 23) electrons can exist in a low spin configuration without localized unpaired electrons, and if further implications can be expected from it. A paradigmatic trimetallic complex with 23 metal electrons is $[Ni_3(dpa)_4]^{3+}$, obtained upon oxidation of $[Ni_3(dpa)_4Cl_2]$.[19,24] In this cationic compound, the two axial chlorine ligands leave the chain to stabilize the new electronic configuration. For the specific issue of electron conduction between two electrodes, the loss of axial ligands is a major defect since they are a fundamental part in the connection of nanowires to an electron source.[25-26]

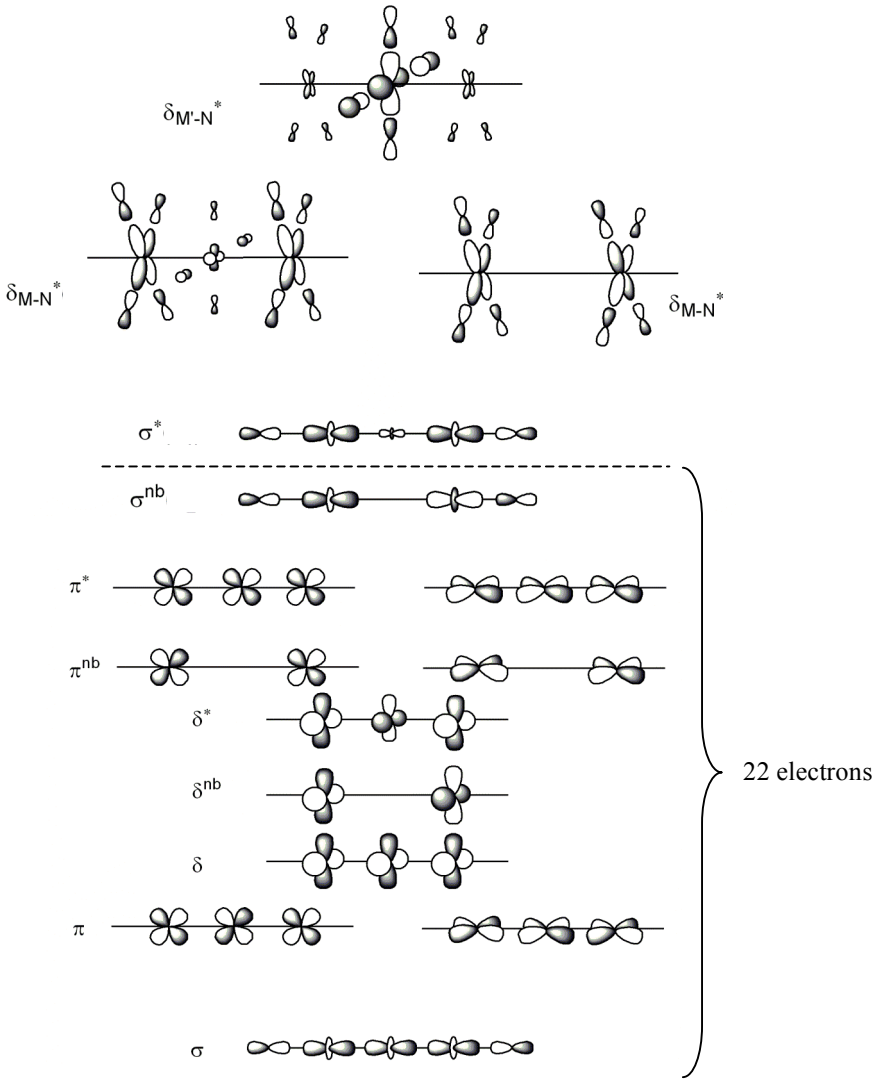

Figure 5.1. Symmetry-adapted molecular orbitals containing the metallic valence electrons for linear M_3 systems. The energy ordering shown may vary from one compound to another. The doubly occupied orbitals in a hypothetical 22-electron closed-shell configuration are indicated.

Recently, Peng, Rohmer *et al*. synthesized and characterized $CoPdCo(dpa)_4Cl_2$ (**1**), the first heterometal string compound.[27] The complex contains the typical combination of equatorial dpa and axial chlorine ligands and has a metallic backbone with 22 valence electrons. This work was readily followed in time by $Cu_2Pt(dpa)_4Cl_2$ and $Cu_2Pd(dpa)_4Cl_2$, reported by the same groups.[28] These works open the door to a subclass of mixed-metal compounds potentially with new properties. For **1**, various electronic configurations have been studied with DFT/B3LYP calculations. The ground state is associated to the $(\delta^{nb})^1(\delta^*)^1(\sigma^{nb})^1(\sigma^*)^1(\delta_{Co\text{-}N}^*)^1(\delta_{Co\text{-}N}^*)^1$ electronic configuration, that corresponds to the antiferromagnetic coupling of high-spin (S = 3/2) Co^{II} ions, separated by a diamagnetic Pd^{II}. The associated ferromagnetic state was found 1.43 kcal mol^{-1} higher in energy. The second set of low-energy states is characterized by an electronic configuration with one unpaired electron per Co (S = ½ terminal metals). The unpaired electrons are coupled through the σ orbitals, while the δ^{nb} and δ* orbitals are doubly occupied. The closed-shell state with the herein interesting $(\sigma^{nb})^2(\sigma^*)^0$ electronic configuration lies as much as 36 kcal mol^{-1} above the ground state, making it unaffordable.

In the present theoretical study we explore hypothetical though plausible compounds that present the unusual, but highly interesting, 22-electron low-spin configuration $(\sigma)^2(\pi)^4(\pi^{nb})^4(\pi^*)^4(\delta)^2(\delta^{nb})^2(\delta^*)^2(\sigma^{nb})^2(\sigma^*)^0$. This will be done via substitution of Co and Pd metal atoms by their group counterparts, and also upon manipulation of the axial donor character by substitution of chlorine ligands by isothiocyanate ($-NCS^-$). These two ligands have been commonly used to saturate the axial positions of the chain, so compounds based on them are stable and well characterized.

5.2. Computational Details

The results discussed have been obtained upon full geometry optimisations of all molecules in the electronic states shown in the text, either using the restricted (closed-shell) or unrestricted (open-shell) formalisms. For complex **1**, previous results available[27] have been taken for comparing the energy ordering of states. We used the DFT formalism with the B3LYP functional as implemented in the

GAUSSIAN 03 package.[29] We applied the maximal D_4 symmetry to all molecules, except when the broken symmetry approach[30] was used to model antiferromagnetic states, a widely used solution when single determinant methods are applied.[31] In such cases, the point symmetry was lowered to C_4 to allow left-right spin polarisation in the metal chain. Valence double-ζ basis sets (D95V) to describe C and H atoms, and a full double-ζ basis sets (D95) supplemented with one d polarisation function for N were used. For the *heavy* atoms (chlorine and metals), the core electrons were modelled with Los Alamos core potentials, and a double-ζ basis was applied for valence electrons (LANL2DZ). For the metal atoms —Ni, Co, Pd and Rh— one f-type polarisation function with exponent 3.13, 2.78, 1.472 and 1.35, respectively, has been added.[32]

CASSCF/CASPT2 calculations were carried out with the MOLCAS 7.4 suite of programs.[33] Atomic natural orbitals of ANO-RCC type were employed as the basis set for all atoms.[34-35] For Rh and Pd atoms the (6s,5p,3d,1f) basis sets and for Cl and S the (4s3p1d) basis sets have been used. For N, C and H atoms the (3s2p1d), (3s2p) and (2s) basis sets have been assigned. The symmetry of molecules has been reduced from D_4 to D_2 avoiding degenerate irreducible representations, which are not supported in MOLCAS. The singlet and triplet state wave functions for which the energy difference was obtained at CASPT2 level feature similar weights of the reference CASSCF wave function.

5.3. Results and Discussion

$Co_2Pd(dpa)_4Cl_2$ is our reference *real* molecule in the present work. It contains 22 metal electrons, but its *aufbau* closed-shell (CS) configuration was computed to be 36 kcal mol^{-1} above the ground state. In order to make the CS (more) stable, we have designed a procedure to increase the energy gap between σ and $\delta_{Co\text{-}N}{}^*$ sets of orbitals via stabilisation of the former ones, eventually converting the σ^{nb} in the highest occupied molecular orbital. This may lead to double occupancy of the lower pure-metal δ orbitals shown in Figure 5.1. Thus, we propose strategic changes in the chemical composition (replacement of metal atoms and axial ligands) and the analysis of the electronic changes associated. The variations in

the composition explored here are in principle achievable and we avoid the obviously unrealistic cases. For example, Pd is an interesting element since it is an electron-rich large atom in the oxidation state II. However, experimentalists have stated that it can only be incorporated to the central position of dpa-based chains and not to the terminal position, since pyridyl nitrogens are worse coordinating agents of Pd than amino nitrogens.[27-28] Structural changes on the dpa ligands have minor effects on the electronic structure of the EMACs, so we have ruled out this pathway.

5.3.1. $Co_2M(dpa)_4X_2$ Compounds

The first series of compounds analyzed are based on the heterometallic symmetric CoMCo chain, with M = Pd, Ni and X = Cl^-, NCS^-. The DFT optimized geometries in their ground states are shown in Table 5.1.

Table 5.1. Selected interatomic distances (in Å) computed for compounds **1**–**4** in their ground states. X is the axial atom linked to the terminal metal, M = Pd or Ni. BS1 and BS2 correspond to the antiferromagnetic broken symmetry solutions of the high spin configurations with six unpaired electrons (S = 3) and two unpaired electrons (S = 1), respectively.

	$Co_2Pd(dpa)_4Cl_2$ **1**	$Co_2Pd(dpa)_4(NCS)_2$ **2**	$Co_2Ni(dpa)_4Cl_2$ **3**	$Co_2Ni(dpa)_4(NCS)_2$ **4**
G.S.[a]	BS1	BS1	BS2	BS2
Co-M	2.538	2.524	2.414	2.410
Co-X	2.451	2.082	2.568	2.148
Co-N	2.178	2.166	2.018	2.013
M-N	2.046	2.047	1.905	1.908

(a) G.S. stands for ground state.

5.3.1.1. $Co_2Pd(dpa)_4Cl_2$ (**1**) and $Co_2Pd(dpa)_4(NCS)_2$ (**2**)

The ground state of **1** has two high-spin Co atoms at both ends of the chain whose six unpaired electrons are antiferromagnetically coupled (broken-symmetry 1, or BS1 solution).[27] As discussed above, the singly occupied orbitals are the (almost) pure metal δ^{nb} and δ^* orbitals, the two $\delta_{Co\text{-}N}{}^*$ orbitals and the

σ^{nb}/σ^* orbitals.[36] Figure 5.2 reflects that the σ orbitals lie above the $\delta_{Co\text{-}N}{}^*$, at variance with the situation depicted in Figure 5.1. In line with the objective of this study, that is, obtaining a stable closed-shell configuration with a $(\sigma^{nb})^2(\sigma^*)^0$ configuration, one may stabilize the σ orbitals to induce the depopulation of the two singly occupied $\delta_{Co\text{-}N}{}^*$ orbitals favouring doubly occupancy of the δ^{nb} and δ* orbitals. This can be done through a diminution of the covalent antibonding interaction along the backbone of the chain. As a first step, the strength of the antibonding interaction between terminal metals and axial ligands is attacked by replacement of Cl^- by NCS^- (isothiocyanate), giving compound **2**. Our calculations reveal that both σ^* and σ^{nb} orbitals are appreciably lowered in energy (by 0.62 and 1.45 eV, respectively) compared to **1.** The effect is especially large for the σ^{nb} orbital, which is now more stable than the two $\delta_{Co\text{-}N}{}^*$ orbitals (see Figure 5.2). Despite this stabilisation of the σ^* and σ^{nb} orbitals in **2**,

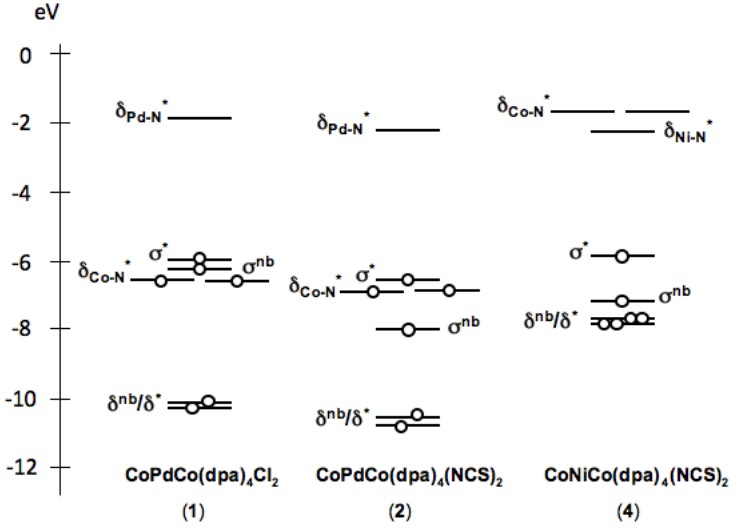

Figure 5.2. Scaled energy representation of the σ and $\delta_{M\text{-}N^*}$ sets of molecular orbitals for compounds **1**, **2** and **4**, summarizing the effects upon central metal and axial ligand replacement. The labels used for molecular orbitals are strictly correct for symmetric (high spin) functions, not for broken symmetry solutions.[36]

no qualitative changes are observed concerning the principal states (septet and triplet and their associated broken symmetry solutions) compared to **1** because the way electrons are shared among orbitals remains unchanged. The Co^{II} ions also keep their high spin configuration, namely, three unpaired electrons are present on each terminal site. Neither the CS state nor states involving partial electron pairing are stable enough to compete with the ground state (Figure 5.3).

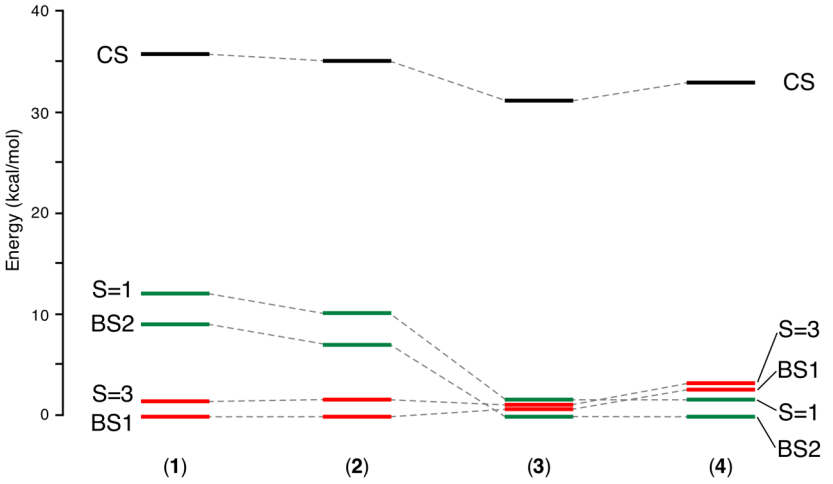

Figure 5.3. Relative energies of the lowest five electronic states computed for systems **1**–**4**. CS stands for the closed shell configuration, whereas BS1 and BS2 correspond to the antiferromagnetic broken symmetry solutions of the high spin configurations with 6 unpaired electrons ($S = 3$) and two unpaired electrons ($S = 1$), respectively.

5.3.1.2 $Co_2Ni(dpa)_4Cl_2$ (**3**) and $Co_2Ni(dpa)_4(NCS)_2$ (**4**)

The second way to stabilize the σ-like orbitals is by weakening the antibonding interaction in the metallic region via substitution of the central Pd atom by a smaller atom, Ni (compound **3**). This substitution would imply a stabilisation of the σ* orbital, which has a significant contribution of the central metal atom. On the contrary, no energy shift is observed for the σ^{nb}, where the central metal does not contribute. Also, when Ni is introduced into the chain, a generalized contraction of the Co-M-Co chain is observed, combined with smaller Co-N and M-N equatorial distances. The reduction of the Ni-N distances is easily

explained by the smaller size of Ni^{II} in comparison to Pd^{II}. On their side, the smaller Co-N distances are a direct consequence of the change in the electronic configuration of the ground state. The stabilisation of the σ* orbital causes the depopulation of the high lying antibonding $\delta_{Co\text{-}N}$* orbitals in favour of the pure metal δ^{nb} and δ* orbitals with no bonding nor antibonding character with equatorial N atoms. The Co^{II} ions are no longer high spin atoms but have now only one unpaired electron. As shown in Figure 5.3, the BS2 state becomes the ground state, although the other open-shell configurations are very close in energy. The CS configuration remains at +31 kcal mol^{-1}. Hence, this small orbital energy alteration induced by the Pd substitution by Ni stabilizes the $(\sigma^{nb})^1(\sigma^*)^1$ configuration, but does not lead to the desired $(\sigma^{nb})^2(\sigma^*)^0$ configuration.

Substitution of the axial Cl^- ligands by NCS^-, together with the incorporation of a Ni atom in central position (compound **4**), produces an extra stabilisation of the $(\sigma^{nb})^1(\sigma^*)^1$ configuration (see Figure 5.3). In this case, the two localized electrons (Co^{II} S = ½) are antiferromagnetically coupled and the energy difference between the ferromagnetic high spin state and the broken symmetry low spin state has been estimated to be ~1000 cm^{-1}. This huge value arises from a σ-type interaction, which is known to be much stronger than the δ type coupling,[37] notably when 4d transition metal atoms are present in the chain.[22,38] Compared to **3**, the energy lowering of the two σ-like orbitals in **4** is more remarkable, achieving complete inversion with respect to the $\delta_{Co\text{-}N}$* orbitals. This causes a further destabilisation of the two states with six unpaired electrons and both the BS2 and the S = 1 state lie now below the BS1 and S = 3 states. Nevertheless, the CS state is still found at very high energies, more than 30 kcal mol^{-1} above the ground state, and we conclude that the $Co_2M(dpa)_4X_2$ complexes are not good candidates for presenting a closed-shell electronic structure.

5.3.2. Rh_2M $(dpa)_4X_2$ Compounds

The chemical changes discussed in the previous section showed that the closed-shell state remains inaccessible in the complexes with a CoNiCo backbone. One

may push the σ* orbital to higher energies with respect to the σ^{nb} orbital by substitution of terminal Co atoms by larger metal ions favouring the closed-shell state. The replacement of 3d by 4d transition metals in terminal positions will destabilize the σ* orbital more than σ^{nb} since the former orbital involves the antibonding interaction in the metal-metal region as well as in the metal-axial ligand region. This replacement also pushes up the two $\delta_{M\text{-}N}^*$ orbitals to higher energies due to the larger antibonding interactions with the N orbitals of dpa ligands, ruling out the possibility of being occupied. Rhodium is a suitable and realistic candidate to fulfil these requirements since Rh-based EMACs have been synthesized before.[39-40]

5.3.2.1. $Rh_2Ni(dpa)_4Cl_2$ (**5**) and $Rh_2Ni(dpa)_4(NCS)_2$ (**6**)

Replacement of the 3d metal atoms (Co in compounds **3** and **4**) by 4d Rh atoms gives compounds **5** and **6**. The most relevant strucural parameters obtained upon DFT full geometry optimisations are listed in Table 5.2. We can observe that the distances related to Rh are longer, notably the Rh-ligand ones, because of the larger size of this metal atom compared to Co. From the electronic point of view, in $Co_2Ni(dpa)_4Cl_2$ (**3**), the energy gap between σ* and σ^{nb} orbitals was found to be modest, around ~0.72 eV for the S = 1 state. For $Rh_2Ni(dpa)_4Cl_2$ (**5**) this energy difference is slightly larger, of the order of 0.85 eV in the same state, in line with our expectations on the replacement of Co by Rh. In addition, the two $\delta_{M\text{-}N}^*$ orbitals are destabilized due to a more effective antibonding Rh-N interaction. The consequences of these changes in the orbital energies are twofold. Firstly, the states arising from the S = 3/2 configurations on the terminal metals are shifted ~100 kcal mol^{-1} to higher energies. Secondly, the $(\sigma^{nb})^2(\sigma^*)^0$ configuration becomes competitive with the states associated to the $(\sigma^{nb})^1(\sigma^*)^1$ configuration. In comparison to the CoMCo-based complexes, the CS state is dramatically stabilized and lies only 2.4 kcal mol^{-1} above the broken symmetry (S = 1/2) ground state, as shown in Figure 5.4.

Although the substitution of chlorine by isothiocyanate in axial position lowers the energy of the σ orbitals due to the weaker antibonding Rh-NCS

interaction, the energy difference between σ^{nb} and σ^* hardly changes leaving the BS2-CS energy gap nearly unaltered with the closed-shell at 2.8 kcal mol^{-1} above the BS2 state (Figure 5.4).

Table 5.2. Selected interatomic distances, in Å, computed for complexes **5** and **6** in their ground states. X is the axial atom linked to the terminal metal.

	$Rh_2Ni(dpa)_4Cl_2$ **5**	$Rh_2Ni(dpa)_4(NCS)_2$ **6**
Ground State	BS2	BS2
Rh-Ni	2.413	2.412
Rh-X	2.711	2.305
Rh-N	2.087	2.085
Ni-N	1.931	1.932

Since the CS states of **5** and **6** are not too far from the ground state, we proceed to the calculation of the one-electron reduced states in these complexes in order to find out if the extra electron can possibly occupy the delocalized σ^* orbital. Our calculations show that the only electronic configuration accessible upon reduction of complexes **5** and **6** is the doublet associated to the configuration $(\sigma^{nb})^2(\delta_{Ni\text{-}N}^*)^1$. The geometry of the reduced complexes **5** and **6** in this electronic configuration display an enlargement of the metal-axial ligand distances of about 0.17–0.19 Å. This significant lengthening upon reduction can be attributed to a weaker Coulombic attraction between the anionic axial ligands and the metallic core, which now carries less positive charge (formal 5+) than in the neutral form (formal 6+). Also, a slight contraction of the metal-metal distances occurs due to the shielding effect that the extra electron localized in the central metal causes on the repulsive metal-metal interactions. Moreover, the occupation of the $\delta_{Ni\text{-}N}^*$ orbital induces a significant increase of 0.12 Å in the Ni-N distances. The quartet state $(\sigma^{nb})^1(\sigma^*)^1(\delta_{Ni\text{-}N}^*)^1$ has been computed to be +12 kcal mol^{-1} above the doublet state just mentioned.

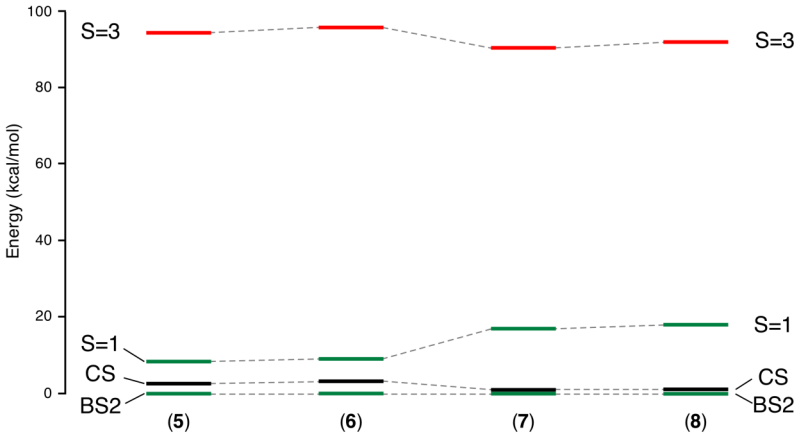

Figure 5.4. Relative energies of the lowest five electronic states computed for compounds **5**–**8**. State labels are equivalent to those in Figure 5.3, but the energy scale is different now.

5.3.2.2. $Rh_2Pd(dpa)_4Cl_2$ (**7**) and $Rh_2Pd(dpa)_4(NCS)_2$ (**8**)

Replacement of the central Ni by Pd in RhNiRh complexes leads to **7** and **8.** The Pd atom at the central position induces a further destabilisation of the σ* orbital with respect to σ^{nb} due to the increased antibonding Rh-Pd interaction. The σ* – σ^{nb} energy gap reaches 1.4 and 1.5 eV in **7** and **8**, respectively (0.96, 0.85 and 0.88 eV in compounds **1**, **5** and **6** respectively) and the CS and the BS2 ground states become indistinguishable. Several evidences for this statement arise: (i) they appear to be energy degenerate with a ΔE = 0.2–0.3 kcal mol^{-1} at the present level of computation, (ii) their geometrical parameters coincide (see Table 5.3) and (iii) the atomic spin populations (0.36) on the terminal Rh atoms and the $S^2 \approx 0.2$ expectation value in the BS2 state are too small to correspond to a *true* antiferromagnetic solution.[41] This indicates that, despite the unrestricted character of the electron density, it tends to collapse to a closed-shell configuration.

Table 5.3. Selected interatomic distances, in Å, computed at the DFT level for complexes **7** and **8** in the closed-shell and BS2 states. X is the axial atom linked to the terminal metal.

	$Rh_2Pd(dpa)_4Cl_2$ **7**		$Rh_2Pd(dpa)_4(NCS)_2$ **8**	
Electronic State	BS2	CS	BS2	CS
Rh-Pd	2.464	2.458	2.463	2.455
Rh-X	2.743	2.746	2.337	2.342
Rh-N	2.108	2.105	2.105	2.102
Pd-N	2.030	2.029	2.032	2.031

As the energy differences found for states BS2 and CS are within the computational uncertainty at the DFT level and, we have performed *ab initio* correlated calculations, i.e., multiconfigurational CASSCF, to clarify the nature of the ground state of **7** and **8**. Taking σ^{nb} and σ^{*} as active orbitals in a CAS(2,2) calculation, the energies of the two spin states —singlet and triplet— have been calculated. The singlet ground state has a marked multiconfigurational character with 71% $\left|\sigma^{nb}\,\bar{\sigma}^{nb}\right|$ and 29% $\left|\sigma^{*}\,\bar{\sigma}^{*}\right|$ in both complexes meaning that the ground state is not totally a closed-shell state and its description with a single determinant is approximate. The energy difference between the singlet ground state and the first triplet state at the second order of perturbation (CASPT2) for **7** and **8** is 26.6 and 27.5 kcal mol^{-1}, respectively, in favour of the singlet state.

Reduction of compound **7** gives rise to the $(\sigma^{nb})^2(\delta_{Pd\text{-}N}^{*})^1$ doublet state, which is 7.7 kcal mol^{-1} more stable than $(\sigma^{nb})^2(\sigma^{*})^1$ with a delocalized electron in the σ channel. The first quartet state that could be obtained upon reduction of **7** is $(\sigma^{nb})^1(\sigma^{*})^1(\delta_{Pd\text{-}N}^{*})^1$ and lies 22 kcal mol^{-1} above the ground state and not of further interest. The geometrical changes arising upon reduction are summarized in Table 5.4. Accommodation of the extra electron in the $\delta_{Pd\text{-}N}^{*}$ orbital induces a modest lengthening of the equatorial Pd-N bond (0.12 Å) so that it becomes longer than the Rh-N ones, a rather unusual fact. In this case, the increase of the

electron density in the metal chain shields the electrostatic repulsive energy between neighbouring positively charged metal ions inducing a very small shrinkage of the Rh-Pd distances (~0.02 Å). In contrast, the extra electron density increases the electrostatic repulsion between terminal metals and axial ligands producing a significant lengthening of the Rh-Cl distances (0.20 Å). Monoreduction of complex **8** gives the same electronic configuration as that of **7**, $(\sigma^{nb})^2(\delta_{Pd\text{-}N}^*)^1$, as the most stable state and the delocalized configuration lies 7.9 kcal mol^{-1} above it. The geometrical changes computed upon reduction roughly coincide to those predicted for **7**, as shown in Table 5.4. The bond distance lengthening of Rh-N(CS) in complex **8** is also significant (~0.16 Å), but smaller than that of **7**. We want to stress that NCS^- as ligand, despite not changing the principal findings made for $X = Cl^-$, has been used preferentially in conductance measurements due to its affinity to Au electrodes.[13,18b] Like complexes derived from Rh_2Ni chains, complexes **7** and **8** also feature a marked change in the M-X distances upon reduction that could be useful in on/off switches.

Table 5.4. Evolution of selected interatomic distances, in Å, upon reduction for complexes **7** and **8**. The oxidized structure has been taken as CS. X represents the axial ligands.

	$RhPdRh(dpa)_4Cl_2$ **7**		$RhPdRh(dpa)_4(NCS)_2$ **8**	
Electronic State	$(\sigma^{nb})^2(\sigma^*)^0$	$(\sigma^{nb})^2(\delta_{cent}^*)^1$	$(\sigma^{nb})^2(\sigma^*)^0$	$(\sigma^{nb})^2(\delta_{cent}^*)^1$
Rh-Pd	2.458	2.435	2.455	2.433
Rh-X	2.746	2.946	2.342	2.501
Rh-N	2.105	2.122	2.102	2.121
Pd-N	2.029	2.151	2.031	2.150

5.4. Conclusions

Chemical strategies for the prediction of trimetallic string complexes featuring low-spin electronic configurations with 22 metal valence electrons have been

computationally tested at the DFT level. Taking the previously reported $Co_2Pd(dpa)_4Cl_2$ complex as 22-electron reference, calculation of the principal (low energy) electronic configurations for eight molecules with compositions $M_2M'(dpa)_4X_2$, with M = Co, Rh; M′ = Pd, Ni and X = Cl^-, NCS^- has allowed us to characterize their ground states and geometries. The main results indicate that compounds based on the Co_2Pd backbone are not predisposed to low-spin configurations. This fact arises from the narrow energy range at which the metal orbitals of high energy σ^{nb}, σ^* and $\delta_{Co\text{-}N}{}^*$ are found, favouring unpairing of electrons. For Co_2Ni based complexes, σ^{nb} and σ^* orbitals are lowered in energy with respect to $\delta_{Co\text{-}N}{}^*$ and a low energy triplet (and its associated broken symmetry state) is found with configuration $(\sigma^{nb})^1(\sigma^*)^1$. Both Co_2Pd and Co_2Ni strings, have closed-shell configurations more than 30 kcal mol^{-1} higher irrespective of the donor strength of the axial ligand.

For systems derived from the Rh_2M backbone the situation is totally different since the voluminous rhodium atoms change dramatically the electronic configuration. The $\delta_{Rh\text{-}N}{}^*$ orbitals are pushed to higher energies, so the states derived from $(\delta^{nb})^1(\delta^*)^1(\sigma^{nb})^1(\sigma^*)^1(\delta_{Rh\text{-}N}{}^*)^1(\delta_{Rh\text{-}N}{}^*)^1$ are inaccessible. In contrast, the $(\sigma^{nb})^1(\sigma^*)^1$ and $(\sigma^{nb})^2(\sigma^*)^0$ configurations are both much lower in energy. Notably, for the two $Rh_2Pd(dpa)_4X_2$ systems computed (X = Cl^- and NCS^-), the closed shell and the broken-symmetry solution related to the $(\sigma^{nb})^1(\sigma^*)^1$ electronic configuration are degenerate. Figure 5.5 shows the evolution of molecular orbital energies and their occupations from the initial $Co_2Pd(dpa)_4Cl_2$ system (**1**) to $Rh_2Pd(dpa)_4(NCS)_2$ (**8**), which can be considered as a concise summary of the main results and could help the development of new EMAC species.

Reduction of some Rh_2M systems may lead to the interesting $(\sigma^{nb})^2(\sigma^*)^1$ 23-electron configuration,[42-43] with one delocalized electron along the σ channel of the metal string. Calculations of reduced complexes rule out this possibility in detriment of the more stable $(\sigma^{nb})^2(\delta_{Pd\text{-}N}{}^*)^1$ situation. We have calculated a notable axial Rh-X lengthening when $(\sigma^{nb})^2(\delta_{Pd\text{-}N}{}^*)^1$ takes place, thus we cannot totally discard that reduced complexes could even loose the axial ligands. This

issue could be interesting in designing the on/off switches. Present calculations indicate that, in general, $(\sigma)^2(\cdots)^{18}(\sigma^{nb})^2(\sigma^*)^1$ configurations produce a concomitant loss of the axial ligands due to the excess antibonding interaction between terminal metals and axial ligands.

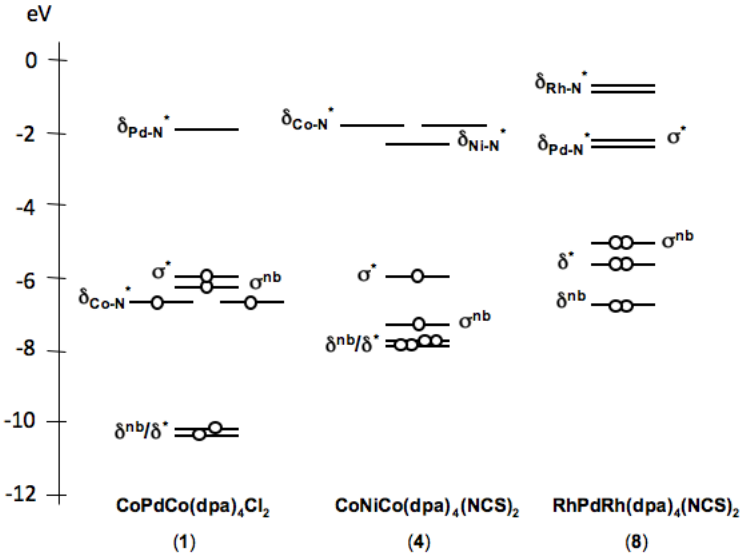

Figure 5.5. Scaled representation of the 1-electron energies for the relevant compounds **1**, **4**, and **8**, summarizing the effect upon metal and axial ligand replacement.

References

[1] A. Aviram, M. Ratner, *Chem. Phys. Lett*. 29 (1974) 277.

[2] M. A. Reed, J. Tour, *Sci. Am*. 282 (2000) 86.

[3] A. Nitzan, M. A. Ratner. *Science* 300 (2003) 1384.

[4] R. L. Carroll, C. B. Gorman. *Angew. Chem. Int. Ed*. 41 (2002) 4378.

[5] D. Q. Andrews, R. Cohen, R. P. Van Duyne, M. A. Ratner. *J. Chem. Phys*. 125 (2006) 174718.

[6] F. Chem, J. Hihath, Z. Huang, X. Li, N. J. Tao. *Annu. Rev. Phys. Chem*. 58 (2007) 535.

[7] C. Joachim, J. K. Gimzewski, A. Aviram, *Nature* 408 (2000) 541.

[8] L. P. Wu, P. Field, T. Morrissey, C. Murphy, P. Nagle, B. Hathaway, C. Simmons and P. Thornton, *J. Chem. Soc., Dalton Trans*. (1990) 3835.

[9] J. S. Miller, *Extended Linear Chain Compounds*, Plenum, New York, Vol. 1-3, 1982.

[10] P. Day, H. J. Keller, *Low-Dimensional Cooperative Phenomena*, Plenum, New York, p. 191, 1974.

[11] R. J. H. Clark, D. E. Brown, *Mixed Valence Compounds*, Reidel, Dordrecht, p.271,1982.

[12] D. H. Chae, J. F. Berry, S. Jung, F. A. Cotton, C. A. Murillo, Z. Yao, *Nano Lett*. 6 (2006) 165.

[13] I. W. P. Chen, M. D. Fu, W. H. Tseng, J. Y. You, S. H. Wu, C. J. Ku, C. H. Chen, S. M. Peng, *Angew. Chem. Int. Ed.* 45 (2006) 5814.

[14] L. Y. Hsu, Q. R. Huang, B. Y. Jin, *J. Phys. Chem. C* 112 (2008) 10538.

[15] T. W. Tsai, Q. R. Huang, S. M. Peng, B. Y. Jin, *J. Phys. Chem. C* 114 (2010) 3641.

[16] V. P. Georgiev, J. E. McGrady, *Inorg. Chem*. 49 (2010) 5591.

[17] V. P. Georgiev, J. E. McGrady, *J. Am. Chem. Soc*. 133 (2011) 12590.

[18] (a) S. Y. Lin, I. W. P. Chen, C. H. Chen, M. H. Hsieh, C. Y. Yeh, T. W. Lin, Y. H. Chen, S. M. Peng, *J. Phys. Chem. B* 108 (2004) 959. (b) K. N. Shih, M. J. Huang, H. C. Lu, M. D. Fu, C. K. Kuo, G. C. Huang, G. H. Lee, C. H. Chen, S. M. Peng, *Chem. Commun*. 46 (2010) 1338.

[19] P. Kiehl, M. M. Rohmer, M. Bénard, *Inorg. Chem*. 43 (2004) 3151.

[20] J. F. Berry, F. A. Cotton, L. M. Daniels, C. A. Murillo, X. Wang, *Inorg. Chem*. 42 (2003) 2418.

[21] M. M. Rohmer, M. Bénard, *Chem. Soc. Rev*. 30 (2001) 340.

[22] X. López, M. Bénard, M. M. Rohmer, *J. Mol. Struct. THEOCHEM* 777 (2006) 53.

[23] Z. Tabookht, X. López, C. de Graaf, *J. Phys. Chem. A* 114 (2010) 2028.

[24] J. F. Berry, F. A. Cotton, T. Lu, C. A. Murillo, X. Wang, *Inorg. Chem*. 42 (2003) 3595.

[25] J. F. Berry, F. A. Cotton, C. A. Murillo, *Dalton Trans*. (2003) 3015.

[26] F. A. Cotton, C. A. Murillo, Q. Wang, *Inorg. Chem. Commun*. 10 (2007) 1088.

[27] M. M. Rohmer, I. P. C. Liu, J. C. Lin, M. J. Chiu, C. H. Lee, G. H. Lee, M. Bénard, X. López, S. M. Peng, *Angew. Chem. Int. Ed*. 46 (2007) 3533.

[28] I. P. C. Liu, G. H. Lee, S. M. Peng, M. Bénard, M. M. Rohmer, *Inorg. Chem*. 46 (2007) 9602.

[29] *Gaussian 03*, Revision B 05; Gaussian: Pittsburgh, PA, 2003.

[30] (a) A. P. Ginsberg, *J. Am. Chem. Soc*. 102 (1980) 111. (b) L. Noodleman, *J. Chem. Phys*. 74 (1981) 5737. (c) L. Noodleman, E. J. Baerends, *J. Am. Chem. Soc*. 106 (1984) 2316. (d) L. Noodleman, D. A. Case, *Adv. Inorg. Chem*. 38 (1992) 423. (e) L. Noodleman, C. Y. Peng, D. A. Case, J. M. Mouesca, *Coord. Chem. Rev.* 144 (1995) 199.

[31] See, for example, the recent work D. Jose, A. Datta, *Cryst. Growth Des*. 11 (2011) 3137.

[32] A. W. Ehlers, M. Böhme, S. Dapprich, A. Gobbi, A. Höllwarth, V. Jonas, K.F. Köhler, R. Stegmann, A. Veldkamp, G. Frenking, *Chem. Phys. Lett*. 208 (1993) 111.

[33] G. Karlström, R. Lindh, P. Å. Malmqvist, B. O. Roos, U. Ryde, V. Veryazov, P. O. Widmark, M. Cossi, B. Schimmelpfennig, P. Neogrady, L. Seijo, *Comput. Mater. Sci.* 28 (2003) 222. *MOLCAS* Version 7.4. Department of Theoretical Chemistry, University of Lund.

[34] B. O. Roos, R. Lindh, P. Å. Malmqvist, V. Veryazov, P. O. Widmark, *J. Phys. Chem. A* 109 **(**2005) 6575.

[35] B. O. Roos, R. Lindh, P. Å. Malmqvist, V. Veryazov, P. O. Widmark, *J. Phys. Chem. A* 108 (2004) 2851.

[36] The use of the σ, σ*, σ^{nb}... labels in molecular orbitals arising from a broken symmetry (BS) calculation is not rigorous since these do not retain the left-right symmetry of the molecule anymore (see Figure S1 in the Supplementary Information). However, to let the reader grasp easily the main character of the orbitals (s for d(z^2)–like, d for d(*xy*)–like, etc.) irrespective of their true symmetry, we use the same notation for BS and triplet or septet solutions, for which these notation is correct.

[37] Z. Tabookht, X. López, M. Bénard, C. de Graaf, *J. Phys. Chem. A* 114 (2010) 12291.

[38] X. López, M. M. Rohmer, M. Bénard, *J. Mol. Struct* 890 (2008) 18.

[39] J. T. Sheu, C. C. Lin, I. Chao, C. C. Wang, S. M. Peng, *Chem. Commun*. (1996) 315.

[40] G. C. Huang, I. P. C. Liu, J. H. Kuo, Y. L. Huang, C. Y. Yeh, G. H. Lee, S. M. Peng, *Dalton Trans*. (2009) 2623.

[41] Broken symmetry calculations performed on systems with two S = ½ centres typically give $\langle S^2 \rangle \approx 1$, which is the zero-overlap limit. Values of $\langle S^2 \rangle$ much smaller than 1 indicate a large overlap between *a* and *b* spinorbitals.

[42] J. F. Berry, F. A. Cotton, L. M. Daniels, C. A. Murillo, *J. Am. Chem .Soc*. 124 (2002) 3212.

[43] J. F. Berry, F. A. Cotton, P. Lei, T. Lu, C. A. Murillo, *Inorg. Chem*. 42 (2003) 3534.

Chapter 6

Charge Ordering and Electrical Conduction in One-dimensional MMX Chains: Theoretical Study of $Ni_2(dta)_4I$ and $Pt_2(dta)_4I$ (dta = $CH_3CS_2^-$)

6.1. Introduction and Objectives

During the last three decades, efforts to find one-dimensional (1-D) materials based on molecular building blocks exhibiting metal-like or semiconducting properties with potential applications in nanoscale technology have steadily increased.[1-4] 'Synthetic metals', or 1-D metals, comprise several classes such as organic metals,[5-10] polysulfur nitrides[11] or metal-containing polymers (metallopolymers).[12-15] In a large group of 1-D metals, the metallic properties arise from interacting metal atoms along the backbone of a chain[16-18] known as

'1-D metallic complexes'. In these complexes, a *short* metal-metal distance (< 3.0 Å) is required for an effective overlap between metal orbitals leading to bond formation. Krogmann has discussed the metallic properties of this class of compounds in terms of a partially filled 1-D band in the metal-atom chain direction.[15] Among 1-D metallic complexes, the halogen-bridged binuclear mixed-valence chains, also known as MMX chains, are promising candidates for molecular electronic devices.[19-21] They are made up of two metallic centers linked by organic ligands that facilitate a short metal-metal distance, and halides that connect the dimetallic subunits. Thus-far synthesized MMX chains are classified into two groups: the neutral $M_2(RCS_2)_4I$ (M = Pt, Ni; R = Me, Et, *n*-Pr, *n*-Bu)[22-25] and the ionic $R_4[Pt_2(pop)_4X]\cdot nH_2O$ (X = Cl, Br, I; R = K, NH_4, Li, Cs; pop = diphosphonate = $H_2P_2O_5^{2-}$)[26-38] chains. The M–M distance in the former family is significantly shorter than in the diphosphonate one,[39] a sufficient reason for their higher conductivity. Important features of the MMX chains arise from the electron distribution and the charge polarization within dimer units due to metal-metal bonding. This property gives them the possibility of having various valence-ordering states, which can be classified as follows:

(1) averaged-valence state (AV):

$$—X^{-}—M^{2.5+}——M^{2.5+}—X^{-}—M^{2.5+}——M^{2.5+}—X^{-}—$$

(2) charge density wave (CDW) state:

$$—X^{-}——M^{2+}——M^{2+}——X^{-}–M^{3+}—M^{3+}–X^{-}——$$

(3) charge-polarization (CP) state:

$$—X^{-}——M^{2+}——M^{3+}–X^{-}——M^{2+}——M^{3+}–X^{-}——$$

(4) alternate charge-polarization (ACP) state:

$$——X^{-}——M^{2+}——M^{3+}–X^{-}–M^{3+}——M^{2+}——X^{-}——$$

In the AV (1) and CDW (2) states, the charge is uniformly distributed within each dimer unit, while in CP (3) and ACP (4) states, the charge is unevenly distributed (polarized) in each dimer. All valence-ordered states except the AV state undergo lattice distortions due to valence alternation. In the AV state, each

M_2 unit possesses a delocalized unpaired electron, while in the CP state there is one unpaired electron localized at the M^{3+} site per M_2 unit. In the CDW and CP states the bridging halogen is shifted away from the midpoint of the two adjacent metal cations since it experiences different Coulomb attractive forces from them. In state 4, the two M^{3+} sites of neighboring dimers, each carrying one unpaired electron, are dimerized. The ground state of neutral MMX 1-D systems depends on the nature of metal ions, bridging halogens and alkyl groups of the dithiocarboxylato ligand. In the diphosphonate family it also depends on the radius of the countercations and the number of water molecules.[25,36]

In the present work we focus on the alkyl-family, $[M_2(dta)_4I]$ (M = Ni, Pt; dta = $CH_3CS_2^-$, dithioacetato). $[Ni_2(dta)_4I]_\infty$ and $[Pt_2(dta)_4I]_\infty$ chains were first synthesized and characterized by Bellito et al. during the 1980s.[22-23] They suggested a "hopping–type" mechanism to describe the observed electrical conductivities with values $7\cdot10^{-3}$ $\Omega^{-1}cm^{-1}$ and $5\cdot10^{-6}$ $\Omega^{-1}cm^{-1}$ for Pt and Ni systems, respectively. In 1992, Yamashita et al. measured a wide range of physical properties of these chains to clarify their electronic structures, concluding that both systems represent a model of one-dimensional Mott-Hubbard-type electronic structure.[40] Experimental techniques confirm a higher electrical conductivity for the $Pt_2(dta)_4I$ chain compared to the Ni analog. The former represents the first example of a halogen-bridged 1-D transition-metal complex exhibiting a clear metallic behavior at standard conditions with no electronic π-system. This is the main reason for the great attention paid to Pt chains.[41-45] Experimentalists have devoted considerable efforts to prepare other derivatives of the Pt chain, including different halogen atoms and modifications of the alkyl group of the dithiocarboxylato ligand.[45-50]

On the other hand, few theoretical studies have been carried out to describe the electronic structure and conduction properties of MMX systems. The major part of the existing works deals with the description of the metal-semiconductor transition, excitation mechanisms and structural distortions.[51-59] Recently, Calzolari et al. presented a study of the 1-D band structure in the framework of density functional theory (DFT) on a single Pt chain.[60] They analyzed the metallicity of the Pt chain under metal, halogen and ligand modifications. The

electronic state of the chain was assigned basically an AV state.[61-62] However, the electronic structure of the homologous Ni chain seems to be less established. X-ray photoelectron spectra for the Ni complexes suggest the valence delocalization on a regular chain structure.[23] According to Yamashita et al., the essential feature of $[Ni_2(dta)_4I]_\infty$ is similar to that of $[Pt_2(dta)_4I]_\infty$, involving uniform dimer units.[40] ^{1}H NMR studies also suggest a strong fluctuation of electron spins and charge over the Ni chain.[63] However, in 2002 Makiura et al. detected different charges for Ni ions along the backbone of the chain by X-ray photoelectron spectroscopy rejecting the prevalence of the AV state.[64] $[Ni_2(dta)_4I]_\infty$ is regarded as a Mott-Hubbard semiconductor due to a relatively large on-site Coulomb repulsion energy U in the Ni atoms.[40] Very few theoretical models have been reported to clarify the elusive electronic ground state of the Ni complex. Nakano et al. reported an AV state from hybrid density functional theory (DFT) calculations. The small $|t_{MXM}|/U_{eff}$ ratio is an indication that the system belongs to the strongly correlated materials.[65] The band structure analysis of $[Ni_2(dta)_4I]_\infty$ carried out by Calzolari with the PBE functional and plane waves shows that the system is metallic and very similar to $[Pt_2(dta)_4I]_\infty$.[60]

The goal of the present work is to explain the observed different electrical conductivities and to clarify the charge-ordering state of Pt and Ni MMX chains. This is done by periodic DFT calculations and through the extraction of electronic structure parameters from correlated *ab initio* calculations performed on dimers (XMMX) and tetramers (XMMXMMX) using the effective Hamiltonian approach. The valence-ordered states of Ni and Pt chains are thus examined and are related to their electrical conductivity properties.

6.2. Computational Details

To study the electronic structure of the title compounds in the one-electron band structure approximation, unrestricted DFT periodic calculations were carried out with the CRYSTAL06 code.[66] We used the PBE,[67] a gradient corrected functional, and a modification of the hybrid B3LYP functional[68] with several amounts of Hartree-Fock (HF) exchange. Atom centered Gaussian type functions are used to construct the Bloch functions. Standard all-electron basis

sets have been used to describe Ni and S, which can be indicated as 86-411(41d)G and 86-311G*, respectively.[69] For C and H atoms, 6-21G* and 3-1p1G basis sets have been used.[70] To represent the inner electrons of Pt and I ions the effective core pseudopotentials have been utilized. [71] There are 836 AOs with 502 electrons per unit cell for the Ni system and 832 AOs with 462 electrons for the Pt system. A shrinking factor of 4 has been used to define a grid of k-points in the reciprocal space.

The *ab initio* calculations reported have been performed using the experimental geometries.[22-23] Most important geometrical parameters, namely, the M–M and M–I distances, are kept as the experimental ones. But to reduce the computational cost of the embedded cluster calculations, the mean value is taken for the distances affecting the dta ligand. In this way, the point group symmetry of the model system is increased to C_2 with the two-fold rotation axis along the I–M–M–I axis as shown in Table 6.1. This symmetrization induces only small changes in the geometry of the dta groups.

Table 6.1. Average distances (Å) and angles (deg) used in Pt and Ni dimeric and tetrameric models with C_2 point group symmetry.

	M–M	M–I[a]	(M–I)'	M-S	C-S	C-C	∠SCS	∠MSC
$[Pt_2(dta)_4I_2]^{-1}$	2.677	2.975	2.981	2.324	1.68	1.52	128.1º	110.0º
$[Ni_2(dta)_4I_2]^{-1}$	2.514	2.928	2.940	2.234	1.677	1.51	122.7º	110.2º

(a) In Figure 6.1, the M–I and (M–I)' distances are labeled *a* and *b*.

Four sulfur atoms surround each metal ion in a pseudo-square-planar arrangement. The two adjacent $[MS_4]$ squares are alternated by 21° and 28° in Pt and Ni systems, respectively. In the dimer calculations, the relatively small size of the systems allows us to use high quality ANO-RCC basis sets: Ni (6s,5p,3d,2f,1g), Pt (8s,7p,5d,3f,2g), I (6s,5p,3d,1f), S (4s,3p,1d), C (3s,2p) and H (2s).[72,73] The affordable basis sets in tetramers are valence-only basis sets with effective core potentials. For Pt, Ni, I, and S we use the *ab initio* model potentials of Barandiarán and co-workers[74-76] with a (3s,3p,4d,2f), (3s,3p,4d,1f),

(3s,4p,3d), (2s,3p,1d) valence basis set, respectively. The C-1s electrons are represented with the Stoll pseudopotential, while the valence electrons are described with the corresponding (2s,2p) basis set.[77] Finally, the 6-31G basis set is used for H.[78]

An accurate description of local electronic structure parameters via a fragment approach can be obtained when the fragment is embedded in an adequate representation of the rest of the crystal. In this work the dimer (I–MM–I) and tetramer (I–MM–I–MM–I) fragments are embedded in a set of model potentials[79] representing the nearest metals and point charges for I and S (see Figure 6.1). We use formal charges in the Ni chain: +2.5, –1.0 and –0.5 for Ni, I and S respectively. To reflect the more covalent nature of the Pt system, we have reduced the point charges in the embedding by 50% in this case.

Experimental geometries, featuring long–short M–I distances (*a* and *b* in Figure 6.1, and Table 6.1), have been used for the *ab initio* calculations. Taking in mind that the difference between *a* and *b* is very small (0.012 Å and 0.006 Å for Ni[23] and Pt[22] chains, respectively), the X-ray structures can be considered "*almost symmetric*".

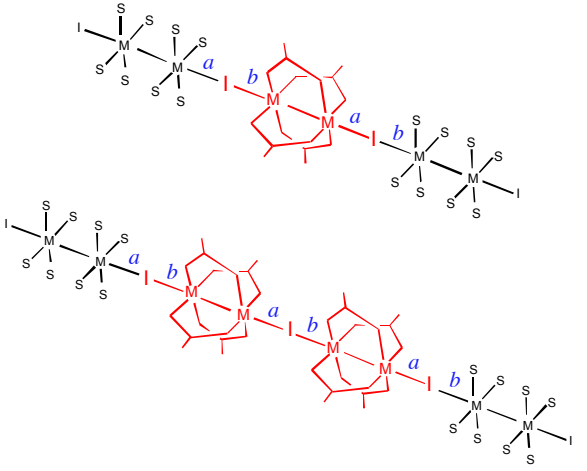

Figure 6.1. Schematic representation of a dimer (top) and tetramer (bottom) MMX fragments with embedding in black. To emphasize that consecutive M–I distances are not identical, they are labeled *a* and *b*.

The MOLCAS[80] and CASDI[81] programs have been employed for performing Complete Active Space Self Consistent Field (CASSCF) and Difference Dedicated Configuration Interaction[82-83] (DDCI) calculations, respectively. The variational DDCI method is considered as one of the most accurate computational techniques for computing electronic energy differences.[84-90]

6.3. Results and Discussion

6.3.1. Periodic DFT Calculations on Pt and Ni Chains

The electronic structure of the two title compounds has been studied with band structure calculations taking the experimental structures. It is well known that the local density approximation (LDA) usually underestimates the band gap and the HF approximation severely overestimates it, both leading to inaccurate descriptions of the electron distribution. So, to check the consistency of the results upon changes in the density functional, we performed calculations with the PBE and with hybrid functionals with a range of 20–60% HF exchange. This interval includes the typical percentages that have been used in the literature to obtain accurate electronic structure parameters (such as J and t) in other transition metal materials.[91-93]

To characterize the electronic ground states of $[Pt_2(dta)_4I]_\infty$ and $[Ni_2(dta)_4I]_\infty$, we have calculated the charge difference ($\Delta q = q_{M(1)}–q_{M(2)}$) and spin density difference ($\Delta s = s_{M(1)}–s_{M(2)}$) between adjacent metal atoms of dimer units using the Mulliken population analysis, represented in Figure 6.2 for the PBE and hybrid functionals with 20–60% HFX. Some important features arise. First, the PBE functional assigns the same charge and spin to adjacent metal atoms for both the $Pt_2(dta)_4I$ and $Ni_2(dta)_4I$ chains, reproducing the main conclusions obtained in the theoretical work of Calzolari et al.[60] Present results show that the B3LYP functional (20% HF exchange) gives a complete electronic delocalization in both cases, which can be interpreted as both chains having roughly the same character. Second, using a hybrid functional with 30% HF exchange (30HFX), Pt still features a uniform charge distribution along the chain with very small Δq and Δs irrespective of the amount of % HF used. On

the other hand, calculations on Ni chains give notably different charge and spin populations on adjacent nickel ions for moderate (and large) amounts of HF exchange, at variance with the PBE functional, highlighting how sensitive to the choice of a density functional can be the study of electronic structures.

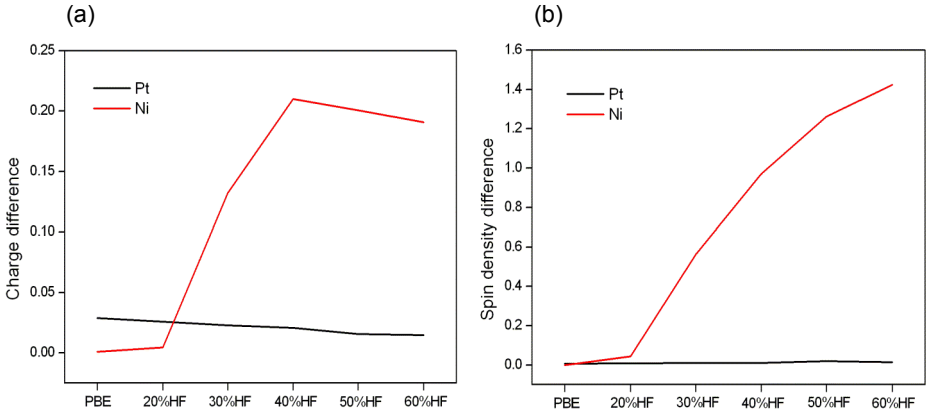

Figure 6.2. (a) Charge and (b) spin atomic population differences on adjacent metal atoms computed with the PBE and various %HF exchange-containing hybrid functionals. The vertical scales are different in (a) and (b).

It is also worth pointing out that Δq values are smaller than Δs. This can be partially explained by a larger charge polarization of the ligands around the metal ion with the higher oxidation state, but could also be attributed to the approximate nature of the Mulliken analysis. In general, spin populations are more reliable since the overlap population, which is the most arbitrary ingredient of the analysis, is smaller due to the rather localized nature of the singly occupied orbitals.

Another issue concerns the dependence of the electron distribution with the geometry. To this end, we have optimized the geometries of the Pt and the Ni compounds with the PBE and the hybrid 30HFX functionals. The optimized geometries retain the essential features of the experimentally determined structures. As can be seen in Table 6.2, the optimized M–M and M–I distances are always within an error of 0.1 Å with respect to the experiments. For Pt,

optimized geometries with either functional are very similar to the experimental one. The Δs and Δq values are very small and highly constant, following the insignificant changes on the geometry. The largest discrepancies between the computed and experimental geometries concern the distances *a* and *b* in the Ni chain. The difference between these two parameters, ($b - a$) increase from 0.012 Å to 0.153 Å upon optimization with 30HFX. A smaller difference (0.029 Å) is obtained with the PBE functional, an expected result owing to the nature of the PBE functional. One may recall that, contrarily to correlated calculations, mean-field calculations often overestimate dimerization effects in systems exhibiting a broken symmetry electron distribution. Despite a slight overestimation of the charge and spin distribution differences between the two metallic sites for the Ni compound which is due to the overestimation of dimerization, we observe a qualitatively good agreement between the Δs and Δq values obtained with the experimental and optimized geometries. These values confirm the prevalence of a fully delocalized nature of the valence electrons in the Pt compound and a polarized Ni^{2+}–Ni^{3+}-like charge ordering in the Ni compound.

Table 6.2. Relationship between experimental and DFT-optimized metal-metal and metal-I distances (in Å) and the total charge difference Δq and spin population difference Δs for $[Pt_2(dta)_4I]_\infty$ and $[Ni_2(dta)_4I]_\infty$ computed with different functionals.

	Pt				Ni			
	Exp.[a]		Opt.		Exp.[b]		Opt.	
	PBE	30% HF	PBE	30% HF	PBE	30% HF	PBE	30% HF
d(M–M')	2.677		2.692	2.691	2.514		2.514	2.552
d(M–I) = *a*	2.975		2.968	2.967	2.928		2.920	2.838
d(M–I)' = *b*	2.981		2.973	2.975	2.940		2.949	2.991
$b - a$	0.006		0.005	0.008	0.012		0.029	0.153
Δq	0.029	0.023	0.012	0.013	0.001	0.132	0.000	0.158
Δs	0.006	0.011	0.006	0.007	0.000	0.561	0.000	0.744

(a) Experimental geometry taken from Ref. 22.
(b) Experimental geometry taken from Ref. 23.

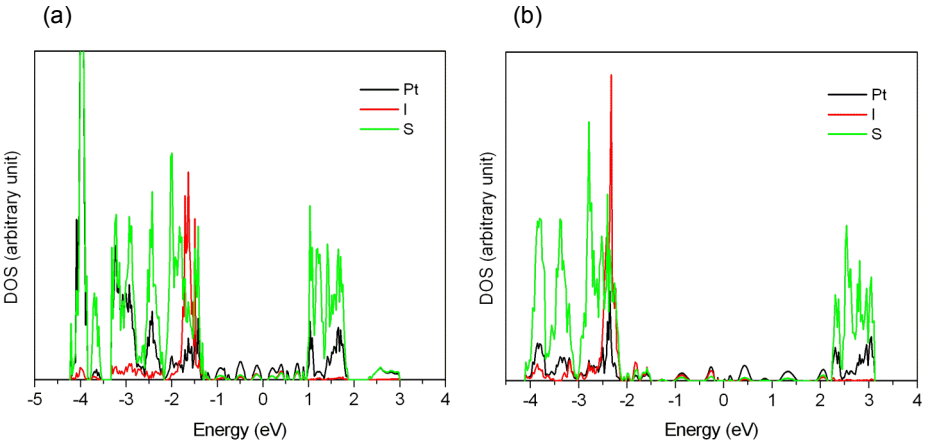

Figure 6.3. Projected density of states for the Pt chain with (a) the PBE and (b) the 30HFX functionals. Pt (black), I (red) and S (green) projected DOS. All energies are referred to the highest occupied states.

Finally, we relate the calculated electronic structure to the different electrical conductivity observed in the Ni and Pt systems via an analysis of the density of states (DOS). Figures 6.3 and 6.4 show the projected DOS for Pt and Ni chains, respectively, obtained with the PBE and the 30HFX functionals. In the Pt case, a gapless DOS can be observed for both functionals, with the Fermi Level (FL) lying at the middle of a band, indicating a conducting state. A deeper analysis on the projected DOS on Pt, I and S, shows that this band is basically composed of the basis functions centered on the atoms responsible of conduction along the chain, namely Pt and I (Figure 6.3, black and red lines). These general results are in agreement with previous theoretical studies.[60] However, the Ni chain presents a different behavior depending on the density functional used. With PBE, an important DOS is observed around the FL (characteristic of a conducting state) whereas the hybrid functional removes it, opening an energy gap between the valence and the conduction states of 1.93 eV, typical of an insulating or semiconducting state.

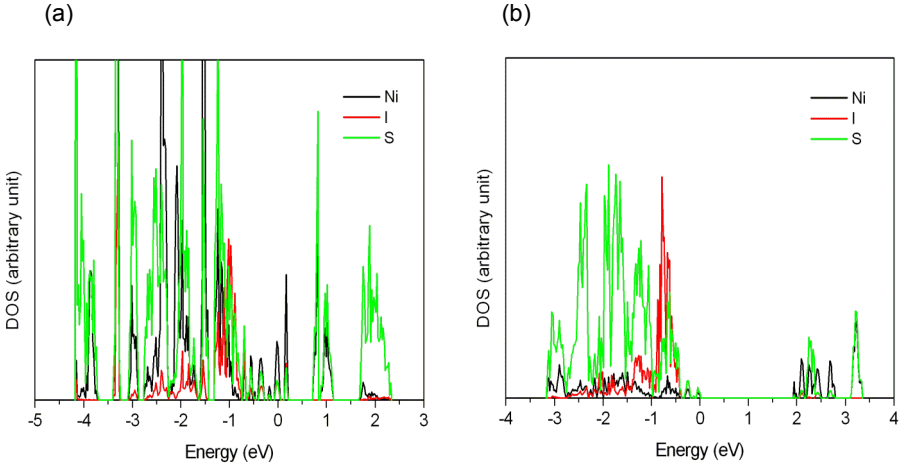

Figure 6.4. Projected density of states for the Ni chain with (a) the PBE and (b) the 30HFX functionals. Ni (black), I (red) and S (green) projected DOS. All energies are referred to the highest occupied states.

Another issue worth being discussed concerns the choice of the basis sets. In previous work, plane waves have been used, while our results have been obtained with a Gaussian-type basis set. Despite the completely opposite nature of the two basis sets (delocalized for the plane waves versus localized for the Gaussian functions), our PBE results largely coincide with those previously obtained in the Ni and Pt compounds.[60] This shows that the Gaussian basis sets used in our work are sufficiently good to correctly describe the physics of the systems studied.

From this analysis one may conclude that the hybrid functional with 30% HF exchange (30HFX) can reproduce the different electrical conductivity for Ni and Pt chains measured by Bellitto et al.[22,23] For a deeper analysis of the physics governing the electron transport in these chains, we have performed *ab initio* calculations on the fundamental MMX units constituting these materials.

6.3.2. *Ab initio* Calculations

6.3.2.1. $[Pt_2(dta)_4I_2]^{-1}$ Dimer Fragment

For each Pt-Pt unit, there are three unpaired electrons accommodated in four molecular orbitals (MOs) that are built from bonding and antibonding combinations of metal d_{z^2} or $d_{x^2-y^2}$ atomic orbitals. These orbitals are optimized for the four lowest quartet states at the CASSCF level to ensure an unbiased orbital optimization process. The final orbitals are represented in Figure 6.5. Linear combinations of the d_{z^2} orbitals lead to σ and σ* orbitals with significant contributions of the I-orbitals, while the $d_{x^2-y^2}$ orbitals give δ and δ* molecular orbitals, which are strongly mixed with the S orbitals. In both cases the metal-ligand interaction is antibonding, as expected. The diagonalization of the Hamiltonian matrix expressed in the $M_S = -1/2$ subspace spanned by this set of molecular orbitals leads to a doublet ground state with an electronic configuration $(\sigma)^2(\sigma^*)^1 = (d_{z^2})_1^2(d_{z^2})_2^1 + (d_{z^2})_1^1(d_{z^2})_2^2$ where the indices refer to the Pt centers 1 and 2. The strong ligand field exerted by the S atoms pushes the δ orbitals to higher energies, while the weak-field of the iodines does not affect the σ orbitals to such a large extent. In consequence the δ orbitals remain unoccupied and the dominant electronic configuration is: $(\sigma)^2(\sigma^*)^1$. The first excited state mainly consists of the determinants with two electrons in σ and one electron in δ orbitals giving rise the $(\sigma)^2(\delta)^1$ electronic configuration.

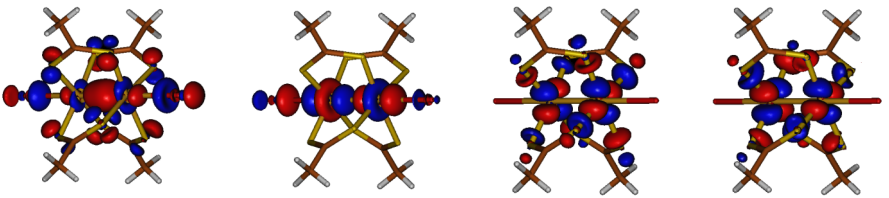

Figure 6.5. State-average optimized orbitals spanning the CAS(3,4) for the Pt dimer.

The $M_S = -1/2$ CAS based on the localized orbitals σ_1 (mainly Pt-$5d_{z^2}$) and δ_1 (mainly Pt-$5d_{x^2-y^2}$) centered on Pt(1) and σ_2 and δ_2 centered on Pt(2) consists of 24 determinants, and defines the full model space *M* of a model Hubbard

Hamiltonian. The extraction of all the interactions of this model is out of the scope of the present study and we will concentrate on the main electronic interactions that govern the electronic structure of the lowest states. In the case of a weak crystal field, the double exchange model would rule the energetic ordering of the lowest states. In the present case, since the dta ligand exert a strong ligand field, the electronic structure is determined by the energy difference D between the δ_i and σ_i orbitals; the hopping integral t_σ between the σ_1 and σ_2 orbitals; the t_δ between the δ_1 and δ_2 orbitals. These interactions and the on-site Coulomb energy U have therefore been extracted from *ab initio* calculations. One may notice that the mentioned parameters can be obtained from different pairs of determinants. For instance, the electron hopping between σ_1 and σ_2 orbitals is the interaction between $\left|\sigma_1\bar{\delta}_1\bar{\delta}_2\right|$ and $\left|\sigma_2\bar{\delta}_1\bar{\delta}_2\right|$, but also between $\left|\sigma_1\bar{\sigma}_2\bar{\delta}_2\right|$ and $\left|\sigma_1\bar{\sigma}_1\bar{\delta}_2\right|$, or $\left|\sigma_1\bar{\sigma}_1\bar{\sigma}_2\right|$ and $\left|\bar{\sigma}_1\sigma_2\bar{\sigma}_2\right|$, etc. All these matrix elements have slightly different values in the extracted effective Hamiltonian, since the electron transfer between σ_1 and σ_2 also depends on the spatial and spin parts of the other electrons in the exact bielectronic Hamiltonian.

Previous studies established that the values of these parameters depend on the level of treatment of electron correlation effects,[94] especially the values of U may change significantly. Hence, to properly evaluate the magnitude of the parameters, large CI expansions are required. In this work, we consider two different, well-defined CI spaces in addition to the space spanned by the 24 determinants. In the first place, we use the DDCI1 space constructed by adding all the Slater determinants in which one electron is moved from (i) the doubly occupied to the σ_i or δ_i and orbitals; (ii) the σ_i or δ_i to the unoccupied orbitals; (iii) the doubly occupied to the unoccupied orbitals. A slightly better wave function can be obtained from the DDCI2 space, which extends the previous space with all Slater determinants with two changes in the occupation of either the inactive or the virtual orbitals.

To numerically determine all the matrix elements of the generalized Hubbard Hamiltonian from the effective Hamiltonian theory,[95] the 24 states with the largest projections onto the model space are *a priori* needed. Due to the

simplicity of the model interactions, the extraction can actually be performed using a smaller model space, and hence a smaller number of roots. Among the 24 determinants, those with all three electrons in the σ orbitals are the most stable ones (group A). The second group of low-energy determinants contains the neutral determinants with two electrons in σ orbitals and one in δ (group B). The determinants with two electrons in σ orbitals and one in δ, with all three electrons on one site, are referred to as ionic determinants and are found at higher energies (group C). The rest of determinants with two or more electrons in δ orbitals lie very high in energy (group D) and the interactions between these are not of interest.

A. Neutral determinants with three electrons in σ orbitals

(1) $|\sigma_1\bar{\sigma}_1\bar{\sigma}_2|$ (2) $|\bar{\sigma}_1\sigma_2\bar{\sigma}_2|$

B. Neutral determinants with two electrons in σ orbitals and one in δ

(3) $|\sigma_1\overline{\sigma_2}\overline{\delta_1}|$ (4) $|\overline{\sigma_1}\sigma_2\overline{\delta_1}|$ (5) $|\overline{\sigma_1}\overline{\sigma_2}\delta_1|$ (6) $|\sigma_1\overline{\sigma_2}\overline{\delta_2}|$

(7) $|\overline{\sigma_1}\sigma_2\overline{\delta_2}|$ (8) $|\overline{\sigma_1}\overline{\sigma_2}\delta_2|$ (9) $|\sigma_1\overline{\sigma_1}\overline{\delta_2}|$ (10) $|\sigma_2\overline{\sigma_2}\delta_1|$

C. Ionic determinants with two electrons in σ orbitals and one in δ

(11) $|\sigma_1\overline{\sigma_1}\overline{\delta_1}|$ (12) $|\sigma_2\overline{\sigma_2}\overline{\delta_2}|$

D. Other determinants with at least two electrons in δ orbitals

(13) $|\sigma_1\overline{\delta_1}\overline{\delta_2}|$ (14) $|\overline{\sigma_1}\delta_1\overline{\delta_2}|$ (15) $|\overline{\sigma_1}\overline{\delta_1}\delta_2|$ (16) $|\sigma_2\overline{\delta_1}\overline{\delta_2}|$

(17) $|\overline{\sigma_2}\delta_1\overline{\delta_2}|$ (18) $|\overline{\sigma_2}\overline{\delta_1}\delta_2|$ (19) $|\overline{\sigma_1}\delta_1\overline{\delta_1}|$ (20) $|\overline{\sigma_2}\delta_2\overline{\delta_2}|$

(21) $|\overline{\sigma_2}\delta_1\overline{\delta_1}|$ (22) $|\overline{\sigma_1}\delta_2\overline{\delta_2}|$ (23) $|\delta_1\overline{\delta_1}\overline{\delta_2}|$ (24) $|\overline{\delta_1}\delta_2\overline{\delta_2}|$

Therefore we have reduced the dimension of the model space to 12 to extract the effective interactions represented in the following CI matrix:

	1	2	3	4	5	6	7	8	9	10	11	12
1	E_1	$-t_\sigma$										
2		E_1										
3			E_4			t_δ	0			t_σ	t_σ	
4				E_3		0	t_δ			$-t_\sigma$	$-t_\sigma$	
5					E_2			t_δ				
6						E_3			t_σ			t_σ
7							E_4		$-t_\sigma$			$-t_\sigma$
8								E_2				
9									E_1+D	0	t_δ	
10										E_1+D		t_δ
11											E_4+U	0
12												E_4+U

The energies of the determinants (diagonal elements of the matrix) have been classified 2 by 2 with the same label, for simplicity. Namely, the energies in (1,1) and (2,2) are labelled E_1 though they are not numerically exactly the same since the right and left sites of the dimer are not strictly equivalent. The same stands for other diagonal elements labelled E_2, E_3 and E_4.

The subspace M' spanned by the first twelve determinants (groups A–C) contains all the information needed to determine t_σ, t_δ, D and U. The twelve states with the largest projections onto the M' model subspace are calculated at the DDCI1 and DDCI2 levels. After an orthonormalization of these projections, the matrix elements of M' were obtained with the effective Hamiltonian theory applying the des Cloizeaux formula:[96]

$$\hat{H}^{eff} = \sum_m \left|\tilde{\Psi}_m\right\rangle E_m \left\langle\tilde{\Psi}_m\right|$$

where $\tilde{\Psi}_m$ are the orthonormalized projections of the 12 computed eigenstates $\tilde{\Psi}_m$ of the exact electronic Hamiltonian projected onto the model space. This method provides exactly the same values of the interactions as the inversion of the matrix of H_{eff} and the use of the computed energies when the number of

unknown interactions is equal to the number of energy differences. As already explained in other papers,[97] owing to the use of both energies and wavefunctions, the effective Hamiltonian theory enables one to determine all the matrix elements of H_{eff} and therefore to extract more information than from the energies only.

As we mentioned above, t_σ and t_δ can be obtained from different matrix elements. Therefore, we have given an averaged value for each parameter. For instance, t_σ results from the interaction between determinants 1 and 2:

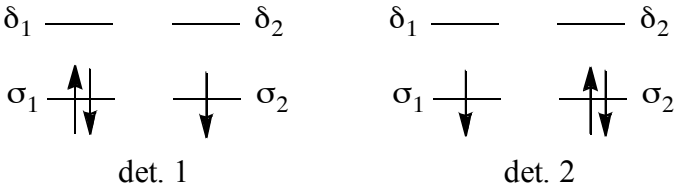

$$t_\sigma = \langle \sigma_1\bar{\sigma}_1\bar{\sigma}_2 | \hat{H} | \bar{\sigma}_1\sigma_2\bar{\sigma}_2 \rangle = -\langle \sigma_1\bar{\sigma}_1\bar{\sigma}_2 | \hat{H} | \sigma_2\bar{\sigma}_1\bar{\sigma}_2 \rangle$$

According to the general Slater-Condon rules, as the Hamiltonian has a bielectronic nature, it leads to

$$t_\sigma = -\langle \sigma_1 | \hat{h} | \sigma_2 \rangle + \langle \sigma_1\sigma_2 | \frac{1-\hat{P}_{12}}{r_{12}} | \bar{\sigma}_1\bar{\sigma}_1 \rangle + \langle \sigma_1\sigma_2 | \frac{1-\hat{P}_{12}}{r_{12}} | \bar{\sigma}_2\bar{\sigma}_2 \rangle$$

Concerning t_δ, it can be obtained similarly. For example, the matrix element (5,8) leads to:

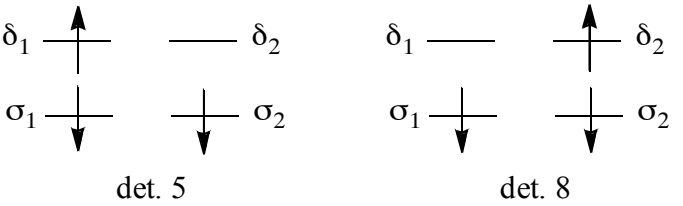

$$t_\delta = \langle \bar{\sigma}_1 \bar{\sigma}_2 \delta_1 | \hat{H} | \bar{\sigma}_1 \bar{\sigma}_2 \delta_2 \rangle =$$

$$\langle \delta_1 | \hat{h} | \delta_2 \rangle + \langle \delta_1 \delta_2 | \frac{1-\hat{P}_{12}}{r_{12}} | \bar{\sigma}_1 \bar{\sigma}_1 \rangle + \langle \delta_1 \delta_2 | \frac{1-\hat{P}_{12}}{r_{12}} | \bar{\sigma}_2 \bar{\sigma}_2 \rangle$$

U is extracted from the energy difference between the diagonal elements (3,3) and (11,11) of the CI matrix for the left site (respectively (7,7) and (12,12) for the right site). These two energy differences are not numerically exactly the same since the right and left sites of the dimer are not equivalent.

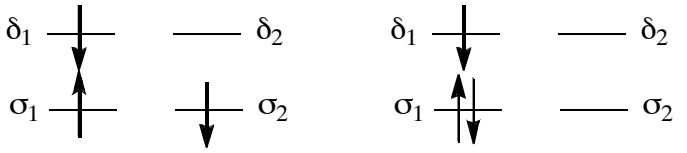

det. 3 det. 11

Another interesting parameter that could be extracted from the diagonal elements of the CI matrix is the energy difference between on-site d_{z^2} and $d_{x^2-y^2}$ atomic orbitals, called *D*. This parameter can be obtained as the energy difference between the following determinants for the left site (respectively determinants 1 and 9 for the right site):

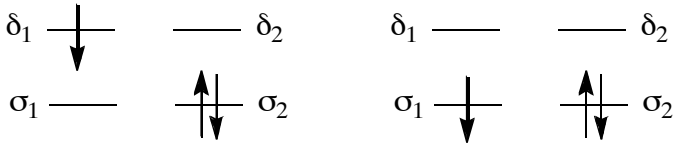

det. 10 det. 2

In Table 6.3 we report mean right-left site values for *U* and *D* as the final values. Concerning electron hopping, it is readily seen that t_σ is roughly one order of magnitude larger than t_δ both at the CASSCF and DDCI2 levels. This is due to the more effective overlap between d_{z^2} atomic orbitals (responsible for the σ hopping) in comparison to the $d_{x^2-y^2}$ ones (δ hopping). The energy difference between d_{z^2} and $d_{x^2-y^2}$ orbitals (*D* parameter) and the relative small value of t_δ are consistent with the obtained $(\sigma)^2(\sigma^*)^1$ electronic structure. One may finally

notice that these interactions depend only slightly on electron correlation, except the on site Coulomb repulsion (U), which becomes smaller when electron correlation is taken into account (38801 and 5911 cm^{-1} at CASSCF and DDCI2 levels, respectively).

Table 6.3. CASCI, DDCI1 and DDCI2 electronic structure parameters (in cm^{-1}) for the Pt dimer.

	t_σ	t_δ	D	U
CASCI	–12156	–1772	26164	38801
DDCI1	–11115	–1617	26866	5838
DDCI2	–11168	–1532	25283	5911

6.3.2.2. $[Ni_2(dta)_4I_2]^{-1}$ Dimer Fragment

For the Ni dimer, we followed the same procedure outlined above for the Pt case. The optimization of the orbitals with respect to the average energy of the four lowest quartet states leads to the set of σ and δ orbitals shown in Figure 6.6. As expected, these orbitals are less diffuse than those of the Pt dimer, and present a weaker antibonding interaction with the ligand orbitals. Contrarily to what was observed for the Pt dimers, the doublet ground state is dominated by the $(\sigma)^2(\delta)^1$ electronic configuration at the CASCI level and shows that the σ bond is highly correlated ($\psi_{GS} = -0.71(\sigma)^2(\delta)^1 + 0.46(\sigma^*)^2(\delta)^1 + \ldots$). Due to the multiconfigurational character of this state, its energy is significantly lower than that of the single determinant $(\sigma)^2(\delta)^1$. However, the inclusion of dynamic electron correlation changes the situation. Due to the compact character of the σ_1 and σ_2 orbitals, dynamic electron correlation stabilizes considerably the state dominated by the configuration $(\sigma)^2(\sigma^*)^1$ which becomes the ground state, although the wave function still has important contributions from other determinants and has a much higher multiconfigurational character than in the Pt case.

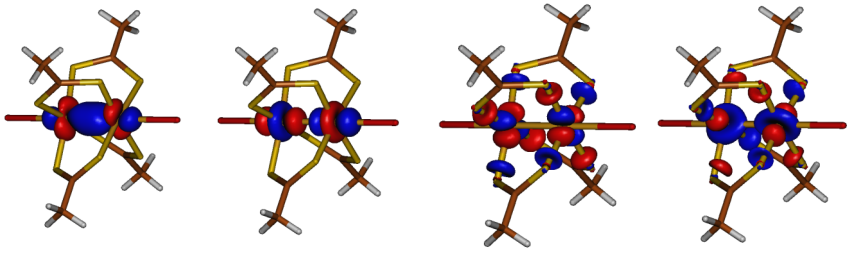

Figure 6.6. State average optimized orbitals spanning the CAS(3,4) for the Ni dimer.

The relevant electronic structure parameters have been extracted from the CASCI, DDCI1 and DDCI2 energies and wave functions as described above for the Pt dimer. Table 6.4 shows that $|t_\sigma|$ is quite large and stronger than $|t_\delta|$ at any level of calculation, indicating here again a large overlap between d_z^2 atomic orbitals of Ni atoms. Moreover, we observe the expected large diminishing of U when electron correlation is accounted for.

Table 6.4. CASCI, DDCI1 and DDCI2 electronic structure parameters (in cm^{-1}) for the Ni dimer.[a]

	t_σ	t_δ	D	U
CASCI	8761	996	23152	240049
DDCI1	6024	1622	21507	21267
DDCI2	5914	1644	22168	26020

(a) t_σ and t_δ extracted from 10×10 CI matrix. D and U extracted from 12×12 CI matrix. See the text for details.

Having a look at the parameters of Tables 6.3 and 6.4, one may notice that the electron transfer integrals (t_σ) are large for both Ni and Pt chains. The large intra-dimer electron transfers arise from the large overlap of adjacent metal d_z^2 atomic orbitals. The main difference between two dimers arises from the magnitude of U. The on site Coulomb repulsion energy of Pt atoms is much smaller than that of Ni due to the size of Pt atoms. At any level, the D for Pt dimer is larger than that of Ni dimer as a result of the stronger antibonding

interaction between Pt and ligand orbitals. For both complexes this parameter reduces slightly taking into account the electron correlation. At correlated levels, both Pt and Ni metal atoms feel a strong ligand field from sulfur atoms so practically only σ MOs are involved in the interactions. Moreover, it can be seen that from three electrons settled in two σ MOs, two of them form the bond and one electron remains unpaired for each M-M unit. It should be noted that the contribution of iodine p_z orbitals in the σ MOs in the Pt dimer is much larger (roughly ×3) than in the Ni one (see Figures 6.5 and 6.6 for a graphical comparison).

The norm of the projections onto the model gives a measure of the reliability of the extracted parameters. In the case of dimer fragments, all projections are very high (>0.97 for Pt; >0.77 for Ni) at the CASCI level, as expected. On the other hand, for DDCI2, the projections in the Pt case are still high (>0.54), but for the Ni dimer the projections of 2 states have a low norm (~0.1), while the rest of the norms are very high (>0.61). This leads to large discrepancies between t_σ (respectively t_δ), which appears in many matrix elements, avoiding extracting a confident averaged value. Therefore, we have extracted these parameters for the Ni dimer from several, smaller model spaces through the effective Hamiltonian approach. For t_σ and t_δ, we observe numerical stability upon changes in the dimension of the model space, which gives robustness to the final parameters reported in Table 6.4, which correspond to the 10×10 CI matrix (determinants 1–10). For the *D* parameter, we report the value extracted from the 12×12 matrix (also consistent to smaller model spaces). Since *U* only appears for model spaces ≥12, to check its validity we refer to the agreement between the present value and previous theoretical studies.[91,98]

6.3.2.3. $[Pt_4(dta)_8I_3]^{-1}$ Tetramer Fragment

Tetranuclear fragments are the smallest units that can represent all the possible charge ordering states mentioned in the Introduction. All experimental and theoretical studies show that the ground state of the Pt system is best described with the AV scheme, with charges uniformly distributed among the Pt sites. According to the schematic representation of this valence-ordered state (Figure

6.7), the active orbitals of the tetramer are expected to be two half-filled σ^* orbitals delocalized on each dimer. In the dimer calculations, we concluded that the dimer can be modeled as a single electron in the σ^* orbital. Therefore, we do not include the δ orbitals in the active space as they do not play any role in the description of the electronic structure of the ground state. The active space of the tetramer contains two σ^* orbitals and two unpaired electrons. The orbitals are optimized for the triplet state and shown in Figure 6.8. Subsequently, the Hubbard Hamiltonian matrix expressed in the $M_S = 0$ subspace is diagonalized, providing the energy and wave function of three singlets and one triplet states. The matrix representation of the $M_S = 0$ subspace is the following:[94]

	$\lvert a\bar{b}\rangle$	$\lvert b\bar{a}\rangle$	$\lvert a\bar{a}\rangle$	$\lvert b\bar{b}\rangle$
$\langle a\bar{b}\rvert$	0	K_{ab}	t_{ab}	t_{ab}
$\langle b\bar{a}\rvert$	K_{ab}	0	t_{ab}	t_{ab}
$\langle a\bar{a}\rvert$	t_{ab}	t_{ab}	U	K'_{ab}
$\langle b\bar{b}\rvert$	t_{ab}	t_{ab}	K'_{ab}	U

where $\lvert a\bar{b}\rangle$ and $\lvert b\bar{a}\rangle$ are the so-called neutral determinants with one electron on each dimer, and $\lvert a\bar{a}\rangle$ and $\lvert b\bar{b}\rangle$ the ionic determinants with two electrons on the same dimer. In this notation, we use $a = \sigma_1^*$ and $b = \sigma_2^*$, the optimized orbitals being localized on dimer 1 or 2, respectively. The energy of the neutral determinants is taken as zero of energy, t_{ab} is the inter-dimer hopping parameter, i.e., from one Pt_2 (or Ni_2) to a neighboring one via the bridging iodine atom and K_{ab} and K'_{ab} are the effective exchange integrals which are different at the correlated levels (for instance spin polarization only affects the coupling between the neutral determinants). Numerical estimates of the relevant parameters are extracted from the *ab initio* results by projecting the four roots with the largest projection onto the $M_S = 0$ subspace and application of the des Cloizeaux formula. In addition, the magnetic exchange interaction J can be

easily calculated from the energy difference between the triplet and singlet states dominated by the neutral determinants. In order to estimate the quality of the extracted interactions, the values of the effective exchange J has also been calculated from the extracted K_{ab}, t_{ab} and U values using the variational expression[94]

$$J^{\text{var}} = 2K_{ab} + \frac{U - \sqrt{U^2 + 16 t_{ab}^2}}{2}$$

As can be seen from the results listed in Table 6.5, the directly computed and extracted values of the effective exchange compare very well. t_{ab} and K_{ab} are only weakly affected by the inclusion of dynamic electron correlation. On the contrary U decreases at the DDCI1 and DDCI2 levels as usually observed.

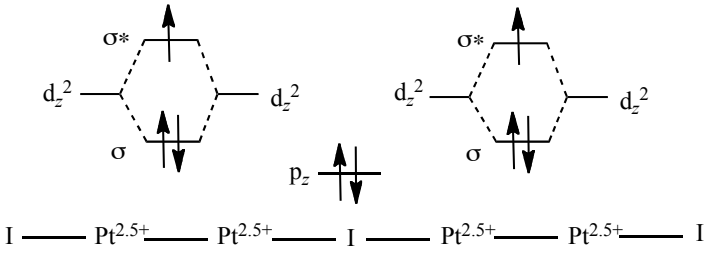

Figure 6.7. Molecular orbital diagram for the Pt tetramer according to the AV state.

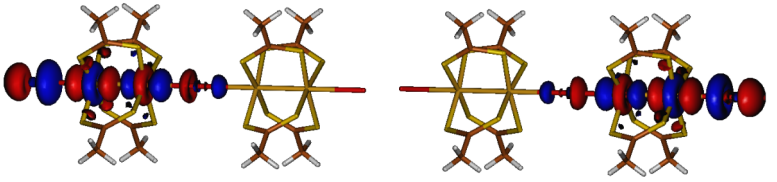

Figure 6.8. Triplet optimized orbitals spanning the CAS(2,2) for the Pt tetramer.

Compared to the Pt dimer, the hopping parameter t_{ab} takes a significantly smaller value, as expected, since two sites (dimer units) are farther from each other in the tetramer than in the dimer and t_{ab} decays rapidly with the distance.

The observation of a smaller U in the Pt dimer with respect to the Pt tetramer can be explained by the fact that the two-center repulsive Coulomb interaction in tetramer is weaker than in the dimer ($J_{ab} \propto 1/r_{ab}$). Hence, the neutral determinants in the tetramer are more stable than those of the dimer. This leads to an increase of the energy difference between the neutral and the ionic determinants ($U = J_{aa} - J_{ab}$).[99] Although J_{inter} is not large enough to unambiguously interpret it as a fingerprint of bond formation of the two σ^* dimer orbitals, it is still at least four times larger than the strong antiferromagnetic coupling measured in the parent compounds of the high-T_c superconductors: $J(La_2CuO_4) \approx -1000$ cm^{-1}.[100]

Table 6.5. CASCI, DDCI1 and DDCI2 electronic structure parameters (in cm^{-1}) for the Pt tetramer.

	K_{ab}	t_{ab}	U	J^{var}	J
CASCI	148	–4420	56529	–1054	–1058
DDCI1	126	–3978	13339	–3460	–3560
DDCI2	144	–4004	10292	–4084	–4271

6.3.2.4. $[Ni_4(dta)_8I_3]^{-1}$ Tetramer Fragment

The valence-ordered state of the $[Ni_2(dta)_4I]_\infty$ chain has not been clarified so far. Previous experimental and theoretical studies[23,40,60,65] state that it has the same electronic structure as the Pt system, namely an AV state. Given the small difference in the two Ni-I bond distances (0.012 Å, see Table 6.1), the AV state seems a logical representation of the electron distribution in the ground state. If this were indeed the case, one would expect the same active orbitals as in the Pt chain. However, the calculation on the tetrameric Ni compound does not feature electron delocalization over dimer units. As Figure 6.9 shows, the orbitals are localized on only one of the Ni atoms within each dimer. With the CAS(2,2), two triplets have been independently optimized with similar energies. In the most stable state, the unpaired electrons are localized on the central Ni atoms in

the fragment (Figure 6.9a), while a second triplet at 0.28 eV higher energy has the active orbitals composed of the terminal Ni-3d_{z^2} orbitals (Figure 6.9b).

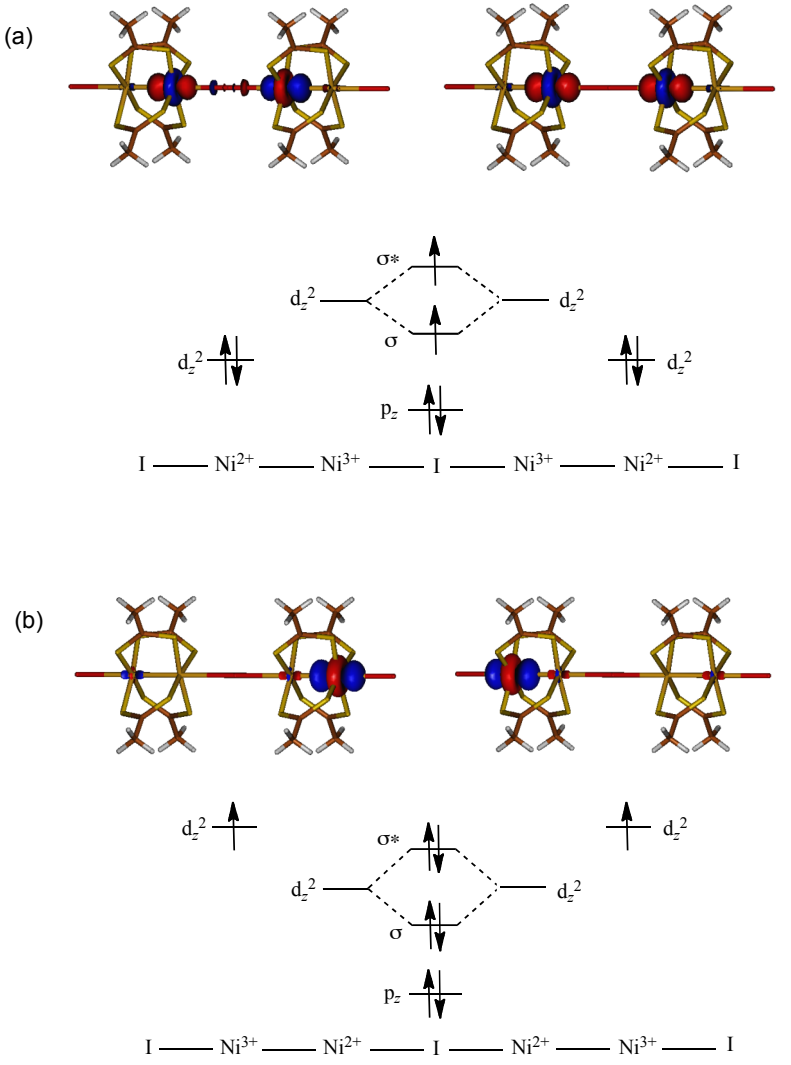

Figure 6.9. Orbitals spanning the CAS(2,2) optimized for (a) the most stable triplet and (b) the second triplet at 0.28 eV, with their corresponding ACP charge-ordering state representations.

Both states represent an ACP state with strong charge fluctuations within each dimer, as schematically shown. The energy difference remains nearly constant (0.3 eV) when dynamic electron correlation effects are taken into account with second-order perturbation theory. We have also expanded the active space to a CAS(6,4) to check if the minimal active space (2,2) could have biased the results. The nearly exact coincidence of the results with both active spaces puts the previous results on a firm basis. There is no indication of an AV state at low energy in the tetramer calculations.

Table 6.6. CASCI, DDCI1 and DDCI2 electronic structure parameters (in cm^{-1}) for the Ni tetramer.

	K_{ab}	t_{ab}	U	J^{var}	J
CASCI	15	–2685	196446	–116	–117
DDCI1	377	–3473	36974	–508	–595
DDCI2	537	–3760	34367	–499	–665

Based on the active orbitals that give the most stable triplet, the electronic structure parameters have been extracted by construction of the valence effective Hamiltonian at different levels of correlation (see Table 6.6). Here again the extracted effective exchange integral from the variational expression compares well with the computed one. The main difference between the Ni and Pt tetramers is the value of U: in the Ni compound it is almost three times larger than that of the Pt compound. This arises from the strongly localized character of the orbitals involved in electron transfer. Consequently, the antiferromagnetic exchange in the Ni fragment is much weaker than in the Pt chain, excluding the possibility of inter dimer bond formation via the $3d_{z^2}$ orbitals.

To exclude the possibility that the observed ACP solution is due to finite cluster size effects, we have repeated the same calculations on a fragment with eight Ni centers. This leads to an active space of four electrons distributed over four dimers. Different starting points in the optimization of the wave function always led to the same final solution: a quintet state with the active orbitals of

mainly $3d_{z^2}$ character localized on the two terminal and the two central Ni ions, see Figure 6.10. This orbital arrangement can be considered as a confirmation of an ACP state, schematically shown for the octameric fragment in Figure 6.11.

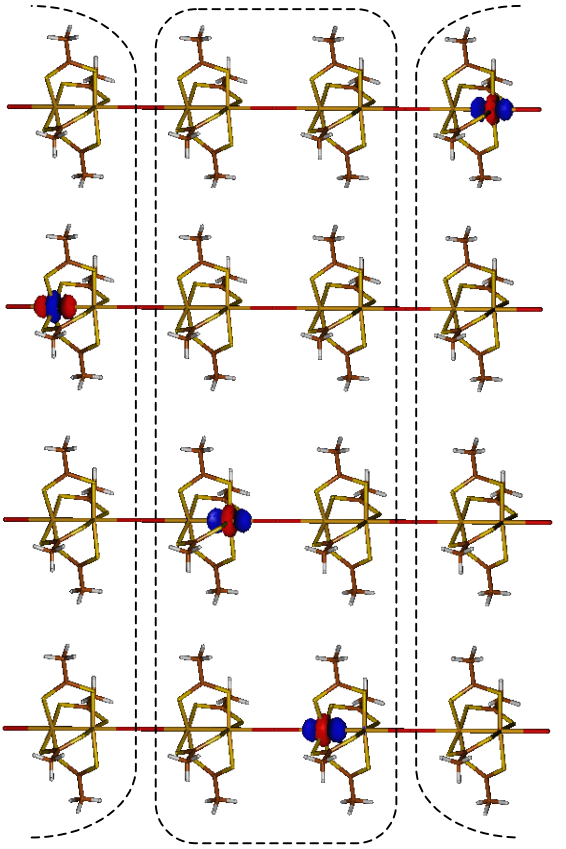

"embedding" tetrameric fragment *"embedding"*

Figure 6.10. Quintet optimized orbitals spanning the CAS(4,4) for the Ni_8 fragment.

This octameric fragment actually may be considered as a tetramer "*embedded*" by two dimers described at the *ab initio* level instead of the set of pseudopotentials and point charges used for the tetramer. A larger fragment also

has been studied: the chain with twelve Ni atoms (two Ni_4 fragments *embedded* by two Ni_2 units at the *ab initio* level). The active space includes six σ electrons over six M–M units. Here again the wave function optimization leads to orbitals (Figure B1 in Appendix B) localized on Ni atoms, implying an ACP charge ordering state as shown in Figure 6.12. It should be mentioned that the geometry of larger fragments also have been taken from Table 6.1.

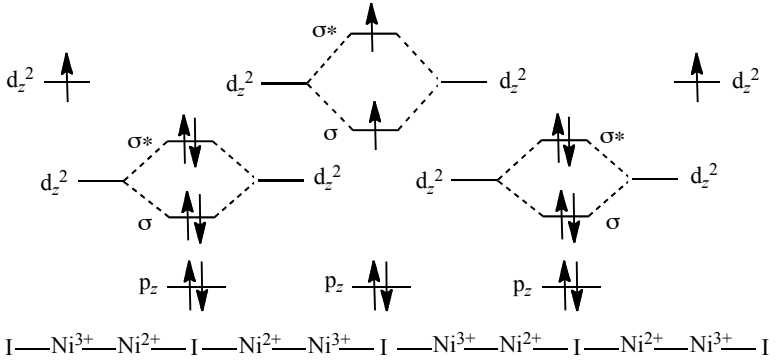

Figure 6.11. Molecular orbital diagram for the Ni_8 fragment according to the ACP state.

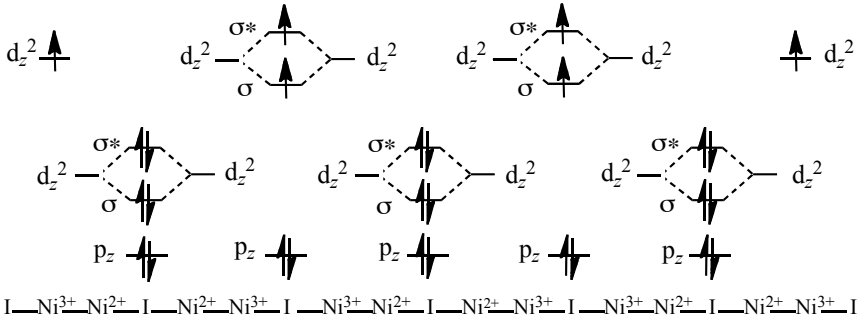

Figure 6.12. Molecular orbital diagram for the Ni_{12} fragment according to the ACP state.

6.4. Conclusions

The present combined wave function and density functional theory study explains the dependence of the physicochemical properties of MMX chains on the chemical nature of the metal ions constituting the chain. Periodic DFT calculations performed with the PBE and a hybrid functional (30% Hartree-Fock exchange) indicate a uniform charge distribution over dimer units in the Pt chain whereas for the Ni compound each functional gives a different behavior, namely, the PBE shows that valence electrons are evenly distributed although the hybrid 30% HF exchange functional tends to some charge polarization. The analysis of the density of states gives an energy gap of 1.93 eV in the Ni system, while in the Pt chain the Fermi level lies within a band with an important contribution of Pt and I atoms. The latter results are in agreement with a difference of three orders of magnitude in their measured electrical conductivities.

Ab initio CI calculations reveal that the observed differences in electrical conductivity for Pt vs. Ni chains can be attributed to the difference between inter-dimer on-site Coulomb repulsion energy U, which is considerably larger for Ni due to the strongly localized character of the σ orbitals in the Ni compound. The correlation of electrical conductivities to the $t_{inter\text{-}dimer}$ values does not make sense since this parameter has different character in Pt and Ni chains. In other words, $t_{inter\text{-}dimer}$ in the Ni case describes the electron delocalization only over a part of the chain while in the Pt case the electron is delocalized over the whole chain. Finally, we have examined the charge-ordering states of Pt and Ni chains by *ab initio* calculations on tetramer fragments. These show that the orbital arrangement coincides with the Alternate Charge Polarization state for Ni and the Averaged Valence state for Pt chains. The ACP state has also been found in Ni_8 and Ni_{12} fragments.

References

[1] M. J. Kelly, *Low-Dimensional Semiconductors (Materials, Physics, Technology, Devices),* Clarendon Press, Oxford, Vol. 16-19, 1995.

[2] C. N. R. Rao, A. Müller, A. K. Cheetham, *Nanomaterials Chemistry (Recent Developments and New Directions),* Wiley-VCH, Weinheim, 2007.

[3] H. Klaud, *Organic Electronics (Materials, Manufacturing and Applications),* Wiley-VCH, Weinheim, 2006.

[4] H. J. Keller, *Chemistry and Physics of One-Dimensional Metals,* Plenum Press, New York, 1977.

[5] A. J. Heeger, J. T. Devreese, R. P. Evrard, V. E. Van Doren, *Highly Conducting One-dimensional Solids,* Plenum Press, New York, p.69, 1979.

[6] L. B Coleman, M. J. Cohen, D. J. Sandman, F. G. Yamagishi, A. F. Garito, A. J. Heeger, *Solid State Commun*. 12 (1973) 1125.

[7] M. Yano, K. Aoyama, Y. Ishida, M. Tasumi, K. Sato, D. Shiomi, T. Takui, *Polyhedron* 22 (2003) 2003.

[8] A. S. Dhindsa, Y. P. Song, J. P. Badyal. M. R. Bryce, Y. M. Lvov, M. C. Petty, J. Yarwood, *Chem. Mater*. 4 (1992) 724.

[9] M. Yano, Y. Ishida, K. Aoyama, M. Tatsumi, K. Sato, D. Shiomi, A. Ichimura, T. Takui, *Synth. Met*. 137 (2003) 1275.

[10] S. S. Khasanov, A. Pérez-Benítez, B. Zh. Narymbetov, L. V. Zorina, R. P. Shibaeva, J. Singleton, A. K. Klehe, V. N. Laukhin, J. Vidal-Gancedo, J. Veciana, E. Canadell, C. Rovira, *J. Mater. Chem*. 12 (2002) 432.

[11] M. M. Labes, P. Love, L. F. Nichols, *Chem. Rev*. 79 (1979) 1.

[12] B. J. Holliday, T. M. Swager, *Chem. Commun*. (2005) 23.

[13] C. Janiak, *Dalton Trans*. (2003) 2781.

[14] R. Mas-Ballesté, J. Gómez-Herrero, F. Zamora, *Chem. Soc. Rev*. 39 (2010) 4420.

[15] K. Krogmann, *Angew. Chem., Int. Ed*. 8 (1969) 35.

[16] J. S. Miller, *Extended Linear Chain Compounds,* Plenum, New York, Vol. 1-3, 1982.

[17] P. Day, H. J. Keller, *Low-Dimensional Cooperative Phenomena*, Plenum, New York, p.191, 1974.

[18] R. J. H. Clark, D. E. Brown, *Mixed Valence Compounds,* Reidel, Dordrecht, p.271, 1982.

[19] F. A. Cotton, R. A. Walton, *Multiple Bonds Between Metal Atoms,* Clarendon, Oxford, 1993.

[20] M. Mitsumi, H. Ueda, K. Furukawa, Y. Ozawa, K. Toriumi, M. Kurmoo, *J. Am. Chem. Soc*. 130 (2008) 14102.

[21] D. Olea, R. González-Prieto, J. L. Priego, M. C. Barral, P. J. de Pablo, M. R. Torres, J. Gómez-Herrero, R. Jiménez-Aparicio, F. Zamora, *Chem. Commun*. (2007) 1591.

[22] C. Bellitto, A. Flamini, L. Gastaldi, L. Scaramuzza, *Inorg. Chem*. 22 (1983) 444.

[23] C. Bellitto, G. Dessy, V. Fares, *Inorg. Chem*. 24 (1985) 2815.

[24] R. J. H. Clark, J. R. Walton, *Inorg. Chim. Acta*. 129 (1987) 163.

[25] M. Mitsumi, Y. Yoshida, A. Kohyama, Y. Kitagawa, Y. Ozawa, M. Kobayashi, K. Toriumi, M. Tadokoro, N. Ikeda, M. Okumura, M. Kurmoo, *Inorg. Chem*. 48 (2009) 6680.

[26] C. M. Che, F. H. Herbstain, W. P. Snaefer, R. E. Marsh, H. B. Gray, *J. Am. Chem. Soc*. 105 (1983) 4604.

[27] M. Kurmoo, R. J. H. Clark, *Inorg. Chem*. 24 (1985) 4420.

[28] R. J. H. Clark, M. Kurmoo, H. M. Dawes, M. B. Hursthouse, *Inorg. Chem*. 25 (1986) 409.

[29] L. G Butler, M. H. Zietlow, C. M. Che, W. P. Schaefer, S. Sridhar, P. J. Grunthaner, B. I. Swanson, R. J. H. Clark, H. B. Gray, *J. Am. Chem. Soc*. 110 (1988) 1155.

[30] M. A. Stroud, H. G. Drickamer, M. H. Zietlow, H. B. Gray, B. I. Swanson, *J. Am. Chem. Soc*. 111 (1989) 66.

[31] M. Yamashita, K. Toriumi, *Inorg. Chim. Acta.* 178 (1990) 143.

[32] T. Mitani, Y. Wada, M. Yamashita, K. Toriumi, A. Kobayashi, H. Kobayashi, *Synth. Met*. 64 (1994) 291.

[33] M. Yamashita, S. Miya, T. Kawashima, T. Manabe, T. Sonoyama, H. Kitagawa, T. Mitani, H. Okamoto, R. Ikeda, *J. Am. Chem. Soc*. 121 (1999) 2321.

[34] H. Matsuzaki, T. Matsuoka, H. Kishida, K. Takizawa, H. Miyasaka, K. Sugiura, M. Yamashita, H. Okamoto, *Phys. Rev. Lett*. 90 (2003) 046401.

[35] H. Mastuzaki, H. Kishida, H. Okamoto, K. Takizawa, S. Matsunaga, S. Takaishi, H. Miyasaka, K. Sugiura, M. Yamashita, *Angew. Chem., Int. Ed.* 44 (2005) 3240.

[36] M. Yamashita, S. Takaishi, A. Kobayashi, H. Kitagawa, H. Matsuzaki, H. Okamoto, *Coord. Chem. Rev*. 250 (2006) 2335.

[37] H. Iguchi, S. Takaishi, T. Kajiwara, H. Miyasaka, M. Yamashita, H. Matsuzaki, H. Okamoto, *J. Am. Chem. Soc*. 130 (2008) 17668.

[38] J. B. Weinrach, M. Hawley, A. P. Sattelberger, B. I. Swanson, *Solid State Commun*. 77 (1991) 853.

[39] N. Kimura, H. Ohki, R. Ikeda, M. Yamashita, *Chem. Phys. Lett*. 220 (1994) 40.

[40] M. Yamashita, Y. Wada, K. Toriumi, T. Mitani, *Mol. Cryst. Liq. Cryst*. 216 (1992) 207.

[41] H. Kitagawa, N. Onodera, T. Sonoyama, M. Yamamoto, T. Fukawa, T. Mitani, M. Seto, Y. Maeda, *J. Am. Chem. Soc*. 121 (1999) 10068.

[42] H. Kitagawa, S. Nakagami, T. Mitani, *Synth. Met*. 116 (2001) 401.

[43] H. Kitagawa, M. Yamamoto, N. Onodera, T. Mitani, *Synth. Met*. 103 (1999) 2151.

[44] H. Kitagawa, T. Sonoyama, T. Mitani, M. Seto, Y. Maeda, *Synth. Met*. 103 (1999) 2159.

[45] M. Mitsumi, T. Yamashita, Y. Aiga, K. Toriumi, H. Kitagawa, T. Mitani, M. Kurmoo, *Inorg. Chem*. 50 (2011) 4368.

[46] A. Kobayashi, H. Kitagawa, R. Ikeda, *Mol. Cryst. Liq. Cryst*. 379 (2002) 315.

[47] M. Mitsumi, T. Murase, H. Kishida, T. Yoshinari, Y. Ozawa, K. Toriumi, T. Sonoyama, H. Kitagawa, T. Mitani, *J. Am. Chem. Soc*. 123 (2001) 11179.

[48] M. Mitsumi, K. Kitamura, A. Morinaga, Y. Ozawa, M. Kobayashi, K. Toriumi, Y. Iso, H. Kitagawa, T. Mitani, *Angew. Chem., Int. Ed*. 41 (2002) 2767.

[49] M. Mitsumi, S. Umebayashi, Y. Ozawa, K. Toriumi, H. Kitagawa, T. Mitani, *Chem. Lett*. 31 (2002) 258.

[50] H. Tanaka, Y. Hasegawa, H. Ito, S. Kuroda, T. Yamashita, M. Mitsumi, K. Toriumi, *Synth. Met*. 152 (2005) 141.

[51] S. A. Borshch, K. Prassides, V. Robert, A. O. Solonenko, *J. Chem. Phys*. 109 (1998) 4562.

[52] V. Robert, S. Petit, S. A. Borshch, *Inorg. Chem*. 38 (1999) 1573.

[53] M. Kuwabara, K. Yonemitsu, *J. Mater. Chem*. 11 (2001) 2163.

[54] S. Yamamoto, *Phys. Rev. B* 63 (2001) 125124.

[55] S. Yamamoto, *Phys. Rev. B* 66 (2002) 165113.

[56] M. Kuwabara, K. Yonemitsu, *Synth. Met*. 120 (2001) 947.

[57] J. Ohara, S. Yamamoto, *Phys. Rev. B* 70 (2004) 115112.

[58] J. Ohara, S. Yamamoto, *J. Phys. Chem. Solids* 66 (2005) 1571.

[59] J. Ohara, S. Yamamoto, *Phys. Rev. B* 73 (2006) 045122.

[60] A. Calzolari, S. S. Alexandre, F. Zamora, R. Di Felice, *J. Am. Chem. Soc*. 130 (2008) 5552.

[61] H. Kitagawa, N. Onodera, J. S. Ahn, T. Mitani, M. Kim, Y. Ozawa, K. Toriumi, K. Yasui, T. Manabe, M. Yamashita, *Mol. Cryst. Liq. Cryst*. 285 (1996) 311.

[62] H. Kitagawa, N. Onodera, J. S. Ahn, T. Mitani, K. Toriumi, M. Yamashita, *Synth. Met*. 86 (1997) 1931.

[63] R. Ikeda, N. Kimura, H. Ohki, T. Furuta, M. Yamashita, *Synth. Met*. 71 (1995) 1907.

[64] R. Makiura, H. Kitagawa, R. Ikeda, *Mol. Cryst. Liq. Cryst*. 379 (2002) 309.

[65] S. Nakano, Y. Kitagawa, T. Kawakami, K. Yamaguchi, *Polyhedron* 22 (2003) 2027.

[66] R. Dovesi, V. R. Saunders, C. Roetti, R. Orlando, C. M. Zicovich-Wilson, F. Pascale, B. Civalleri, K. Doll, N. M. Harrison, I. J. Bush, P. D´Arco, M. Llunell, CRYSTAL06, User´s Manual, University of Torino, Torino, 2006.

[67] J. P. Perdew, K. Burke, M. Ernzerhof, *Phys. Rev. Lett*. 77 (1996) 3865.

[68] (a) A. D. Becke, *J. Chem. Phys*. 98 (1993) 5648. (b) C. Lee, W. Yang, R. G. Parr, *Phys. Rev. B* 37 (1988) 785.

[69] For Ni: M. D. Towler, N. L. Allan, N. M. Harrison, V. R. Saunders, W. C. Mackrodt, E. Apra, *Phys. Rev. B* 50 (1994) 5041. For S: A. Lichanot, E. Apra, R. Dovesi, *Phys. Stat. Sol. (b)* 177 (1993) 157.

[70] For C: R. Dovesi, M. Causa, R. Orlando, C. Roetti, V. R. Saunders, *J. Chem. Phys.,* 92 (1990) 7402. For H: C. Gatti, V. R. Saunders, C. Roetti, *J. Chem. Phys*. 101 (1994) 10686.

[71] For Pt: K. Doll, *Surface Science,* 573 (2004) 464. For I: K. Doll, H. Stoll, *Phys. Rev. B* 57 (1998) 4327.

[72] B. O. Roos, R. Lindh, P. Å. Malmqvist, V. Veryazov, P. O. Widmark, *J. Phys. Chem. A* 108 (2004) 2851.

[73] B. O. Roos, R. Lindh, P. Å. Malmqvist, V. Veryazov, P. O. Widmark, *J. Phys. Chem. A* 109 (2005) 6575.

[74] M. Casarrubios, L. Seijo, *J. Chem. Phys*. 110 (1999) 784.

[75] Z. Barandiaran, L. Seijo, *Can. J. Chem*. 70 (1992) 409.

[76] Z. Barandiaran, L. Seijo, *J. Chem. Phys*. 101 (1994) 4049.

[77] A. Bergner, M. Dolg, W. Kuechle, H. Stoll, H. Preuss, *Mol. Phys*. 80 (1993) 1431.

[78] W. J. Hehre, R. Ditchfield, J. A. Pople, *J. Chem. Phys*. 56 (1972) 2257.

[79] Z. Barandiarán, L. Seijo, *J. Chem. Phys*. 89 (1988) 5739.

[80] MOLCAS Version 7.4. Department of Theoretical Chemistry, University of Lund, G. Karlström, R. Lindh, P. Å. Malmqvist, B. O. Roos, U. Ryde, V. Veryazov, P. O. Widmark, M. Cossi, B. Schimmelpfennig, P. Neogrady, L. Seijo, *Comput. Mater. Sci*. 28 (2003) 222.

[81] (a) CASDI program: N. Benamor, D. Maynau, *Chem. Phys. Lett*. 286 (1998) 211. (b) D. Maynau, N. Benamor, J. Pitarch-Ruiz, CASDI program, Laboratoire de Chimie et de Physique Quantiques, Toulouse University, Toulouse, France, 1999.

[82] J. Miralles, J. P. Daudey, R. Caballol, *Chem. Phys. Lett*. 198 (1992) 555.

[83] J. Miralles, O. Castell, R. Caballol, J. P. Malrieu, *Chem. Phys*. 172 (1993) 33.

[84] O. Castell, R. Caballol, V. M. García, K. Handrick, *Inorg. Chem*. 35 (1996) 1609.

[85] O. Castell, R. Caballol, *Inorg. Chem*. 38 (1999) 668.

[86] J. Cabrero, N. Benamor, C. de Graaf, F. Illas, R. Caballol, *J. Phys. Chem. A* 104 (2000) 9983.

[87] C. J. Calzado, J. F. Sanz, J. P. Malrieu, F. Illas, *Chem. Phys. Lett*. 307 (1999) 102.

[88] C. J. Calzado, J. F. Sanz, J. P. Malrieu, *J. Chem. Phys*. 112 (2000) 5158.

[89] I. de P. R. Moreira, F. Illas, C. J. Calzado, J. F. Sanz, J. P. Malrieu, N. Benamor, D. Maynau, *Phys. Rev. B* 59 (1999) R6593.

[90] N. Suaud, M. B. Lepetit, *Phys. Rev. B* 62 (2000) 402.

[91] P. Labèguerie, C. Boilleau, R. Bastardis, N. Suaud, N. Guihéry, J. P. Malrieu, *J. Chem. Phys*. 129 (2008) 154110.

[92] I. de P. R. Moreira, F. Illas, R. L. Martin, *Phys. Rev. B* 65 (2002) 155102.

[93] X. Feng, N. M. Harrison, *Phys. Rev. B* 70 (2004) 092402.

[94] C. J. Calzado, J. Cabrero, J. P. Malrieu, R. Caballol, *J. Chem. Phys*. 116 (2002) 3985.

[95] C. Bloch, *Nucl. Phys*. 6 (1958) 329.

[96] J. des Cloizeaux, *Nucl. Phys*. 20 (1960) 321.

[97] (a) R. Maurice, R. Bastardis, C. de Graaf, N. Suaud, T. Mallah, N. Guihéry, *J. Chem. Theory Comput.* 5 (2009) 297. (b) R. Maurice, N. Guihéry, R. Bastardis, C. de Graaf, *J. Chem. Theory Comput.* 6 (2010) 55 and *J. Chem. Theory Comput.* 6 (2010) 977. (c) R. Maurice, A. M. Pradipto, N. Guihéry, R. Broer, C. de Graaf, *J. Chem. Theory Comput.* 6 (2010) 3092.

[98] Z. Tabookht, X. López, M. Bénard, C. de Graaf, *J. Phys. Chem. A* 114 (2010) 12291.

[99] P. J. Hay, J. C. Thibeault, R. Hoffmann, *J. Am. Chem. Soc*. 97 (1975) 4884.

[100] R. R. P. Singh, P. A. Fleury, K. B. Lyons, P. E. Sulewski, *Phys. Rev. Lett*. 62 (1989) 2736.

General Conclusions

In this thesis, the electronic structure of linear nanowires and the features derived from it have been analyzed by means of computational tools. Two main families of compounds have been studied, namely, extended metal atom chains (EMACs) and 1-D compounds of the MMX type. For this goal, different computational strategies have been applied to reproduce, explain or propose relevant molecular characeristics with potential interest in technology, such as electronic structure parameters related to magnetic and conduction properties.

The magnetic interactions have been comprehensively described for a series of well-known trinuclear EMAC complexes and some related hypothetical compounds with wave function based methods. At CASSCF/CASPT2 level, the J parameter in $[Cu_3(dpa)_4Cl_2]^+$, containing two S = ½ centers, is nicely reproduced, but CASPT2 calculations for $Cu_3(dpa)_4Cl_2$ (three S = ½ centers) and

$Ni_3(dpa)_4Cl_2$ (two $S = 1$ centers) provide only 33% and 60% of their respective experimental J values. For the latter complex, the J strongly depends on the metal-metal distance so that, with the experimental Ni-Ni distance, ~75% of the measured J is recovered, suggesting that the σ interaction, which takes place directly through the Ni-Ni axis, dominates the overall magnetic interaction. However, for the neutral $Cu_3(dpa)_4Cl_2$ complex, efforts to obtain an accteptable value of J were unsuccessful. Unfortunately, we have not been able to pinpoint the shortcomings in the theoretical treatment of the coupling in such system. More effort will be dedicated in the near future to further clarify the origin of the mismatch between theory and experiment. This study establishes the applicability of correlated *ab initio* wave function-based methods in large polynuclear transition metal complexes.

The performance of the standard Heisenberg Hamiltonian on trimetallic EMACs has been examined through the calculation of the biquadratic exchange parameter by DFT in trimetallic complexes with two $S = 1$ sites. For the real $Ni_3(dpa)_4Cl_2$ complex, the hypothesis that the origin for the previously reported underestimation of J at the DFT/B3LYP level arises from the poor performance of the simple Heisenberg Hamiltonian was rejected since the deviations computed from this spin Hamiltonian are small. On the other hand, calculations on the hypothetical $Pd_3(dpa)_4Cl_2$ complex show that the deviation is considerably large and using a more elaborate form of the Heisenberg Hamiltonian is recommended, confirming our prediction for transition metals of the second period. The contribution of σ and δ pathways existing in compounds with $S = 1$ magnetic centers to the total J has been also determined. In all of them, the σ interaction is largely dominant (90-95%) and may be attributed to its shorter, thus more effective, pathway in comparison to the δ-like interaction.

The origin of the uncommon underestimation of the DFT-computed J for $Ni_3(dpa)_4Cl_2$ and also $Ni_5(tpda)_4Cl_2$ is ascribed to the poor description of the above-mentioned σ interaction with the B3LYP functional. This dominant interaction takes place between neighboring metal atoms separated by longer distances than the ususal covalent ones (characteristic of the δ pathway).

Different amounts of exact exchange have been introduced to the hybrid functional to observe how J_σ and J_δ couplings vary. It comes out that the dominant σ-like interaction is much more sensitive to this variation. Thus, the B3LYP functional not only does not overstimate the σ fraction of *J* —contrarily to most *J* typically computed— but strongly underestimates it, being the responsible for the underestimation of the total *J*. Confirmation of this conclusion and a significant improvement of *J* is provided when using the range-separated LC-ωPBE functional, which achieves a better description of the long-range interaction of σ type, partially solving the underestimation of the dominant part of *J*.

Hypothetical heterometallic EMACs formally containing 22 valence metal electrons were studied via DFT calculations. The search for low-spin ground states without strongly localized unpaired electrons may open the door to new electrical properties. It has been found that $RhPdRh(dpa)_4Cl_2$ and $RhPdRh(dpa)_4(NCS)_2$ trimetallic complexes could feature, if they were synthesized, double occupancy of σ^{nb} and empty σ^* orbitals, namely, a closed shell configuration. This configuration can be a good precursor for a delocalized configuration, $(\sigma^{nb})^2(\sigma^*)^1$, upon reduction. However, the latter configuration is not accessible energetically and the $(\sigma^{nb})^2(\delta_{Pd\text{-}N}^*)^1$ situation is the preferred one. This configuration, although not implying any electron delocalization along the metal backbone, is along with a notable axial Rh-X lengthening, which is potentially interesting in on/off switches.

Finally, for the MMX linear $Ni_2(dta)_4Cl$ and $Pt_2(dta)_4Cl$ compounds, the marked different electrical conductivity of Pt- vs. Ni-based chains has been explained by comparison of their electronic structure parameters via the application of the effective Hamiltonian theory. Electronic structure parameters extracted from accurate CI calculations reveal that the larger electrical conductivity of the Pt chain is ascribed to the smaller inter-dimer on-site Coulomb repulsion energy, *U*. The simple correlation of the different electrical conductivities with the geometry is ruled out since both chains are almost symmetric (experimental geometries), neither is this feature related to the

hopping integrals. Instead, we ascribe the difference in conductivity to the appearance of different charge-ordering states. These states in Pt and Ni chains were examined by *ab initio* calculations on tetramer fragments revealing an Alternate Charge Polarization state for the Ni chain and an Average Valence state for the Pt chain. The ACP state has also been found in Ni_8 and Ni_{12} fragments. Periodic DFT calculations were also used to give additional evidence for the explanation of the different conductivities in Pt and Ni chains in terms of charge ordering states. The hybrid functional with 30% Hartree-Fock exchange, which outperforms PBE, shows a different amount of charge polarization in these chains, a uniform charge distribution over dimer units in the Pt chain and a strong charge polarization in the Ni compound. The density of states gives an energy gap of 1.93 eV in the latter while in the Pt chain the Fermi level was found within a band with an important contribution of the Pt and I atoms.

Appendix A

UNIVERSITAT ROVIRA I VIRGILI
THEORETICAL STUDY OF MAGNETIC AND CONDUCTING PROPERTIES OF TRANSITION METAL NANOWIRES
Zahra Tabookht
DL:T-1807-2011

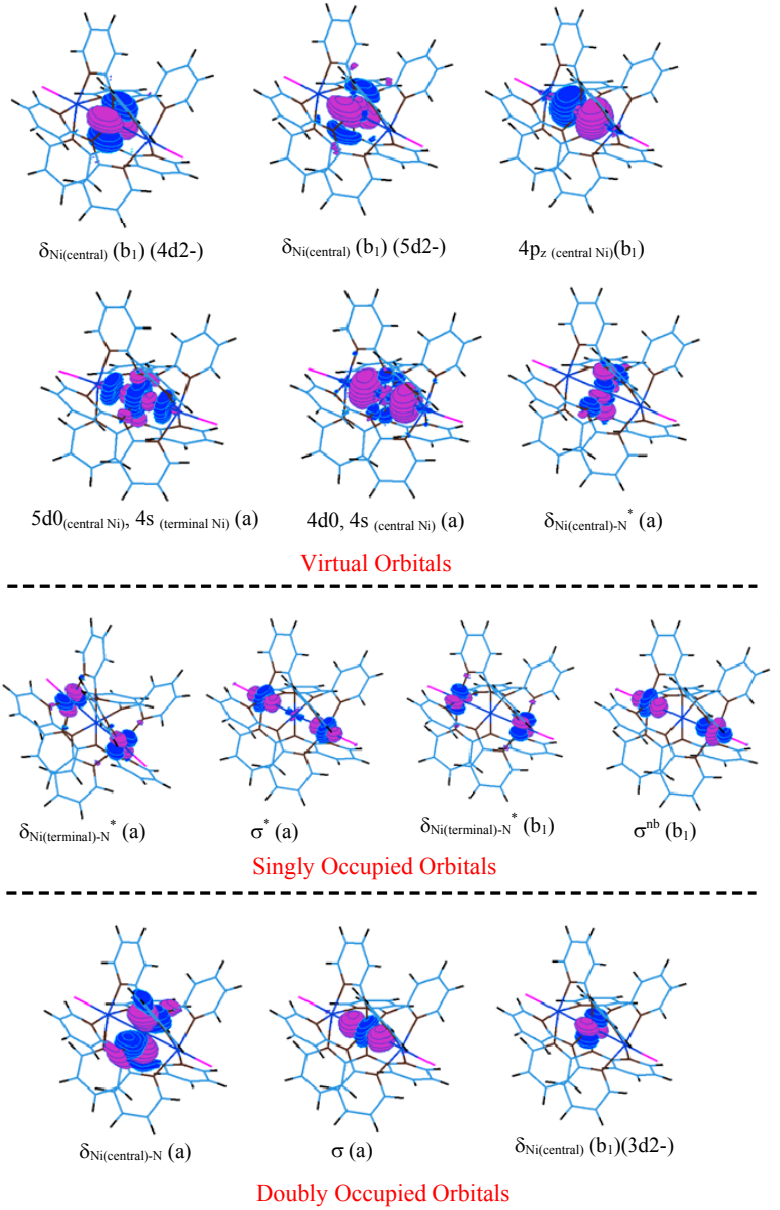

Figure A1. Extended CAS (10,13) for $Ni_3(dpa)_4Cl_2$ (**1**). The symmetry of each orbital is given in parentheses. Labelling of d orbitals: $d_{x^2-y^2}$ = d2+ ; d_{xy} = d2- ; d_{z^2} = d0.

UNIVERSITAT ROVIRA I VIRGILI
THEORETICAL STUDY OF MAGNETIC AND CONDUCTING PROPERTIES OF TRANSITION METAL NANOWIRES
Zahra Tabookht
DL:T-1807-2011

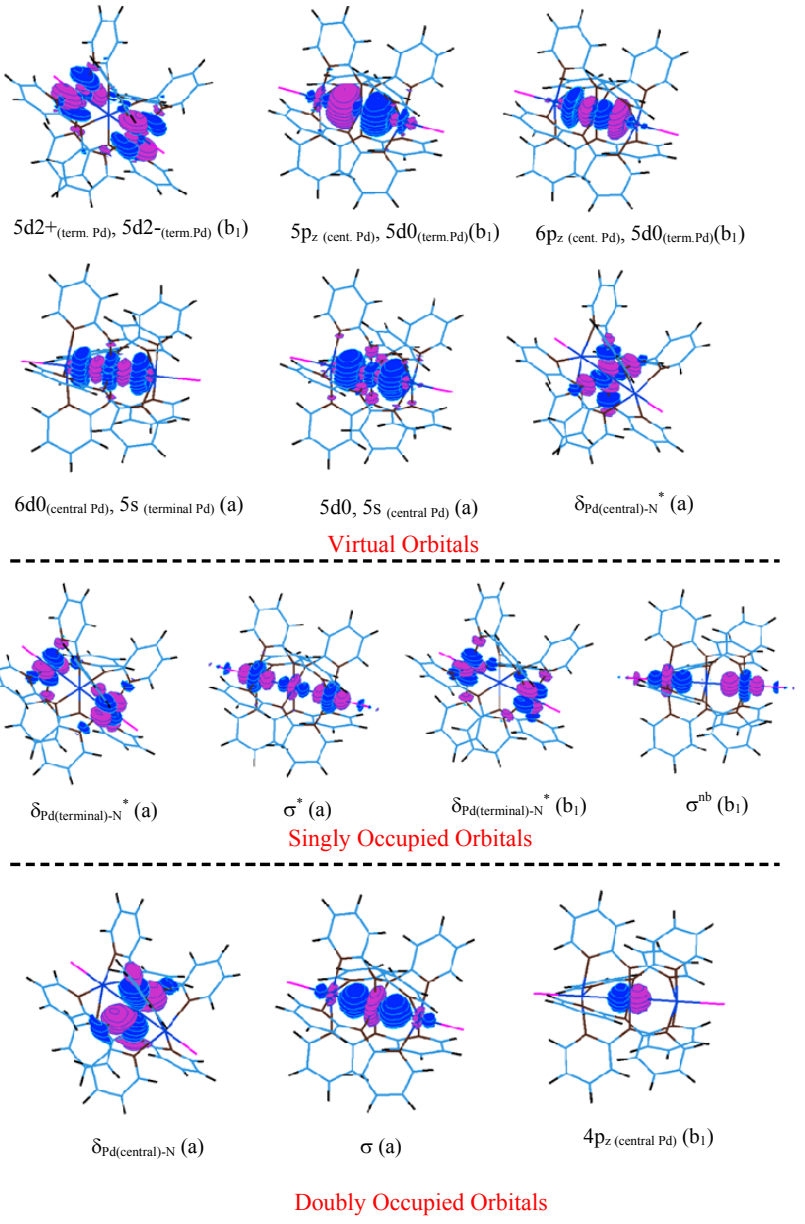

Figure A2. Extended CAS (10,13) for $Pd_3(dpa)_4Cl_2$ (**2**)

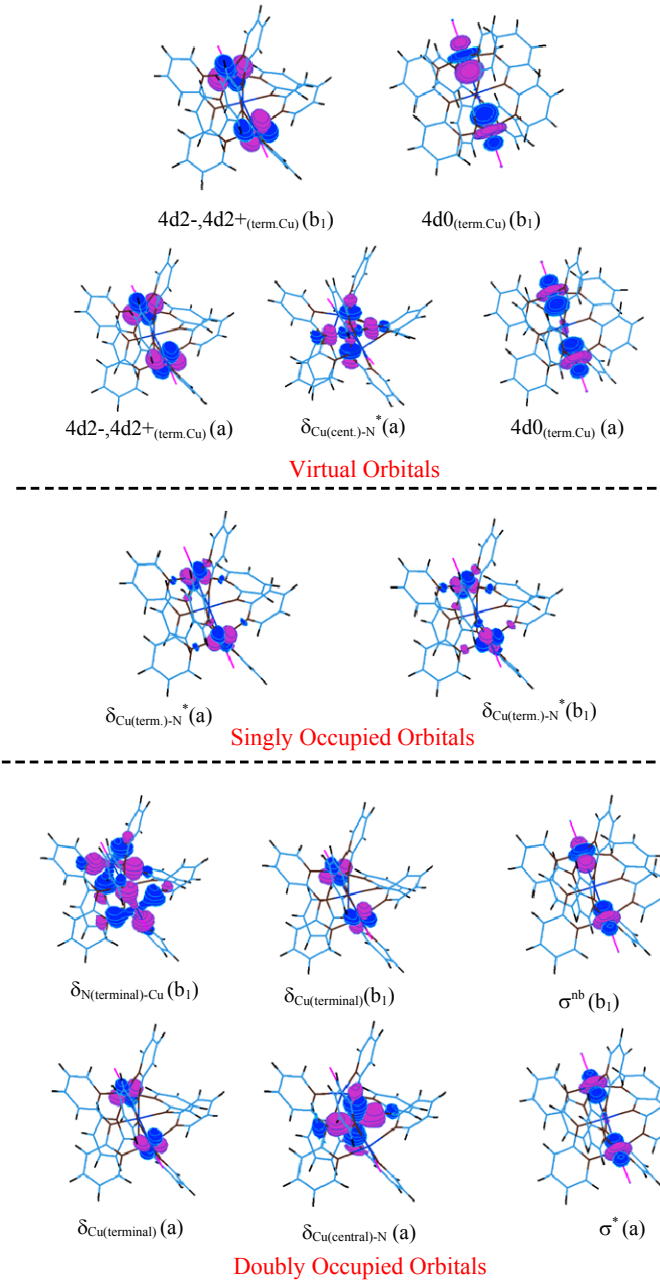

Figure A3. Extended CAS (14,13) for $[Cu_3(dpa)_4Cl_2]^+$ (**3**$^+$)

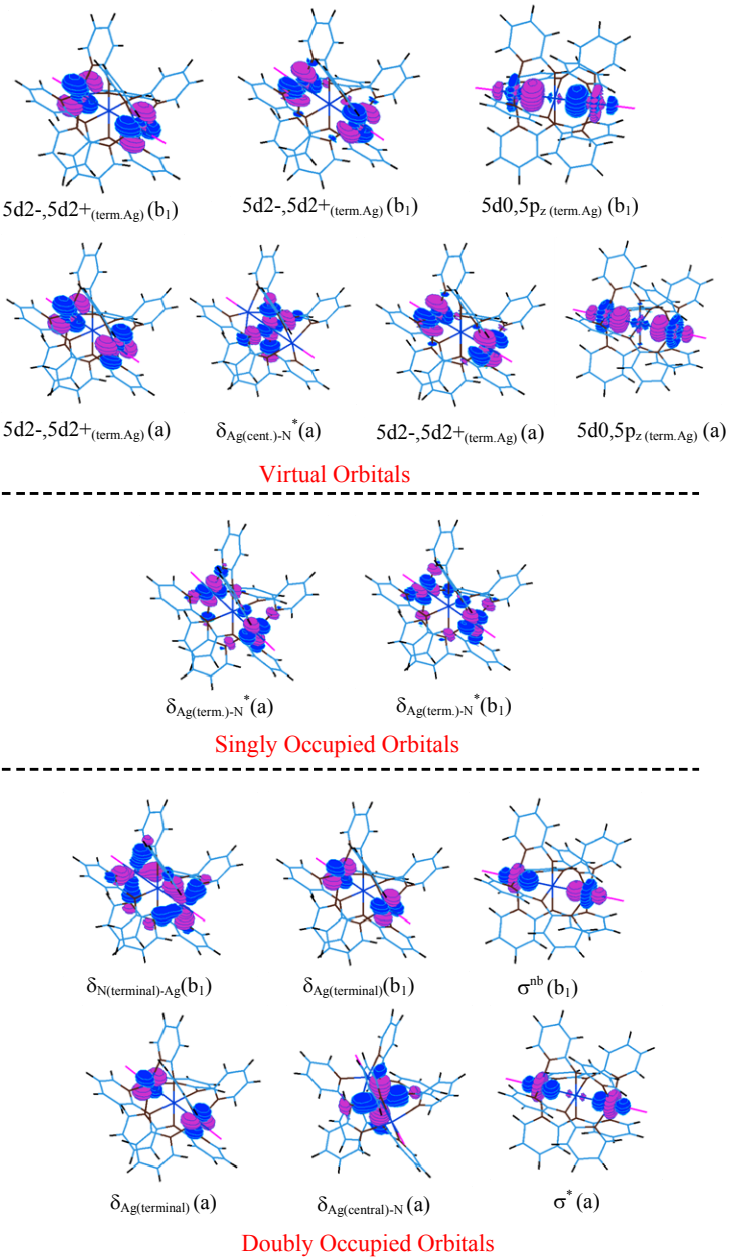

Figure A4. Extended CAS (14,15) for $[Ag_3(dpa)_4Cl_2]^+$ (**4**$^+$)

UNIVERSITAT ROVIRA I VIRGILI
THEORETICAL STUDY OF MAGNETIC AND CONDUCTING PROPERTIES OF TRANSITION METAL NANOWIRES
Zahra Tabookht
DL:T-1807-2011

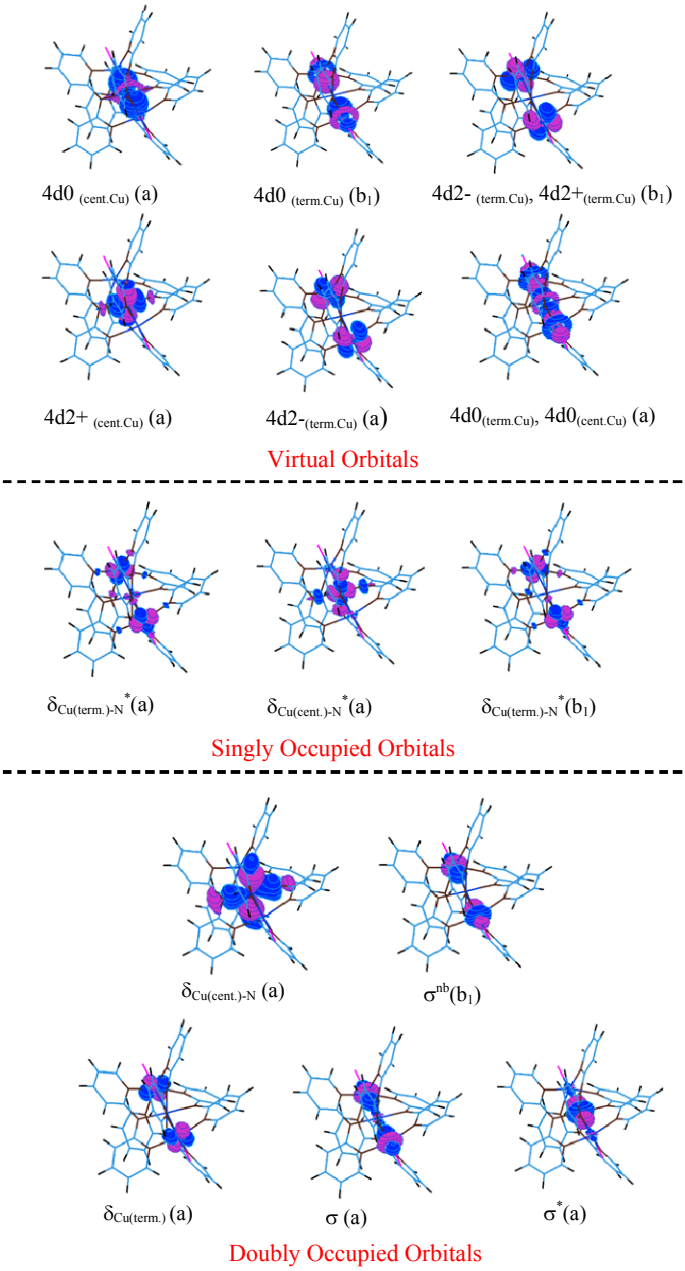

Figure A5. Extended CAS (13,14) for $Cu_3(dpa)_4Cl_2$ (**3**)

UNIVERSITAT ROVIRA I VIRGILI
THEORETICAL STUDY OF MAGNETIC AND CONDUCTING PROPERTIES OF TRANSITION METAL NANOWIRES
Zahra Tabookht
DL:T-1807-2011

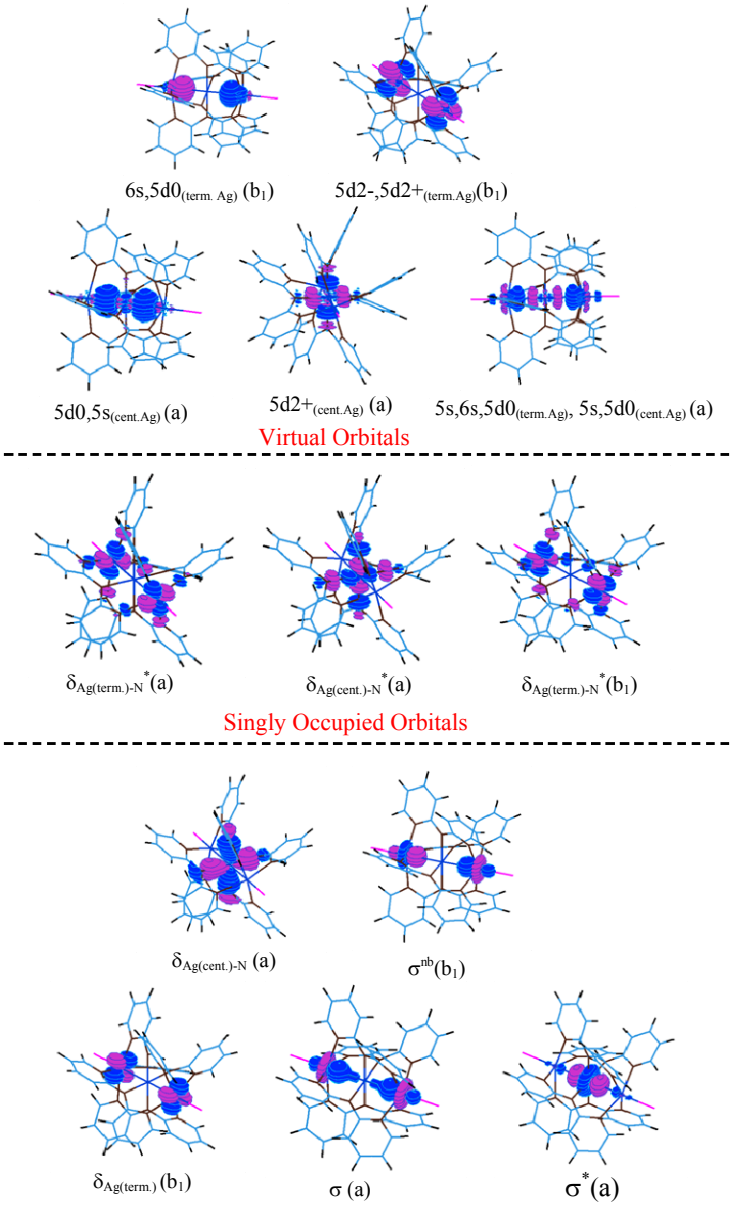

Figure A6. Extended CAS (13,13) for $Ag_3(dpa)_4Cl_2$ (**4**)

Appendix B

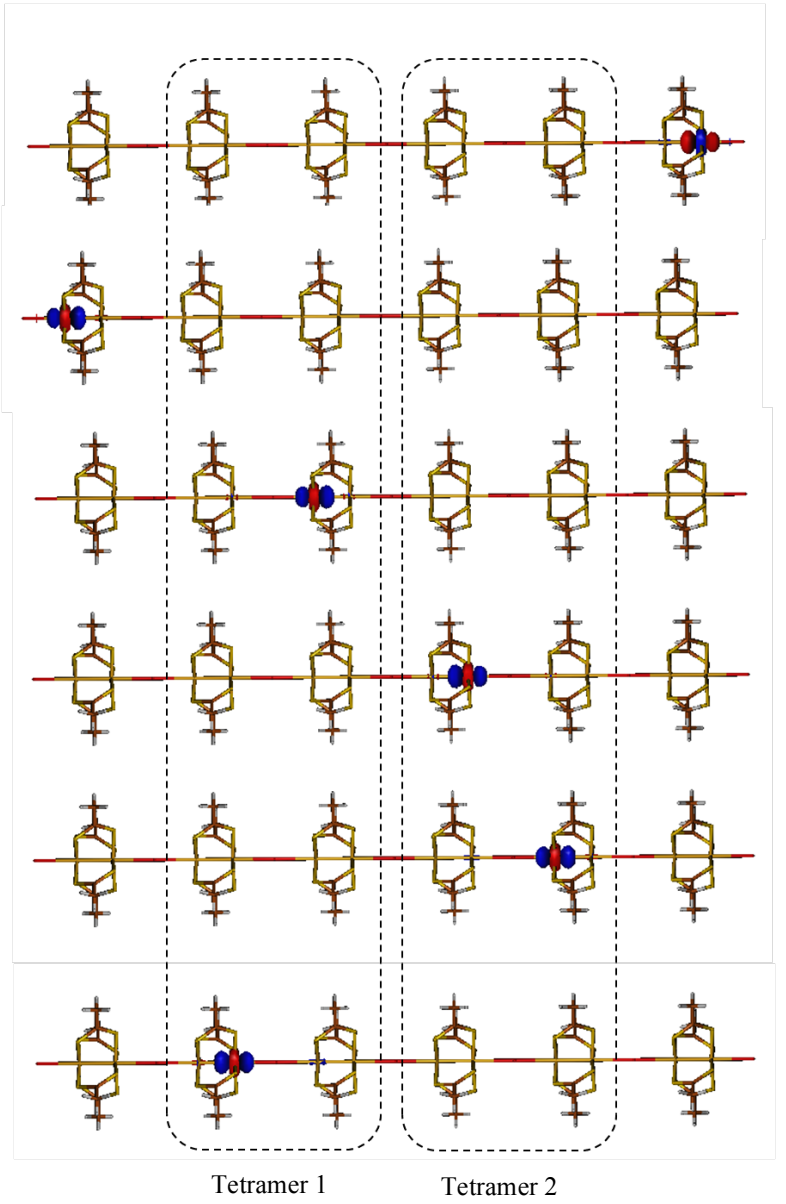

Figure B1. Representation of the septet orbital optimized for the Ni_{12} fragment spanning the CAS(6,6), which may be viewed as two tetramers connected by a I ligand, surrounded by two dimers at both ends of the fragment.

List of Publications

1. "Analysis of the Magnetic Coupling in $M_3(dpa)_4Cl_2$ Systems (M = Ni, Pd, Cu, Ag) by Ab initio Calculations " Z. Tabookht, X. López, C. de Graaf*, J. Phys. Chem. A,* 2010, 114, 2028.

2. "Isotropic non-Heisenberg behavior in $M_3(dpa)_4Cl_2$ Extended Metal Atom Chains" Z. Tabookht, X. López, M. Bénard, C. de Graaf, *J. Phys. Chem. A,* 2010, 114, 12291.

3. "Simple vs. Composite Nature of the Magnetic Coupling in Copper and Nickel-based metallic Chains. Over- and Underestimation of *J*" N. A. G. Bandeira, Z. Tabookht, C. de Graaf, X. López, *C. R. Chimie* DOI: 10.1016/j.crci.2011.10.002.

4. "Towards a Low-Spin Configuration in Extended Metal Atom Chains. Theoretical Study of Trimetallic Systems with 22 Metal Electrons" Z. Tabookht, C. de Graaf, X. López, *Dalton Trans.* DOI:10.1039/C1DT11260K.

5. "Charge-ordering and electrical conduction in MMX chains: theoretical study of $Ni_2(dta)_4I$ and $Pt_2(dta)_4I$ (dta = $CH_3CS_2^-$)" Z. Tabookht, X. López, C. de Graaf, N. Guihéry, N. Suaud, N. Benamor, submitted to *Inorg. Chem*.